NASA CONTRACTOR REPORT 177401

NONLINEAR SYSTEM CONTROLLER DESIGN BASED ON DOMAIN OF ATTRACTION: AN APPLICATION TO CELSS ANALYSIS AND CONTROL

P. S. BABCOCK IV

NASA COOPERATIVE AGREEMENT NCC 2-67
MARCH 1986

NASA

CELSS

NASA CONTRACTOR REPORT 177401

NONLINEAR SYSTEM CONTROLLER DESIGN BASED ON DOMAIN OF ATTRACTION: AN APPLICATION TO CELSS ANALYSIS AND CONTROL

P. S. BARCOCK IV
DEPARTMENT OF MECHANICAL ENGINEERING
UNIVERSITY OF CALIFORNIA - BERKELEY
BERKELEY, CALIFORNIA

PREPARED FOR
AMES RESEARCH CENTER
UNDER COOPERATIVE AGREEMENT NCC 2-67

MARCH 1986

National Aeronautics and
Space Administration

Ames Research Center
Moffett Field, California 94035

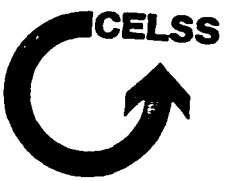

TABLE OF CONTENTS

1. INTRODUCTION

In anticipation of long-duration, manned space flights, NASA has been investigating Closed Ecological Life Support Systems (CELSS). The CELSS would contain a combination of biological, chemical, and mechanical components. It would provide for the crew's nutritional, atmospheric, and waste processing needs. The system is closed to mass but open to energy. Its goal is the long-term survival of the human crew.

The CELSS can be thought of as containing a replenishing food supply (usually plants), a waste processor, the human crew, and various storage tanks. In addition to supplying food for the crew, the plants, through photosynthesis, remove carbon dioxide and provide oxygen to the atmosphere. As the humans consume the food, they partially reoxidize it, using oxygen from the atmosphere and generating carbon dioxide. The waste from the humans is run through a waste processor, completing the oxidation that the humans started. In this way, the human/waste processor components complement the growing food components. The mass flow follows a loop and the mass is conserved.

After considering this general view of a CELSS, the following question was raised: Where might problems develop in system behavior due to these component relationships? There are three areas of concern. First, how do the long time delays of plant growth affect the ability to control the system and insure its survival? Second, what are the effects of nonlinearities on the system behavior? Lastly, does system mass, and its relation to storage tank capacities, determine the possible system behaviors?

To address these questions, a series of abstract dynamic models of a CELSS were developed [2]. They were used to investigate the interaction of long-term dynamics with finite size storage tanks. The variety of missions a CELSS can be used on increases as the total system mass and size is reduced [5]. However, the smaller the storage tanks, the greater the possibility of a tank overflow during a component failure. The series of CELSS models looks at the dynamic consequences of such a component failure as a function of tank capacity and control scheme.

Since no CELSS has been constructed, and the models' nonlinear state equations do not resemble any common engineering system, an investigation of the abstract models was undertaken. In the simplest model there are 5 state variables. In addition to nonlinear functions for plant growth, there are 7 switching functions representing empty and overflowing storage tanks. While the state space is bounded, the determination of the existence of equilibrium points is quite time consuming. This simple 5 dimension system only permits one harvest per growing time. The more realistic models have multiple harvests in a growing period, resulting in 8 to 182 state variables. Even in the case of only 8, the traditional approach to locating equilibrium points is not practical.

To explore all possible behaviors of these systems, a Monte Carlo search of admissible initial conditions was performed. This uncovered all possible equilibrium points (and some more complex attracting regions) and showed a pattern of bifurcations and reverse bifurcations as the storage tank capacities were varied. The relationship between system behavior and tank capacity could now be shown.

It is important to be able to tell when one controller is superior to another from the viewpoint of system survival. Assuming that the major threat to a CELSS is a component failure, and that a failure moves the system along a random vector in state space, the best controller is the one that recovers from the largest variety of failures. This is equivalent to returning the system to the desired equilibrium from the largest region of the state space. The component failure is viewed as an event that moves the system away from the desired behavior. It is assumed that the component can be repaired and that it is then the controller's job to return the system to its desired operation.

The domain of attraction of an equilibrium point is the region in state space that is attracted to the equilibrium point. Initial conditions within this region tend toward the equilibrium point asymptotically. The attractors do not have to be points, they may be limit cycles, or higher-dimension attractors. The present use of domain of attraction is of interest only in nonlinear systems because in linear systems it is trivial, either being the entire state space or null.

The domain of attraction can be refined so that a settling time, overshoot, or other criteria are included. The resulting region is called a domain of performance. While the domain of attraction is not particularly enlightening when used with linear systems, the domain of performance is useful in investigations of both linear and nonlinear systems.

The control-design goal for the CELSS may be stated as developing the controller that gives the system the largest domain of attraction around the desired operating point. If this includes the entire

admissible state space, then system survival is guaranteed for all possible component failures.

This dissertation explores the characterization and use of the domain of attraction and its subset, the domain of performance. Investigations of the domain of attraction are performed by Monte Carlo searches of admissible initial conditions, identifying those that lead toward the desired equilibrium point (pass) and those that do not (fail). The resulting pass region can then be measured (total volume, minimum radius, maximum radius) and a measure of interest can be optimized. This technique is not greatly burdened by high dimensional systems because a random search is used and the performance measure is a set of scalars.

It is possible to mathematically calculate the error associated with the Monte Carlo determination of the domain's volume when the sample distribution is known. If the domain has a regular shape and low dimension, the volume can be used to obtain a minimum and maximum radius. The minimum radius is a reasonable measure of the system's ability to recover from random perturbations of the state due to a component failure. The maximum gives some measure of the elongation of the domain.

For the CELSS models the domain of attraction has an irregular shape and a high dimension. The constant mass constraint results in a nonuniform sample distribution of initial conditions that is analytically unknown. Hence, direct mathematical determinations of volume, minimum radius, and associated errors are impossible. Local densities are used to obtain volume information from the counts of initial

conditions that are contained in the domain. Similarly, the minimum radius is found through Monte Carlo simulations and its error is established statistically.

In the following chapter, the domain of attraction is compared with more conventional measures of system stability and performance. Methods for measuring the domain and its associated error are shown for both uniform and nonuniform distributions. In Chapter 3, controller design using the domain as a performance measure is contrasted with more conventional control designs. Finally, in Chapters 4 and 5, these techniques are used to examine the CELSS models' behavior as well as some properties of CELSS control.

2. THE DOMAIN OF ATTRACTION

2.1 Stability, Performance, and The Domain

A system's equilibrium point (or more complex attractor) is stable if nearby points approach it in some specified fashion (e.g.: Lyapunov stable, asymptotically stable, etc.). The domain of attraction is the entire region about the stable equilibrium point that tends toward it. In linear systems, a stable equilibrium point attracts the entire state space. Nonlinear systems may have many attractors, each with their own domain of attraction. In these cases, both the local and global stability properties are important.

Consider a system that has its state perturbed suddenly from a stable equilibrium. If this is a linear system, it will eventually return to the equilibrium. However, if the system is nonlinear, the perturbed state may be outside the domain of attraction of the original equilibrium. Then the system would not return to the starting equilibrium point. Therefore, the size of the domain of attraction in a nonlinear system is a measure of its ability to recover from displacements in its state.

By including performance criteria, a domain of performance can be found. This is a subset of the domain of attraction. The size of the domain of performance is an indicator of both linear and nonlinear system performance under impulse perturbations of the state. This is because many performance criteria are inherently nonlinear (such as settling time). Since they do not scale with initial conditions, the domain of performance may not be global in stable linear systems.

In this dissertation the domains of attraction and performance will be used to investigate system behavior. In addition, the measures of the domain will be used as a selection parameter in controller design.

It is very difficult to find necessary and sufficient conditions for the stability of nonlinear systems. For example, Lyapunov's second method gives only sufficient conditions. Therefore, the region where the Lyapunov function exists is a conservative estimate of the domain of attraction. Since this is only a sufficient condition, it may be possible to find Lyapunov functions that will approximate the domain of attraction better.

Lyapunov's first method can also be used to determine the size of the domain for a nonlinear system [17]. The system is decomposed into linear and nonlinear parts about the equilibrium point of interest. A Lyapunov function is found for the linear part. The system is locally asymptotically stable if the gradient along trajectories due to the linear and nonlinear parts is negative definite. The domain of attraction is approximated by finding the region where the linear contribution to the gradient dominates that of the nonlinear part. Since this is based on the second method, it is only a sufficient condition and the domain estimate is conservative.

A method for designing controllers and obtaining Lyapunov functions for nonlinear systems has been presented by Su, Meyer, and Hunt [16]. The nonlinear system is transformed into a canonical linear form. A controller can then be designed using standard, linear methods. The equivalent controller for the nonlinear system is found by applying the inverse transformation to the linear system's control.

A Lyapunov function for the nonlinear system can be made by applying the inverse transformation to the linear system's Lyapunov function. Since this function showed global stability of the linear system, it also shows stability over the entire region for which the transformation applies. Within this region the nonlinear system can recover from state perturbations.

There are three limitations to this approach. First, the transformation must be continuous and smooth [7]. A system with switching points or other discontinuities cannot be transformed into a linear system. Secondly, the transformation and results only apply to a limited region of the state space. The region can only contain one attractor of the uncontrolled, nonlinear system. As a result, cases where the controller greatly increases the domain of attraction cannot be detected. Finally, a direct measure of the size of the attracting neighborhood is not obtained; only its lower bounds. This makes selection of control strategies more difficult.

The technique proposed in this dissertation avoids many of the usual problems associated with determining the domain of attraction. By relying on simulation and Monte Carlo selection of initial conditions, the procedure is relatively insensitive to system dimension, nonlinearities, and complexity of form. By finding all attractors, all possible system behaviors are discovered. The domain of attraction about a given attractor gives a direct measure of the system's ability to recover from state perturbations. Controller design can then be accomplished by using a Monte Carlo search of control parameters, effectively creating a nested Monte Carlo program. Performance measures are easily included,

generating a domain of performance that is a subset of the domain of attraction. It is also easy to deal with questions of robustness against conditions such as parameter uncertainty or disturbance rejection.

2.2 Measures of the Domain

The domain of attraction is the set of points in state space that has trajectories that approach an equilibrium point (or other attractor) asymptotically [9]. The domain of attraction is also referred to as the basin of attraction [4, 10, 14] and the domain of stability [9]. This region can be mapped out through simulation using randomly selected initial conditions from the admissible state space. Initial conditions that are attracted to the given equilibrium are labeled as passes; those that are not attracted are called fails. In this section, a method for finding equilibria and mathematically calculating the volume of the domain of attraction will be presented. This applies to both continuous and discrete systems.

Consider the nonlinear, dynamic system:

$$\dot{x}(t) = f(x(t),u(t),z) \tag{2.1}$$

where x(t) is the state vector, u(t) is an input or forcing vector, and z is a vector of parameters. To perform a simulation of this system, u(t), z, and an initial condition for x must be specified. While there are no restrictions on the form of u(t), it is often taken as a function of x(t), giving the system a closed-loop feedback form. The z vector represents parameters of the system that can be selected during the design process such as controller gains.

The equilibrium points are solutions of:

$$f(x(t),u(t),z) = 0 \tag{2.2}$$

Finding these solutions can be very time consuming if the dimension of the state vector is large or if the function f has many switching points. Instead of solving for the equilibrium points directly, a simulation approach is used with randomly selected initial conditions of x. State trajectories are followed until they become (a) stationary within specified tolerances, (b) leave a given region, or (c) remain in a bounded volume but do not converge to a point. Case (a) is the result of a stable equilibrium point. Case (b) occurs when sample initial conditions are within the domain of attraction of a point outside the region being investigated. Higher dimensional attractors (such as limit cycles) appear in case (c).

All attractors (equilibrium points, limit cycles, strange attractors, etc.) can now be found for a given region in the state space. However, specifying the exact nature of the attractor is not always simple. For equilibrium points the trajectory comes to rest within a small volume. Limit cycles repeat their motion and can be recognized by a repeating pattern of trajectory points. Higher dimensional attractors are much more difficult to classify. For example, motion on a torus (which has a finite number of frequencies) and motion on a strange attractor (which has an infinite number of frequencies) can only be distinguished through their spectra or with a calculation of Lyapunov exponents [4, 10]. In the examples in this and the following chapter, only equilibrium points are encountered. More complex attractors occur in Chapter 5.

Once the attractors have been found, the domain of attraction for each may be examined. For simplicity, we will restrict the discussion to the domain of one attractor. A random selection of initial conditions of x are grouped into passes and fails depending on whether the trajectory goes to the attractor of interest. The set of passes indicates the region of attraction. This region can be analytically measured.

To bring this discussion into clearer focus, consider Figure 1. The region of interest R (two-dimensional in this case) is the set of points:

$$R = \{(x,y): a \leq x \leq b, c \leq y \leq d\} \tag{2.3}$$

The domain of attraction D of point (x_o,y_o) is:

$$D = \{(x,y): x(t) \rightarrow x_o, y(t) \rightarrow y_o, \text{ as } t \rightarrow \infty, \text{and } (x,y) \in R\} \tag{2.4}$$

A Monte Carlo integration [6, 12] can be used to determine the area of D. If the initial conditions are uniformly distributed on the region R, their probability density function is:

$$p(x,y) = \frac{1}{(b-a)(d-c)} \tag{2.5}$$

The probability P that an initial condition is in D (i.e.: a pass) is:

$$P = \frac{\text{area } D}{\text{area } R} = \frac{A}{(b-a)(d-c)} \tag{2.6}$$

If N random initial conditions are generated, we denote the number of passes (in region D) as N_p. P can be estimated by:

$$\hat{P} = \frac{N_p}{N} \tag{2.7}$$

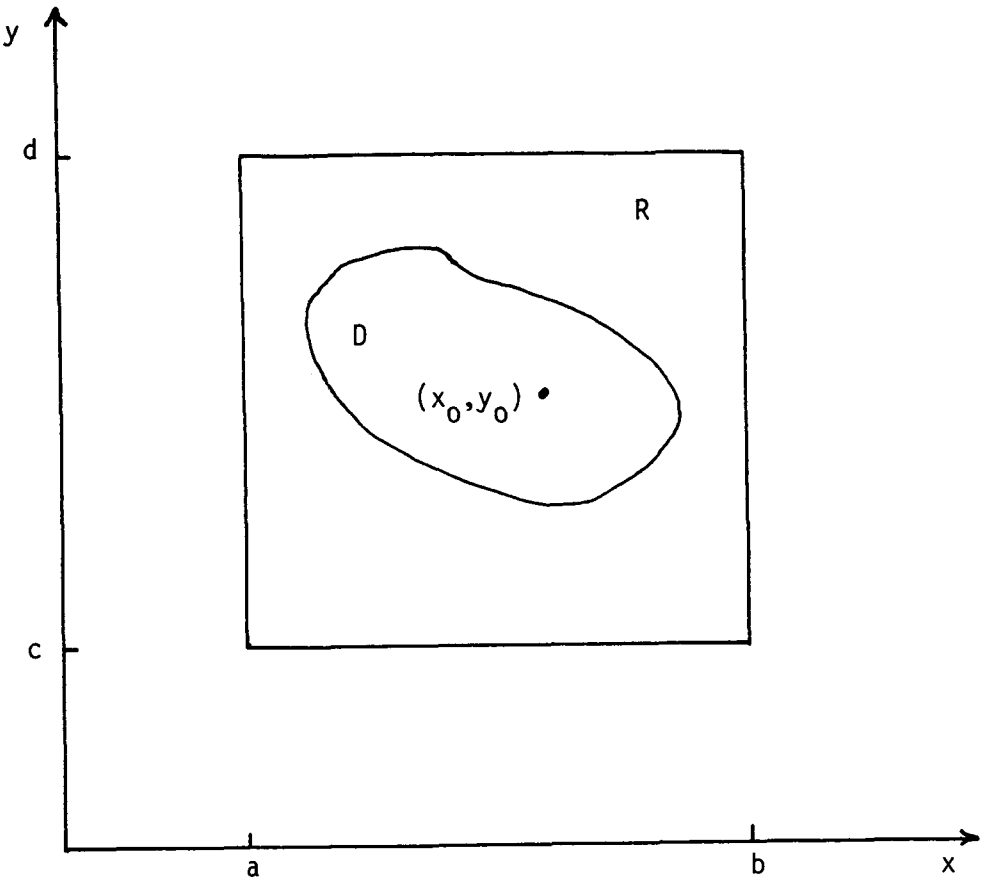

Figure 1: The Domain of Attraction of (x_0,y_0)

Using equations 2.6 and 2.7, the area of D can be approximated by:

$$\text{area } D = A \simeq \hat{A} = (b-a)(d-c)\cdot\frac{N_p}{N} \tag{2.8}$$

Each of the N trials is independent and a binary selection criteria is used. Therefore, these are Bernoulli trials with probability P of a pass. $\hat{A}$ is an unbiased estimator of A because:

$$E(\hat{A}) = (b-a)(d-c)\cdot\frac{E(N_p)}{N} = (b-a)(d-c)P = A \tag{2.9}$$

The variance of $\hat{A}$ is:

$$\text{var}\hat{A} = [(b-a)(d-c)]^2 \text{ var}\hat{P} = \frac{A\cdot[(b-a)(d-c) - A]}{N} \tag{2.10}$$

where the variance of $\hat{P}$ is:

$$\text{var}\hat{P} = \text{var}(N_p / N) = \frac{P(1-P)}{N} \tag{2.11}$$

$$\text{var}\hat{P} = \frac{A\cdot[(b-a)(d-c) - A]}{N\cdot[(b-a)(d-c)]^2}$$

The standard deviation of $\hat{A}$ is:

$$\text{s.d.}(\hat{A}) = [\text{var}\hat{A}]^{1/2} \tag{2.12}$$

The precision of the estimate $\hat{A}$ is proportional to $N^{-1/2}$.

This technique of estimating area (or volume) and error of the domain of attraction requires that the initial conditions are uniformly distributed. In systems where constraints cannot be substituted in explicitly the uniformity of sample points cannot be achieved. An implicit solution for this case is demonstrated in the next section.

Since the domain indicates the region of initial conditions that returns to the attractor, the minimum radius of the domain can be used as a worst-case measure for a system whose state experiences a random perturbation. This is particularly true when the domain has a complex shape such as branches off of a central region. If the perturbation moves the system further from the equilibrium point than the minimum radius, there is no guarantee that the system is still within the domain of attraction.

2.3 Example: The Damped Pendulum

A damped pendulum is used to demonstrate some of the techniques for finding attractors and measuring their domains. The system has many stable equilibrium points, the domain of attraction about one of which is examined here. Using a uniform sample of initial conditions, the area and error calculations of the last section are compared with a more general technique. Since the minimum radius is a more versatile measure of the domain indicating the worst-case system response from a random perturbation of the state, a general method of finding it and its associated error is shown. These techniques are then extended to include the case where a nonuniform sample distribution is used.

The damped pendulum in Figure 2 is represented by the nonlinear state equations:

$$\begin{aligned} \dot{x} &= y \\ \dot{y} &= -\sin(x) - b \cdot y \end{aligned} \tag{2.13}$$

where x is angular position, y is angular velocity, and b is the damping coefficient. Pendulum length and mass have been selected to give unity

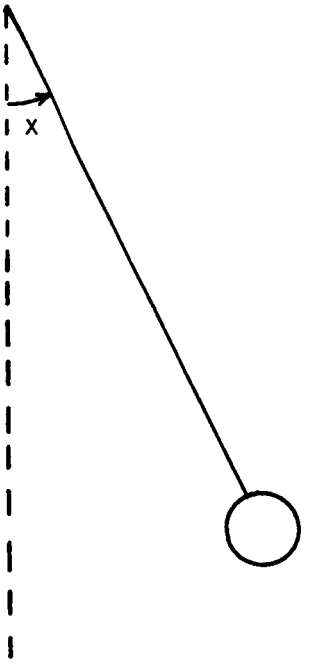

Figure 2: The Pendulum

coefficients. The value of b is set to 0.5 and a time step of 0.05 is used with a fourth-order Runge-Kutta integration. The sample region of initial conditions is:

$$\{(x,y): -10 \leq x \leq 10, -5 \leq y \leq 5\} \qquad (2.14)$$

To discover all attractors that can be reached from this region, a series of simulations can be performed using initial conditions randomly selected from a uniform distribution. The initial conditions are grouped according to the equilibrium point that attracts them. A result for 1000 initial conditions is shown in Figure 3. Points in this region are attracted to 7 stable equilibria. Table 1 gives the distribution of initial conditions with respect to the attractors, and some representative trajectories are shown in Figure 4.

The origin is selected as the attractor for the investigation of the domain of attraction. As a first check of the reliability of the Monte Carlo integration, Figure 5 shows that the fraction of initial conditions attracted to the origin converges to 31.04%. The total region sampled has an area of 200. Therefore, using equation 2.8, the area attracted by the origin is 62.08.

Since the randomly selected initial conditions came from a uniform distribution, the accuracy of this area calculation can be established using equation 2.12. Area and error results for a variety of sample sizes are contained in Table 2. In the standard deviation calculation, it is assumed that the true area is 62.

In most cases, the domain of attraction is not spherical so its

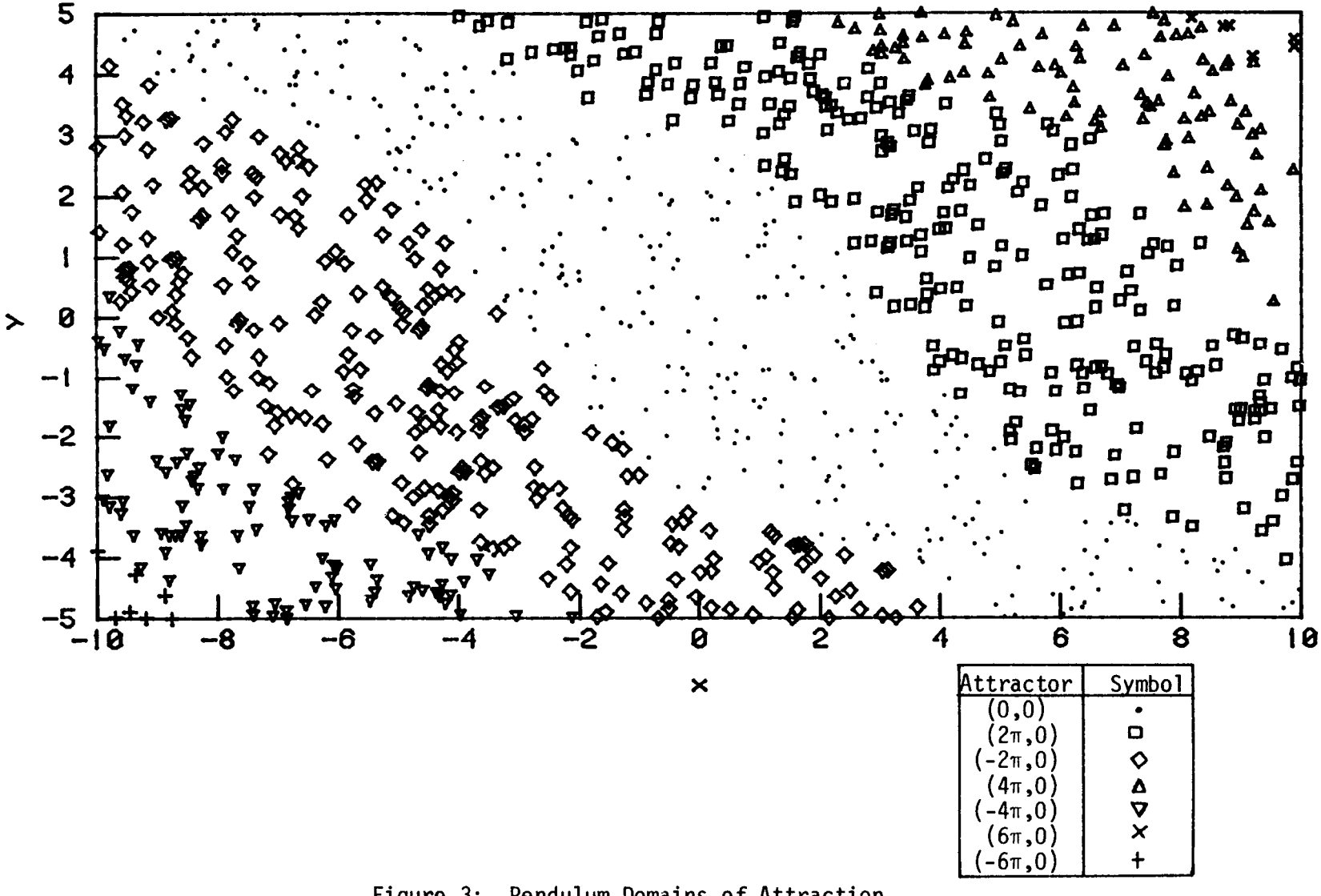

Attractor	Symbol
(0,0)	•
(2π,0)	□
(-2π,0)	◇
(4π,0)	△
(-4π,0)	▽
(6π,0)	×
(-6π,0)	+

Figure 3: Pendulum Domains of Attraction

Table 1: Size of Pendulum Domains (1000 sample points)

Equilibrium (x_o, y_o)	Number of Points
0,0	309
2π,0	253
-2π,0	246
4π,0	87
-4π,0	92
6π,0	6
-6π,0	7

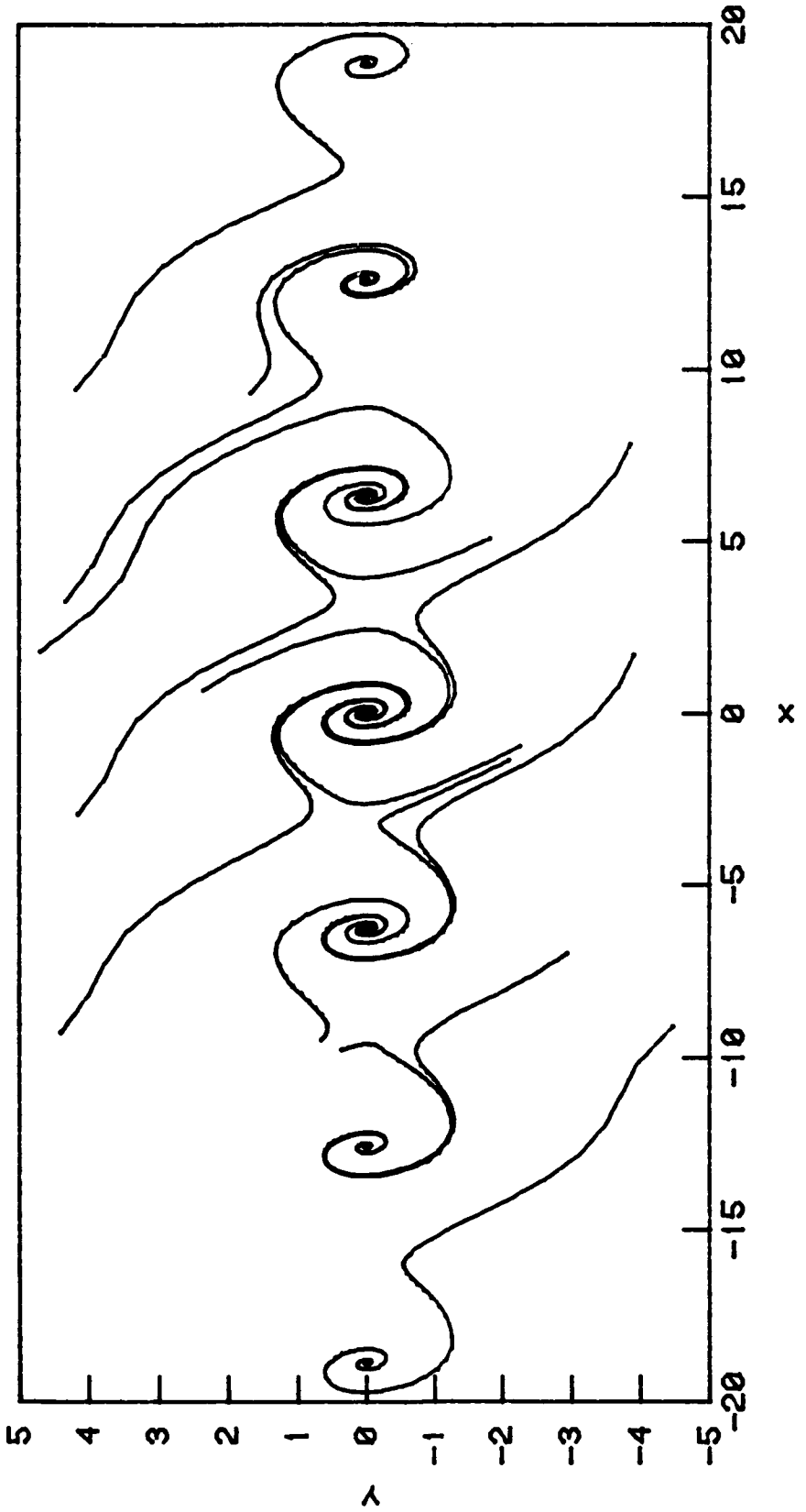

Figure 4: Some Pendulum Trajectories

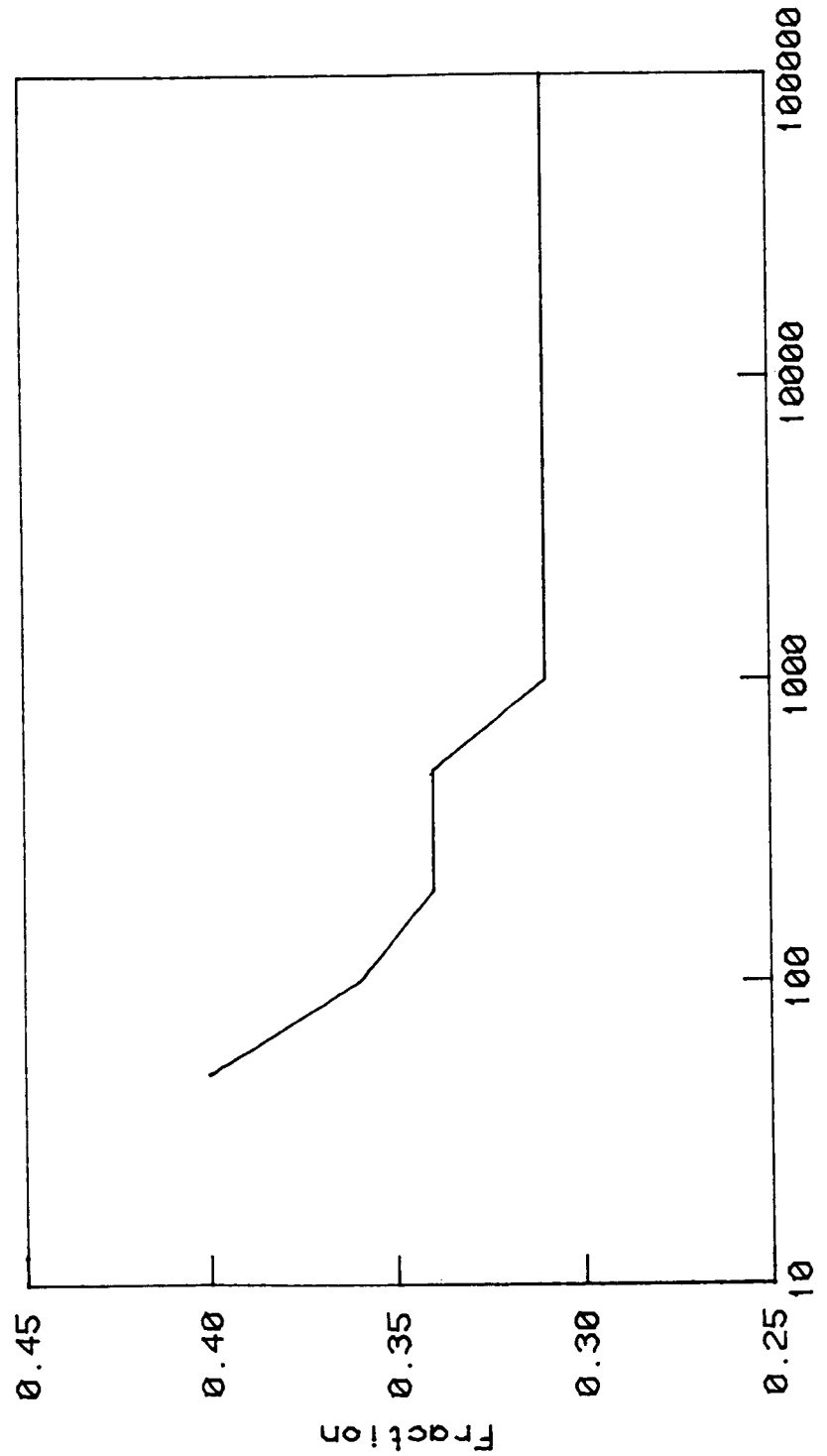

Figure 5: Domain Area of (0,0) vs. Number of Samples

Table 2: Area of Pendulum Origin's Domain of Attraction

Number of Samples	Area $\pm$ Standard Deviation $A \pm a$
100	$72. \pm 9.25$
1000	61.8 ± 2.93
10000	62.0 ± 0.93
100000	62.08 ± 0.29

volume is not a good measure of system recovery from a random disturbance. The minimum radius is more appropriate because it reflects the size of the region where recovery is guaranteed, independent of the orientation of the disturbance vector. For systems where the perturbation has preferred directions, more detailed geometric information on the domain may be useful.

It is possible to get an estimate of the pendulum domain's minimum radius by taking advantage of the domain's regular shape. In Figure 6 a parallelogram is superposed on the pattern of pass and fail initial conditions. Its height (y direction) is fixed at 10. The area of the parallelogram is:

$$A = B \cdot H \tag{2.15}$$

where B is the length of the base (x direction) and H is the height (y direction). For a fixed height, errors in area result from errors in the base measurement:

$$A \pm a = B \cdot H \pm b \cdot H \tag{2.16}$$

where a and b are the errors in area and base, respectively.

Using the information on domain area and error in Table 2 with equation 2.16, a table of base length and error can be made. The base length, however, is not directly a measure of the minimum radius. Using the geometry in Figure 7 a measure of the minimum radius r of the domain can be found:

$$r = \frac{B \cdot \cos\phi}{2} \tag{2.17}$$

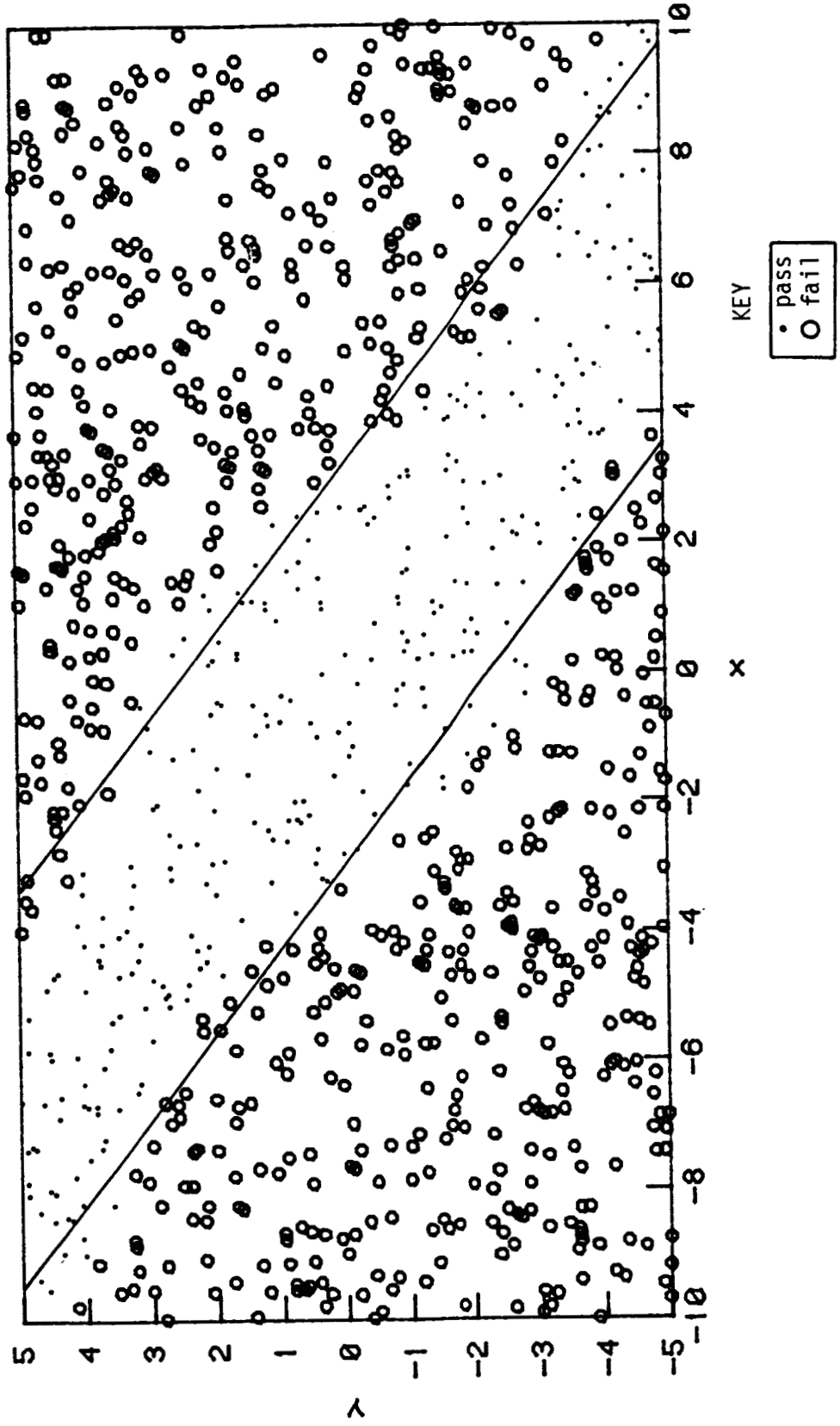

Figure 6: Domain of Attraction about (0,0) with Superposed Parallelogram

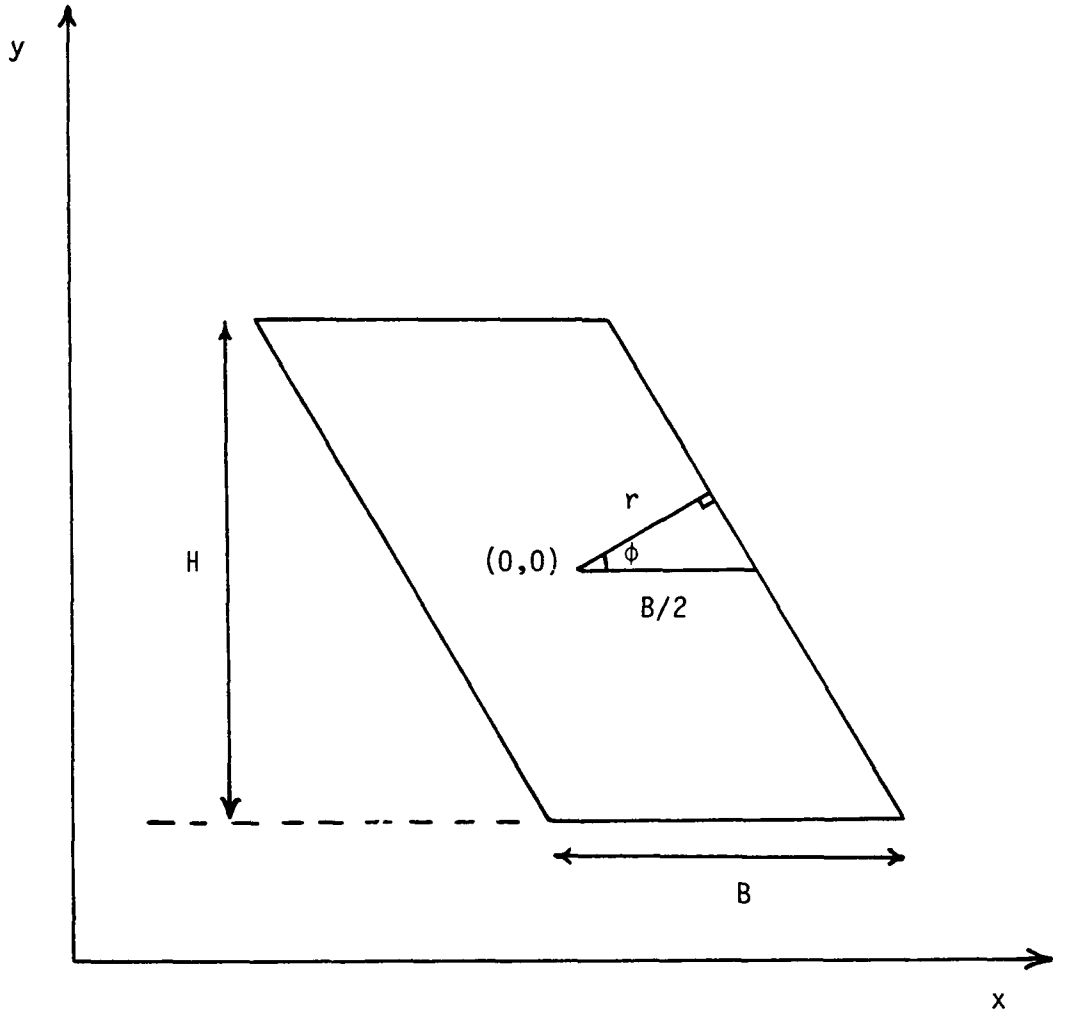

Figure 7: Geometry of a Parallelogram Domain

Using the error of the area (Table 2), the minimum radius error can be calculated:

$$\sigma_r = \frac{a \cdot \cos\phi}{2H} \tag{2.18}$$

The minimum radius and error using equations 2.17, 2.18 and Table 2 for 1000 sample points is:

$$\hat{r} = 1.82 \pm 0.09 \tag{2.19}$$

Figure 6 was used to set ϕ to 53 degrees.

The above is an approximate method for finding the minimum radius relying on the sample distribution being uniform (to find the area) and the region being somewhat regular (to relate area to minimum radius). There are two problems with this. First, the domain of attraction is rarely regular, and second, in higher dimensions a relationship between area and minimum radius cannot usually be found.

To determine the domain's area, minimum radius, and their associated errors more directly, the simulation with 1000 uniformly distributed initial conditions was repeated many times with independent sample sets. The area results of these repetitions were stored. The mean and standard deviation of the set of area calculations converged before 100 repetitions were completed (a total of 1000 repetitions were performed). The result for 100 repetitions is:

$$\hat{A} = 62.08 \pm 2.42 \tag{2.20}$$

where the number of sample points that passed has been converted into an area (equation 2.8). This area agrees with the Table 2 result for

100,000 samples (because this is a 100,000 sample result). The error agrees with the Table 2 result for 1000 samples. Therefore, the area and error calculations using equations 2.8 and 2.12 can be duplicated through repeated simulations of the domain of attraction.

Since the domain's boundary, and therefore its minimum radius, lie somewhere between the pass and fail points, it is not possible to get a direct measurement of the minimum radius using Monte Carlo simulations. However, a first approximation can be found by locating the initial condition nearest the attractor that is not in its domain (i.e. a point from the fail set). For the pendulum example, this point is shown in Figure 8 for 1000 randomly selected initial conditions. The minimum radius is the distance from the attractor to the boundary of the domain. This point, a fail point, is simply the nearest point that is not in the domain. The uniformity of the sample distribution can be used to infer the location of the boundary from this point.

For example, 1000 points uniformly distributed on an area of 200 gives an expected area per point of 0.2. If this area is in the shape of a circle, its radius is 0.25. Assuming the domain's boundary evenly divides the region between neighboring passes and fails, the boundary would be 0.25 closer than the nearest fail point.

This approximation of the minimum radius can be refined by replacing the point's area with an ellipse when the region sampled is not a square, but a rectangle. Assuming the ratio of the semimajor to semiminor axis is 2, the axes measurements for an area of 0.2 would be 0.38 and 0.18, respectively. Using other shapes for the point's area, such as squares, hexagons, etc. can be justified. Such refinements are usually

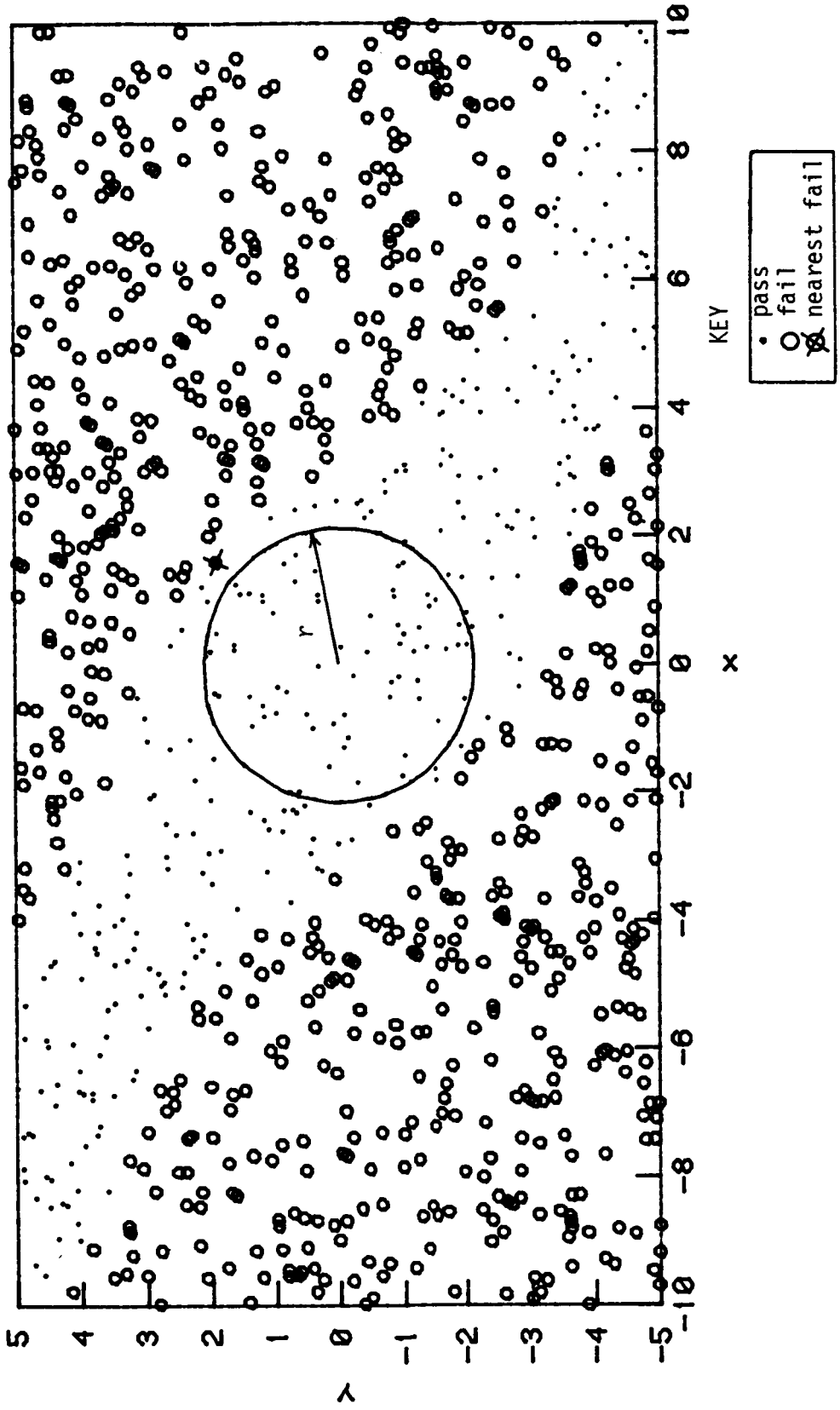

Figure 8: Nearest Fail and Minimum Radius for Domain of Attraction

less significant than the errors associated with the minimum radius measurement. A more precise refinement of the radius could be obtained by concentrating sample points near the nearest fail point.

Repeated simulations of 1000 uniformly distributed initial conditions to find the minimum radius (nearest fail point minus the circular radius about that point) gives:

$$\hat{r} = 2.26 \pm 0.06 \tag{2.21}$$

(see Figure 8). As before, 100 repetitions were used. While the error measurement is similar to that in equation 2.19, this radius is noticeably larger because the domain is not exactly a parallelogram. Rather, it has curves on its edges and the minimum radius is at a bulge (see Figures 6 and 8).

In many systems the state variables have constraints that cannot be substituted in explicitly. Therefore, a uniform distribution of sample points cannot be achieved and an implicit solution for measuring the domain is needed. When nonuniform distributions are used, the number of pass points no longer directly relates to the volume. The volume can be found, however, if the sample distribution is known and can be inverted or if the sample point counts are converted to volumes by using the local density. The minimum radius of the domain of attraction can be found as it was for the uniform distribution. The only difference is that the volume per point, used to infer the boundary location from the nearest fail point, is now dependent on the local density.

The pendulum example is repeated with the uniform sample distribution replaced by a transformed sample:

$$V = \frac{1 - U}{1 + U} \tag{2.22}$$

where U is a sample from a uniform distribution over the range 0 to 1. V is a nonuniform sample over the range 0 to 1. This is used for both x and y coordinates of the initial conditions. A distribution histogram for V is shown in Figure 9.

A 1000 point Monte Carlo simulation is shown in Figure 10 using the nonuniform distribution. Clearly, the fraction of initial conditions attracted to the origin is not proportional to the domain's volume. However, if the state space is divided into moderately sized, identical squares, the initial conditions can be assumed to be uniformly distributed in each. The number of points in each square gives the local density. Therefore, the area of the domain of attraction is:

$$A = \sum_{i=1}^{K} \frac{(N_p)_i}{d_i} \tag{2.23}$$

where $(N_p)_i$ is the number of pass points and d_i is the local density of points in square i. The number of squares in the state space is K. The area of the domain of attraction using equation 2.23 is:

$$\hat{A} = 64.12 \pm 2.44 \tag{2.24}$$

The nearest fail point is indicated and the local density is 0.25 area units per point. Converting this to a circular radius brings the domain boundary 0.28 closer than the nearest fail. Repeating this simulation 100 times and storing minimum radii (nearest fail point minus the circular radius about that point) gives the following measure:

$$\hat{r} = 2.34 \pm 0.06 \tag{2.25}$$

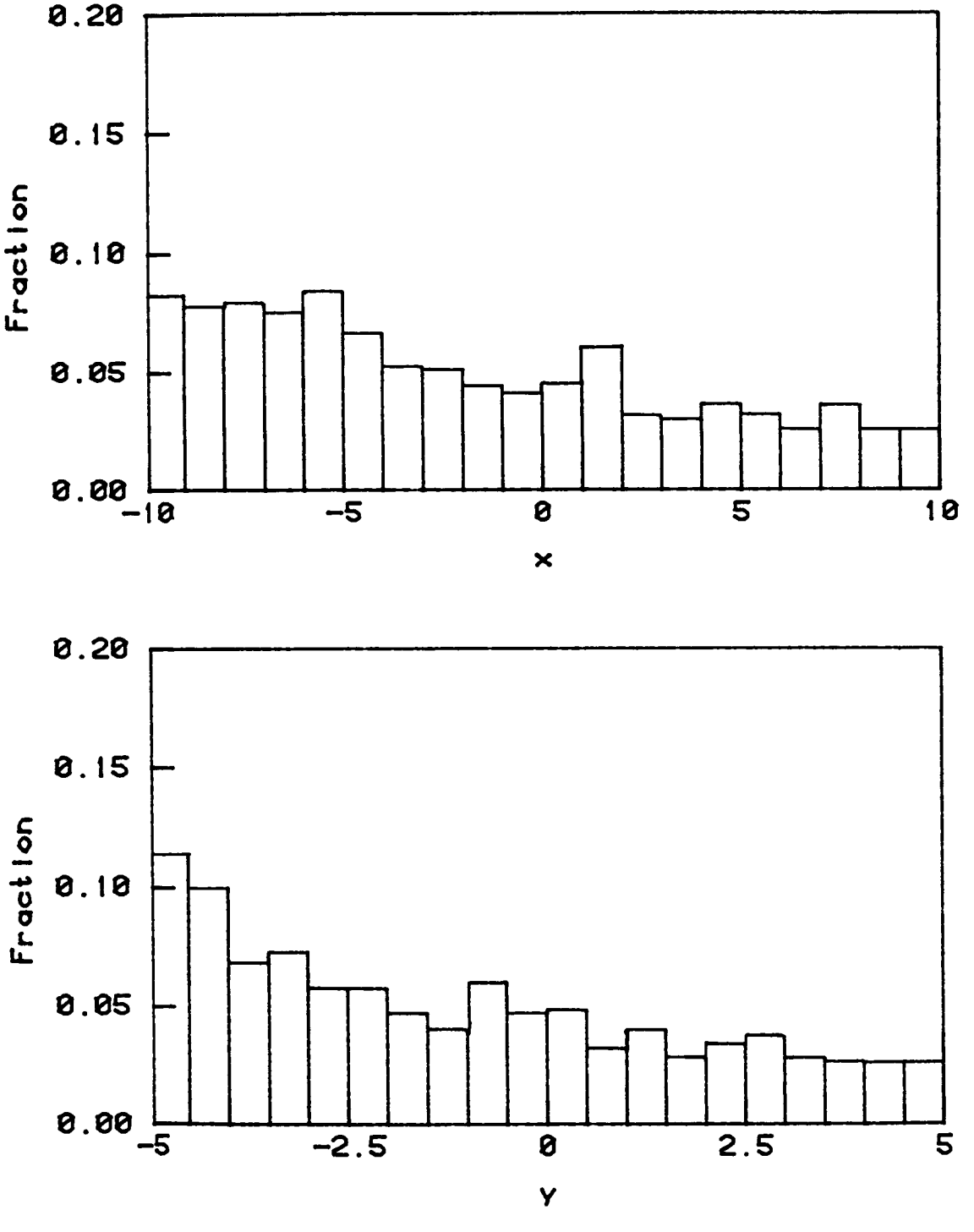

Figure 9: Nonuniform Distribution Histogram

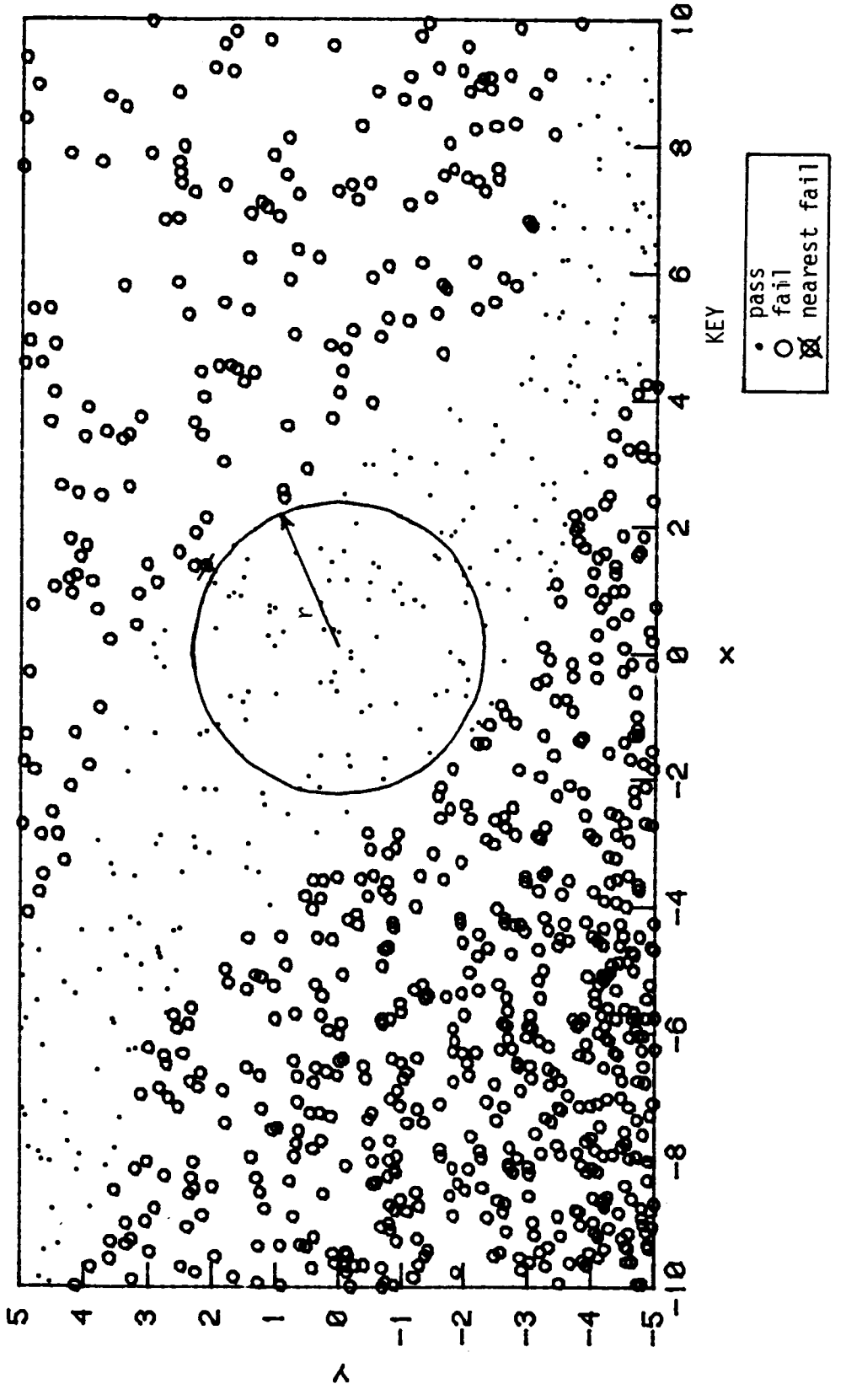

Figure 10: Nearest Fail and Minimum Radius for Domain of Attraction - Nonuniform Sample Density

These results agree with those obtained from the uniform distribution (equations 2.20 and 2.21).

The ability to directly calculate an irregular domain's volume, its minimum radius, and their associated error permits this technique to be useful for a wide variety of systems. For those where uniform samples are not possible (such as constant mass systems), the volume determination requires that the sample counts be converted using local densities. The minimum radius calculation is virtually unchanged. This means that a system's ability to recover from state perturbations can be measured regardless of its dimension, the uniformity of the initial condition sample set, or the complex shape of the domain of attraction.

3. CONTROLLER DESIGN USING DOMAIN OF ATTRACTION

3.1 Example: The Inverted Pendulum

An inverted pendulum was chosen to investigate controller design techniques (see Figure 11). A variety of controllers are then presented to contrast the usual design techniques with those based on the domain of attraction.

The pendulum is constrained to motion in a plane. The controller input is the force applied to the cart at the pendulum's base and the control goal is to return the cart to the origin with the pendulum upright. It is assumed that all four state variables are available to the controller.

The full nonlinear state equations for the inverted pendulum are:

$$\dot{x}_1 = x_2 \tag{3.1}$$

$$\dot{x}_2 = \frac{m_1 L (x_4)^2 \sin x_3 + F - m_1 g \cos x_3 \cdot \sin x_3}{m_1 + m_2 + m_1 \cos^2 x_3}$$

$$\dot{x}_3 = x_4$$

$$\dot{x}_4 = \frac{1}{L} \cdot \frac{(m_1 + m_2) \cdot g \cdot \sin x_3 - m_1 L (x_4)^2 \cos x_3 \cdot \sin x_3 - F \cdot \cos x_3}{m_1 + m_2 + m_1 \cos^2 x_3}$$

where x_1 is the cart position, x_2 is the cart velocity, x_3 is the pendulum position (radians), and x_4 is the pendulum velocity. Control is exerted through force F. The acceleration of gravity is represented by

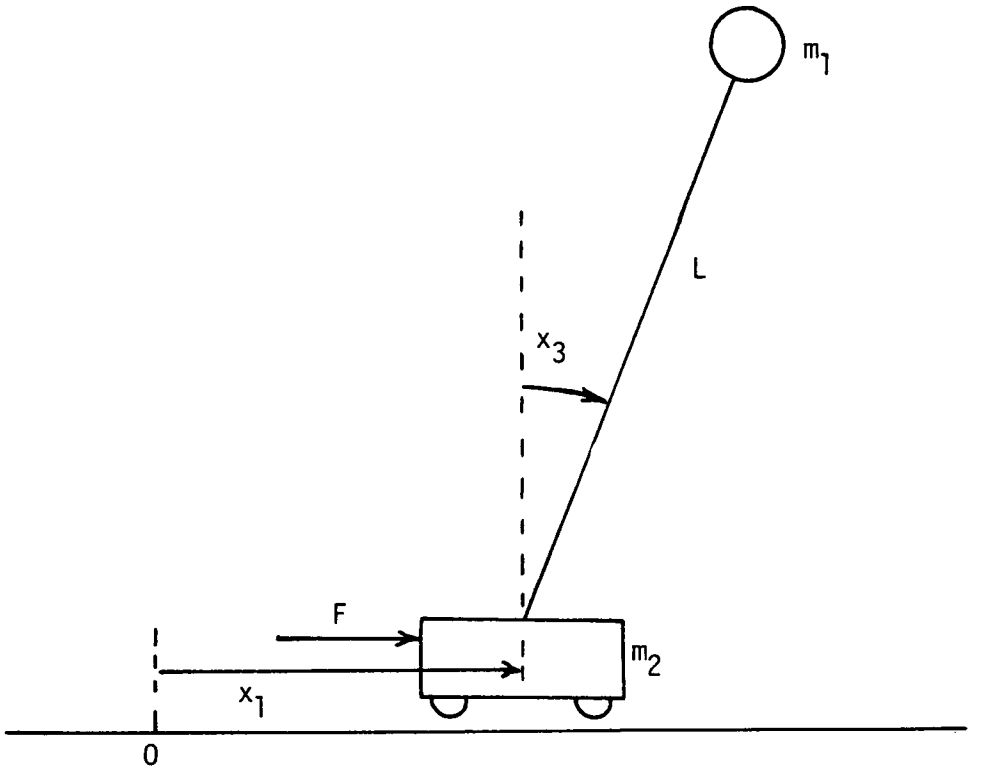

Figure 11: The Inverted Pendulum

g. The following values are used:

$$m_1 = 0.1 \tag{3.2}$$

$$m_2 = 1$$

$$L = 1$$

$$g = 10$$

These equations are simulated with a fourth-order Runge-Kutta integration with a time step of 0.001.

For some traditional controller designs, a linear model of the system is needed. Linearizing equation 3.1 about the origin gives:

$$\dot{x}_1 = x_2 \tag{3.3}$$

$$\dot{x}_2 = \frac{F - m_1 g x_3}{m_2}$$

$$\dot{x}_3 = x_4$$

$$\dot{x}_4 = \frac{(m_1 + m_2)\cdot g \cdot x_3 - F}{L \cdot m_2}$$

In matrix form this would be:

$$\dot{x} = Ax + bF \tag{3.4}$$

where x is the vector of state variables and F is the forcing input.

The local stability about the origin can be found by examining the poles (eigenvalues) of equation 3.4 (with F = 0). The poles are:

$$s = 0,\ 0,\ \pm[(m_1+m_2)g\ /\ Lm_2]^{1/2} \tag{3.5}$$

Substituting the values of equation 3.2 into 3.5 gives:

$$s = 0,\ 0,\ 3.32,\ -3.32 \tag{3.6}$$

Hence the origin is unstable (a saddle point) when no control is applied. This is equivalent to saying that without control the origin's domain of attraction is null. The unstable eigenvalue is due to the upright pendulum. The two 0 eigenvalues are due to the inertia of the cart.

A further examination of the linear system shows that it is controllable using only F as an input. Therefore, the linear system can be moved to any point in the state space in a finite time. Also, the system is observable for output vectors that contain x_1. In these control examples the entire state vector is known so no state observer is needed.

The control goal is to stabilize the nonlinear (and therefore, the linear) system about the origin and to insure that this design can recover from the largest class of state perturbations. To show the effect of a settling time constraint, a performance criteria is set so that the return to the origin (stationary with the cart at zero and the pendulum upright) must be within 5 units of time. For investigations of control behavior, the domain of attraction will be used with the sample initial conditions from the region:

$$\{(x_1,x_2,x_3,x_4):\ -10 \leq x_1 \leq 10,\ x_2=0, \qquad (3.7)$$
$$-3.14 \leq x_3 \leq 3.14,\ x_4=0\}$$

This region is selected to be two dimensional ($x_2 = x_4 = 0$) for clarity. A three or four dimensional region could be used.

3.2 Minimum Error Squared Control

A common technique in modern control design is optimal control where a performance measure such as transient time or squared error is minimized. Optimal controllers that minimize transient time or squared error for linear systems can be expressed in closed form [17]. For most nonlinear systems, however, analytic solutions cannot be found. The following controller will be in a linear state feedback form and it is assumed that the entire state vector is either available or observable. Since the controller form is specified, this restricted problem is not a true optimal control. Rather, it is the minimization of a performance measure by performing a parameter search.

To design a controller for the inverted pendulum that minimizes a squared error, a Monte Carlo search can be performed on a range of feedback gains. The controller has the feedback form:

$$F = k \cdot x \qquad (3.8)$$

The state x is a column vector, the gain k is a row vector, and the applied force F is a scalar. The error cost function is:

$$J = \int_0^t (x_1^2 + w \cdot x_3^2)dt \qquad (3.9)$$

Thus, error accumulates when the cart is not at the origin or the pendu-

lum is not upright. The weighting factor w adjusts the emphasis between the two errors. This parameter is part of the controller design and its value has a strong effect on the resulting gains.

An initial condition of:

$$x_1 = 5, \quad x_2 = 0, \quad x_3 = 0.2, \quad x_4 = 0 \tag{3.10}$$

is used to find the control gains that minimize the cost function (equation 3.9). To insure that the pendulum is quickly moved toward the upright position, a weighting factor of w = 1000 is used. Five hundred sets of gains were randomly selected from uniform distributions with the following ranges:

$$\{0 \leq k_1 \leq 100, \; 0 \leq k_2 \leq 100, \tag{3.11}$$
$$0 \leq k_3 \leq 400, \; 0 \leq k_4 \leq 200\}$$

The minimum cost function (J = 78.1) was obtained with the gain:

$$k = [15.2, \; 49.2, \; 305., \; 64.4] \tag{3.12}$$

This gain was used in a Monte Carlo simulation of 2000 initial conditions randomly sampled from the range in equation 3.7. The domain attracted to the origin in $t \leq 5$ is shown in Figure 12. The minimum radius is:

$$\hat{r}_{perf} = 0.35 \pm 0.06 \tag{3.13}$$

This region is not the total domain of attraction. There is a larger set of initial conditions that have trajectories that lead to the origin. Figure 13 shows the stability region for this control. Here, all

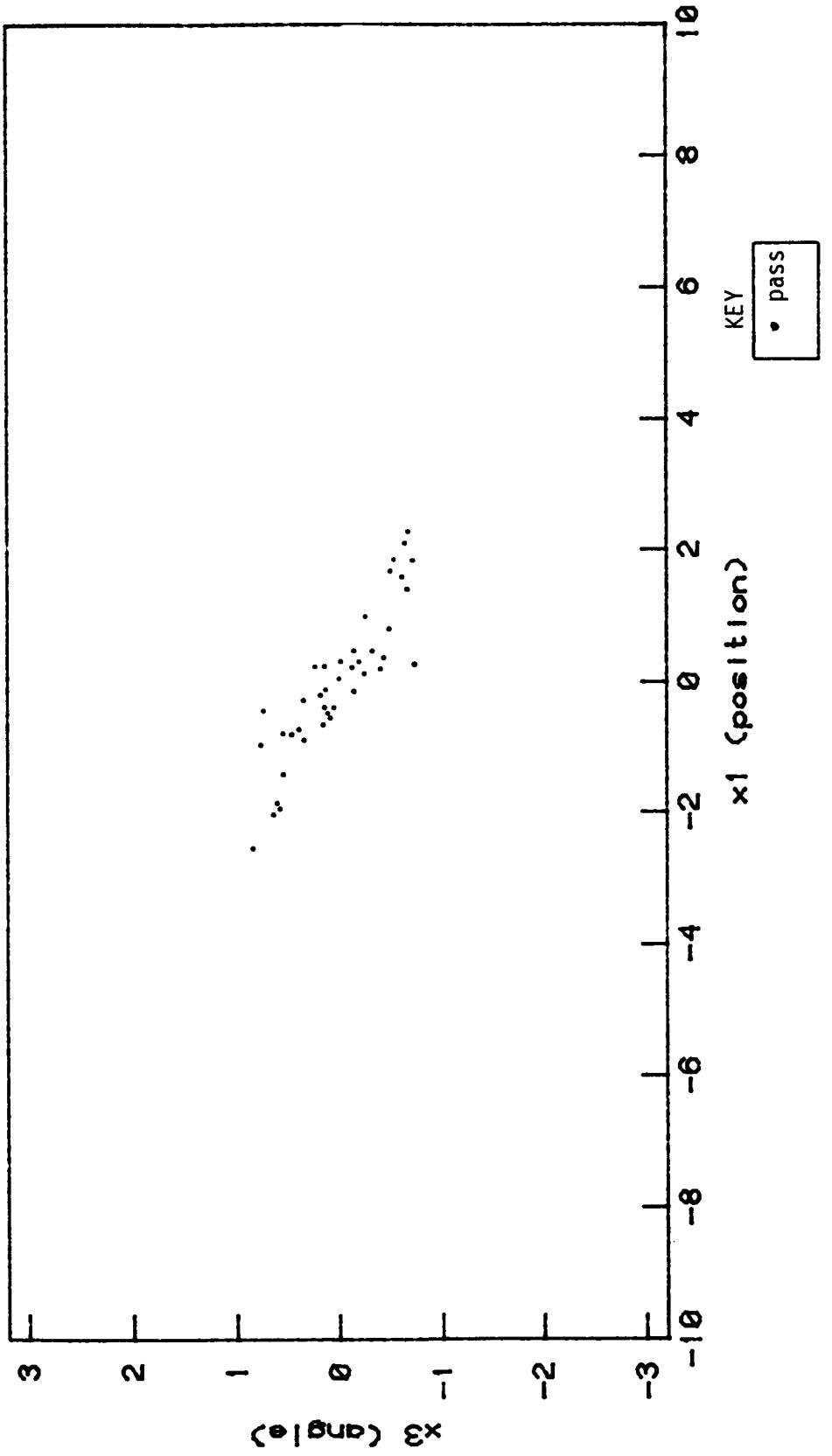

Figure 12: Domain of Performance for Minimum Error Squared Control

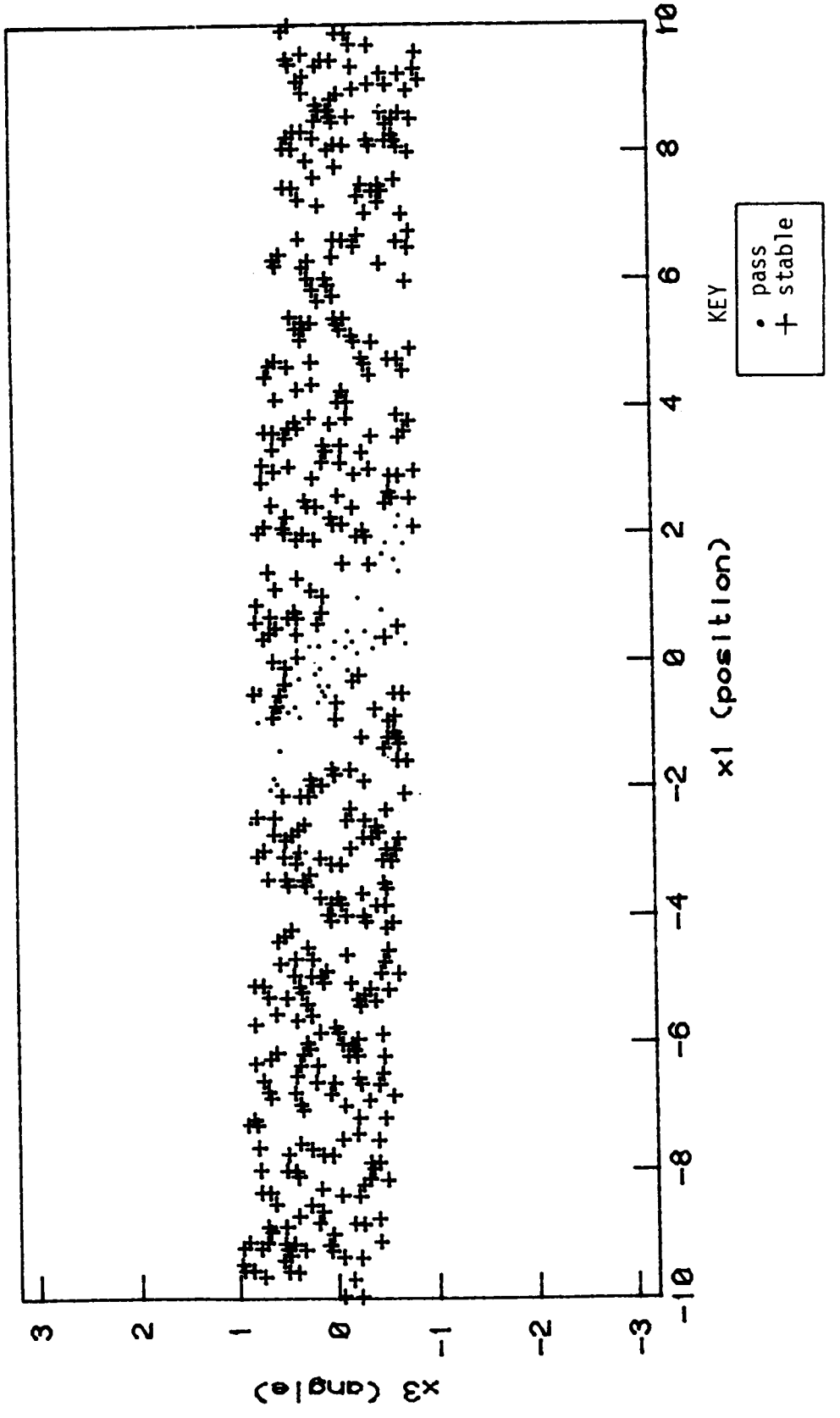

Figure 13: Domains of Performance and Attraction for Minimum Error Squared Control

initial conditions get to the origin in $t \leq 20$. The minimum radius is:

$$\hat{r}_{stab} = 0.81 \pm 0.03 \tag{3.14}$$

Figure 14 shows all 2000 initial conditions.

To distinguish between the various regions in the state space, the following terms are introduced.

Stable set:

Initial conditions that are attracted to the equilibrium point.

Unstable set:

Initial conditions that are not attracted to the equilibrium point (complement of the stable set).

Pass set:

Initial conditions that satisfy the performance criteria (a subset of the stable set).

Fail set:

Initial conditions that do not satisfy the performance criteria (complement of the pass set).

Domain of performance:

Region delineated by the pass set.

Domain of attraction:

Region delineated by the stable set.

Figure 15 shows a typical trajectory from an initial condition in the stable region. The cart motion does not meet the settling time criteria. Trajectories in the pass region are similar but have faster responses. A typical unstable trajectory is shown in Figure 16. The failure is dramatic. The pendulum starts spinning rapidly and the cart

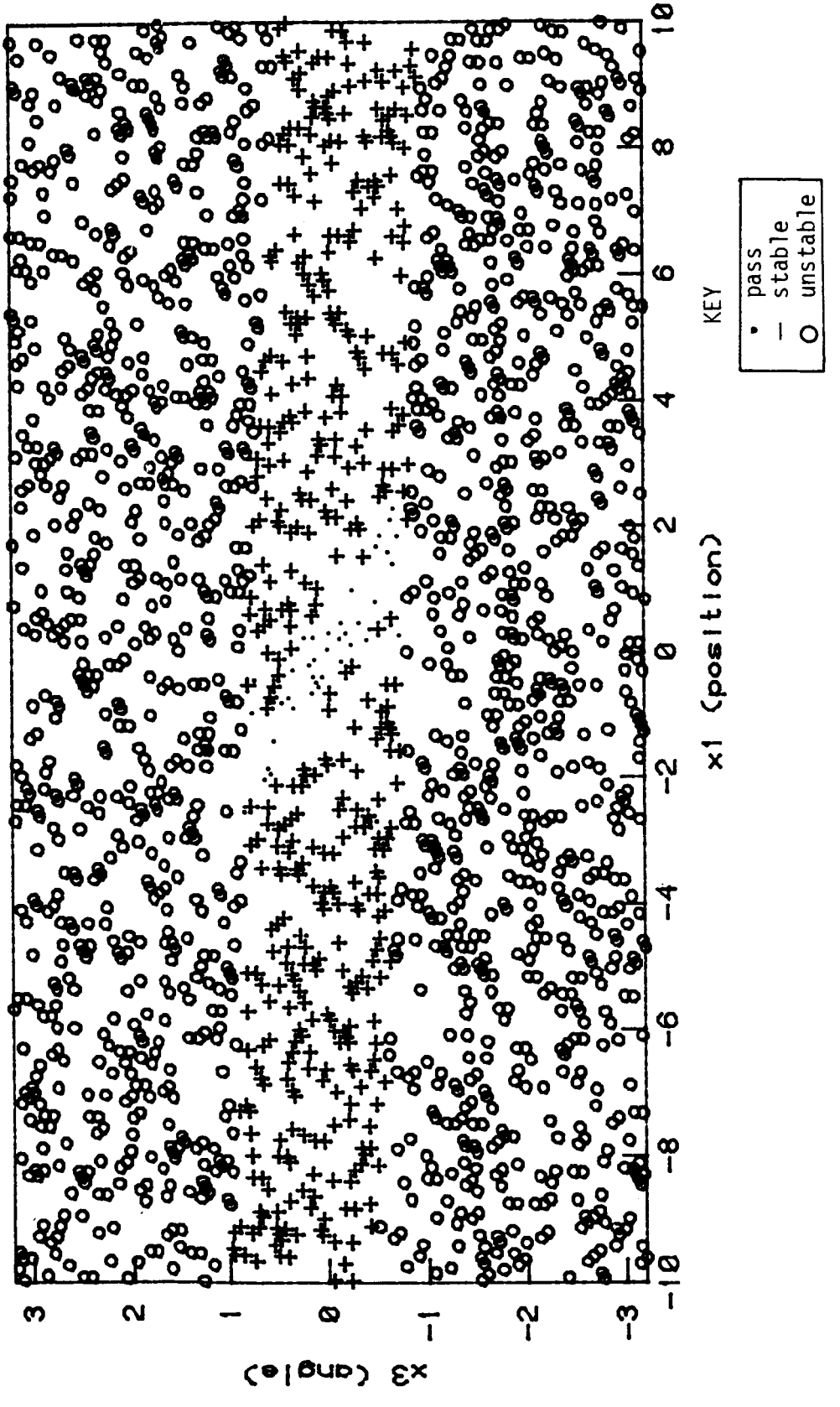

Figure 14: 2000 Initial Conditions for Minimum Error Squared Control

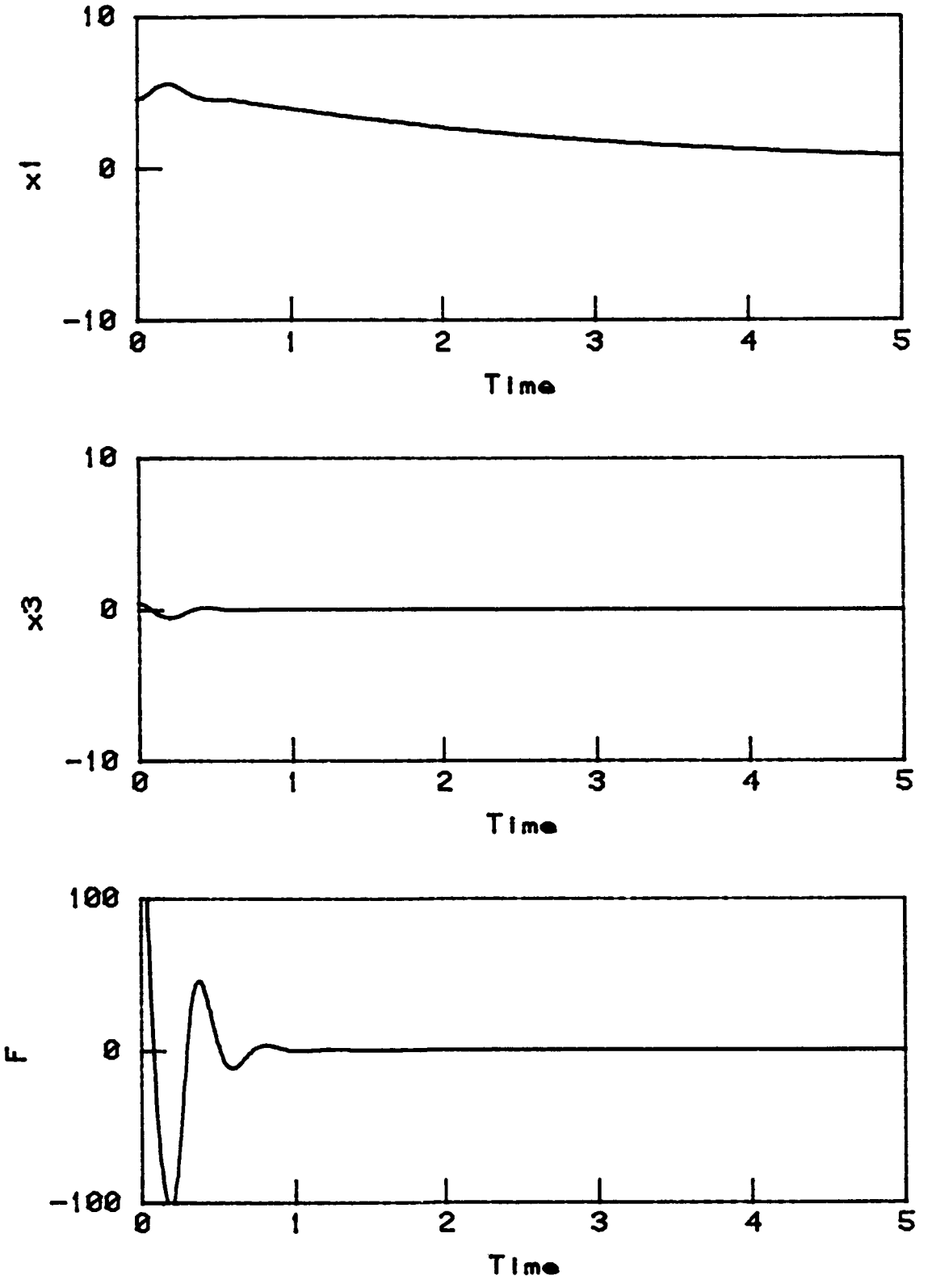

Figure 15: A Stable Trajectory for Minimum Error Squared Control

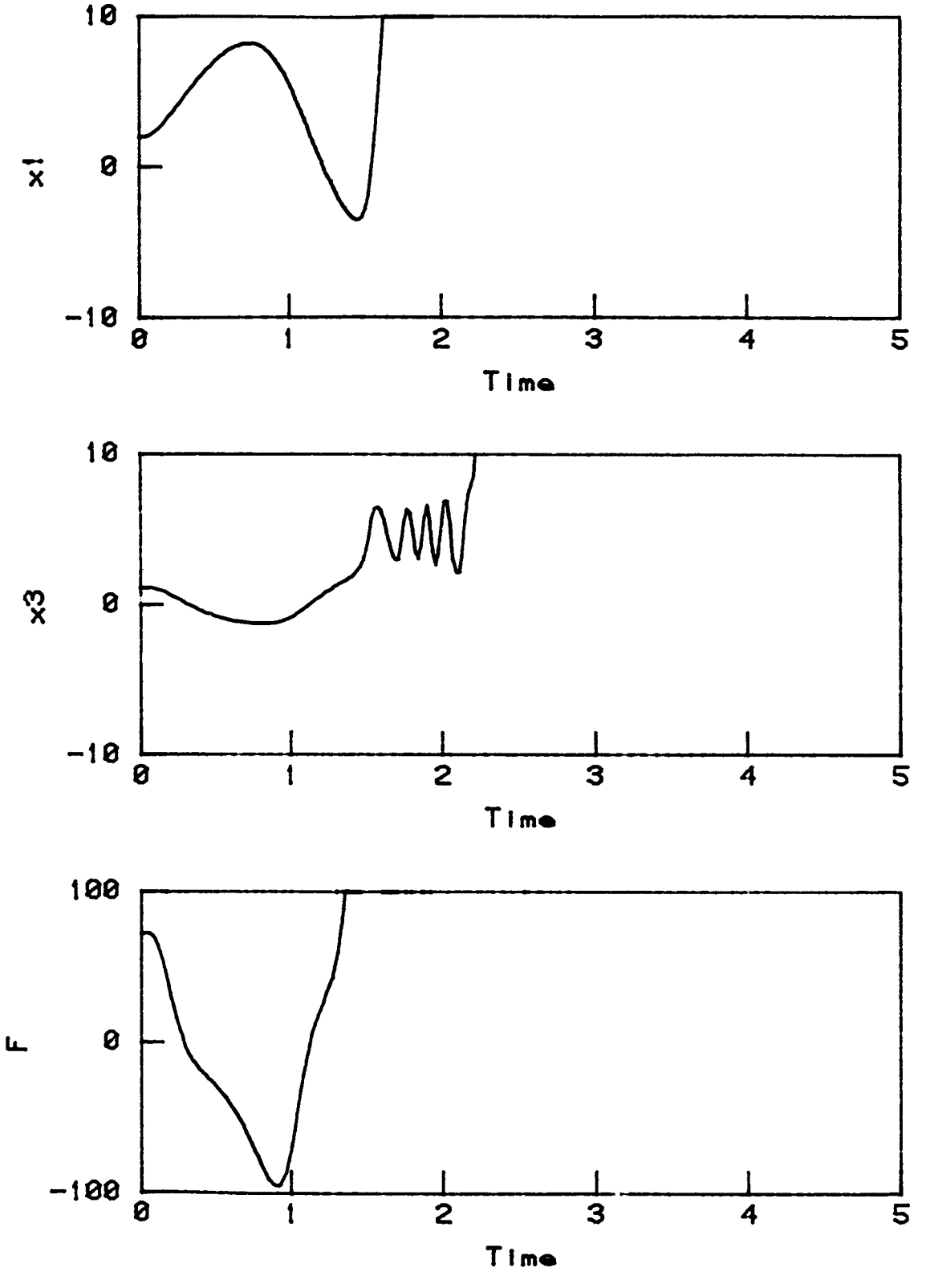

Figure 16: An Unstable Trajectory for Minimum Error Squared Control

accelerates away from the origin. At this point, the controller is completely confused by the nonlinearities of the system.

Although this control design minimizes the squared error for a specific initial condition, the optimization is very local. This gain would not be optimal for other initial conditions since the system is nonlinear. The design therefore depends on two parameters: the weighting factor and the initial condition. There is no a priori way of determining an appropriate choice for them or their effect on the system's global behavior. In this case, the optimization of a local region occurred at the expense of system response from a more global set of initial conditions.

3.3 Minimum Time Control

An alternative cost function for the optimal control design is minimum time. The previous example showed a very small domain of performance but a reasonable size stability region. Hopefully, using time as the cost function will enlarge the region that passes the time limited performance criteria. Since the controller form is restricted to linear, state feedback, this design is not an optimal control. Rather, it is the minimization of the system settling time given this controller form.

Using a state feedback controller (equation 3.8), the cost function is now:

$$J = t: x_i \leq 0.01;\ i=1,2,3,4 \tag{3.15}$$

where t is the time it takes the system to settle to within the tolerance band about the origin.

The initial condition in equation 3.10 was used to find the gains that minimize the cost function J. Five hundred sets of gains were randomly selected from uniform distributions over the range in equation 3.11. The minimum cost function (J = 2.86) was obtained with the gain:

$$k = [48.3,\ 59.5,\ 352.,\ 91.0] \tag{3.16}$$

This gain was used in a Monte Carlo simulation of 2000 initial conditions randomly sampled from the range in equation 3.7. The domain attracted to the origin in $t \leq 5$ is shown in Figure 17. The pass region is identical to the stability region. In fact, all initial conditions surpass the performance criteria and arrive at the origin in $t \leq 3.5$. The minimum radius is:

$$\hat{r}_{perf} = \hat{r}_{stab} = 0.89 \pm 0.03 \tag{3.17}$$

While this control design insured that the selected initial condition met the performance criteria, it did not generate a domain of performance reaching very far beyond it. The sharp edge of the domain ($t \leq 3.5$ for attracted points) is a result of the local optimization. Other initial conditions would generate different results. While this design meets the performance criteria for a larger set of state perturbations than the minimum squared error design, the consequences of local design decisions (the initial conditions) on the global result (domain size) are not easily predicted.

3.4 Pole Placement Control

Pole placement control design permits the manipulation of system

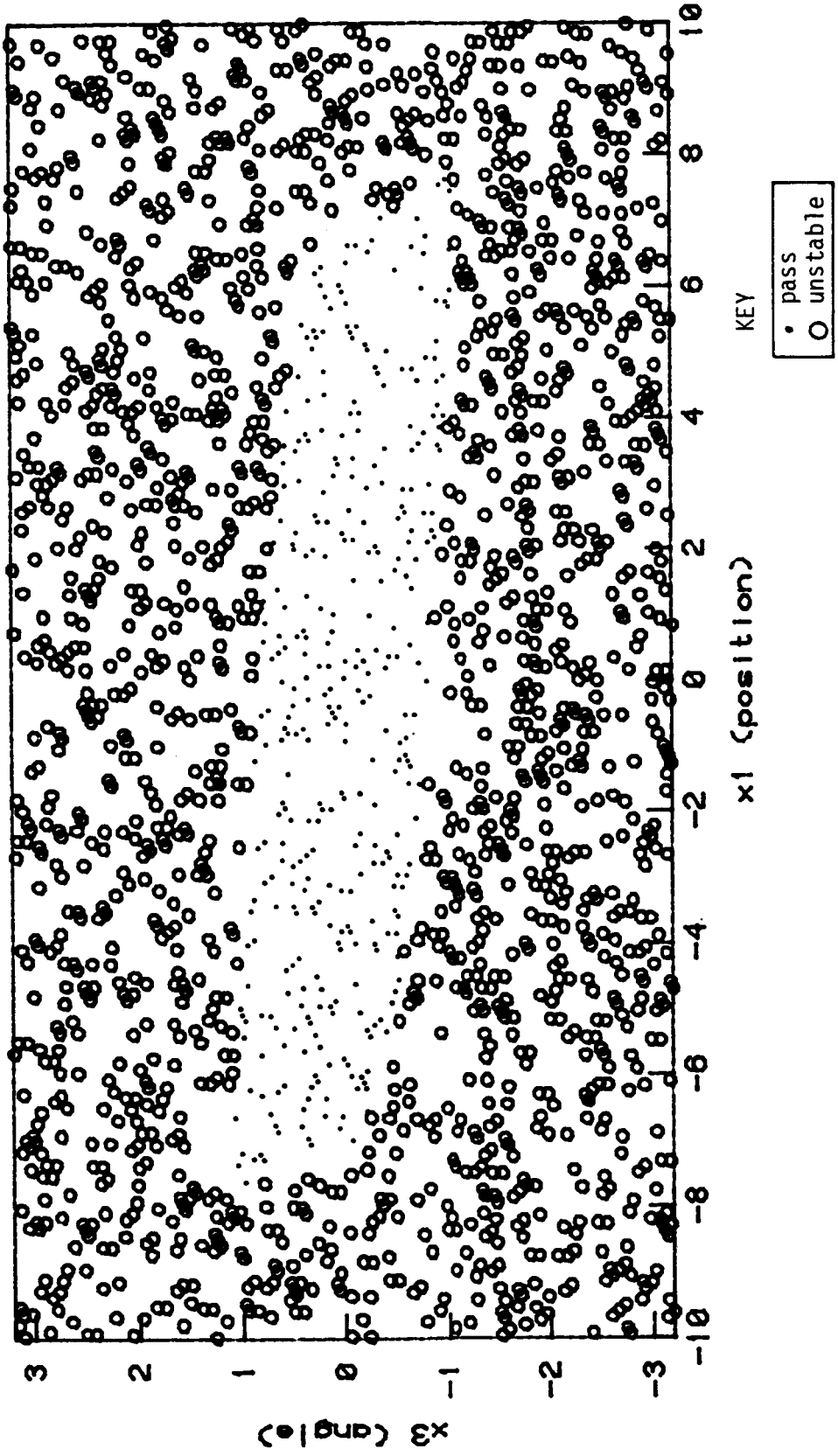

Figure 17: 2000 Initial Conditions for Minimum Time Control

performance through the selection of closed loop poles. The system model is linearized so the design is only insured for behavior near the equilibrium point. The controller is in a state feedback form and it is assumed that the entire state vector is either available or observable. For controllable systems, the system/controller poles can be placed wherever desired.

Using the linearized system described in equations 3.3 and 3.4, the control is expressed in a state feedback form (equation 3.8). Combining equations 3.4 and 3.8 gives:

$$\dot{x} = (A + b \cdot k)\, x \qquad (3.18)$$

where A is the system matrix and b is a column vector. The poles (eigenvalues) of equation 3.18 can be placed arbitrarily because the system (A,b) is controllable [3]. Transforming the system to a control canonical form aids in finding the gain k that yields the desired poles.

It is difficult to determine which pole locations will satisfy the system design criteria. The poles are selected in a linear environment but the system is highly nonlinear. Therefore, the task is to find poles that will permit the nonlinear system to recover from the largest range of perturbations with $t \leq 5$.

For instance, if the poles are placed at s = -1, -1, -5, -5 the gain vector is:

$$k = [2.5,\ 6,\ 59.5,\ 18] \qquad (3.19)$$

Equations 3.8 and 3.19 show that the slow poles (-1) cause a moderate reaction to cart position and velocity errors while the fast poles (-5)

cause a stronger reaction to pendulum position and velocity errors.

Two thousand uniformly distributed initial conditions from the range in equation 3.7 were simulated using the gain in equation 3.19. The domain of performance (attracted to the origin in $t \leq 5$) is shown in Figure 18. It has a central region and two separated wings. The wings are isolated from the main body of the attractor by a region that is stable but does not meet the settling time limit. The total set of initial conditions is shown in Figure 19.

Given the performance criteria of $t \leq 5$, the controller's behavior can be measured using the pass region. The region's wings and long extensions along the x axis do not contribute to the system's ability to recover from random state perturbations. Rather, perturbation recovery is measured with the minimum radius of the domain of attraction:

$$\hat{r}_{perf} = 0.45 \pm 0.03 \tag{3.20}$$

For comparison, the minimum radius of the stability region is:

$$\hat{r}_{stab} = 1.20 \pm 0.03 \tag{3.21}$$

To increase the system's ability to recover from perturbations, the main body of the domain of performance needs to be expanded toward the wings, filling in the stable region. Since this region was not satisfying the time constraint, it would seem reasonable to use faster poles to improve the system behavior. However, increasing the speed of all the poles has been found to shrink the region. For example, using poles at s = -5, -5, -5, -5 gives a performance minimum radius of 0.31 ± 0.05. Through trial and error, it was found that good results were obtained

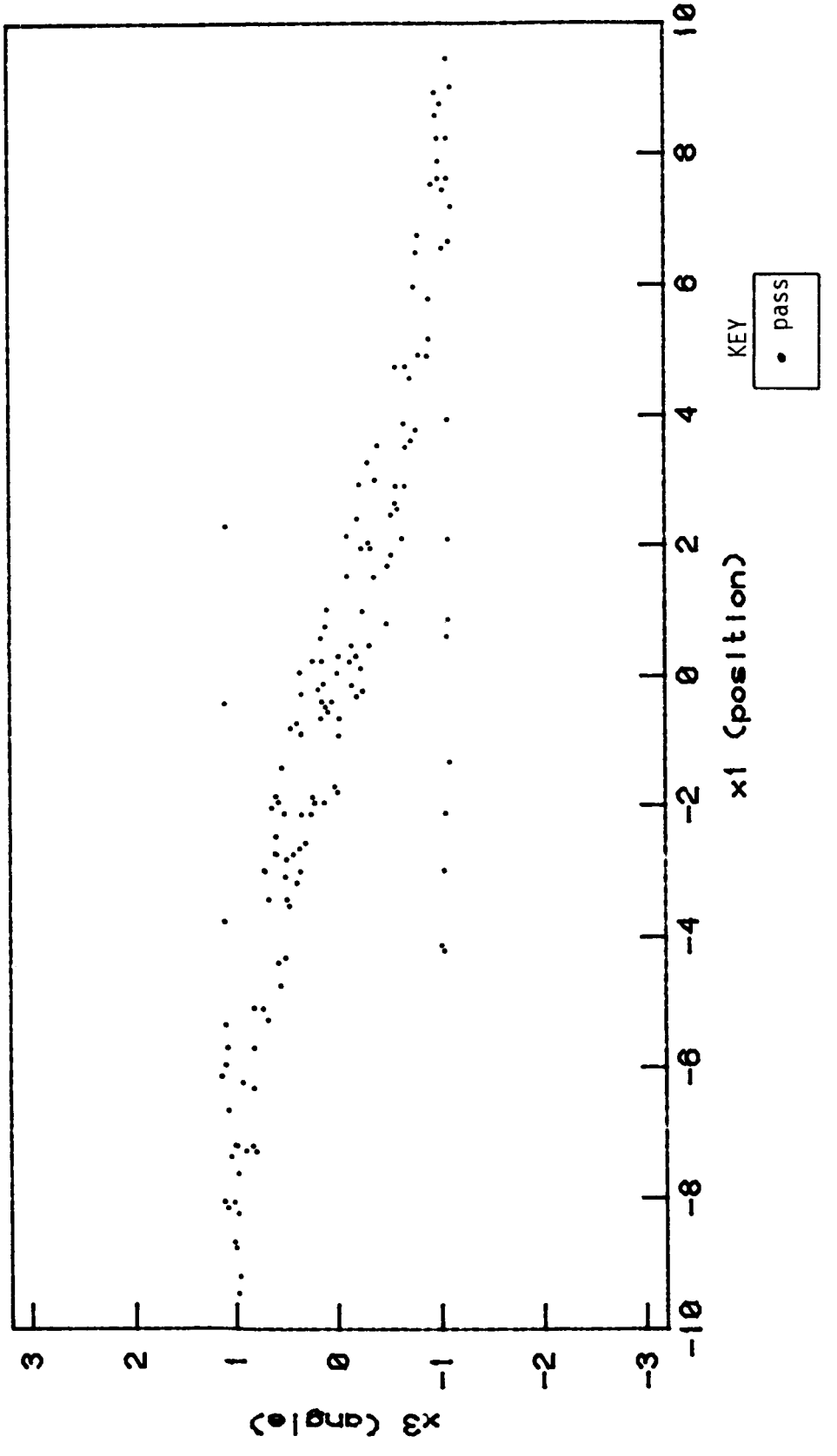

Figure 18: Domain of Performance for Pole Placement Control

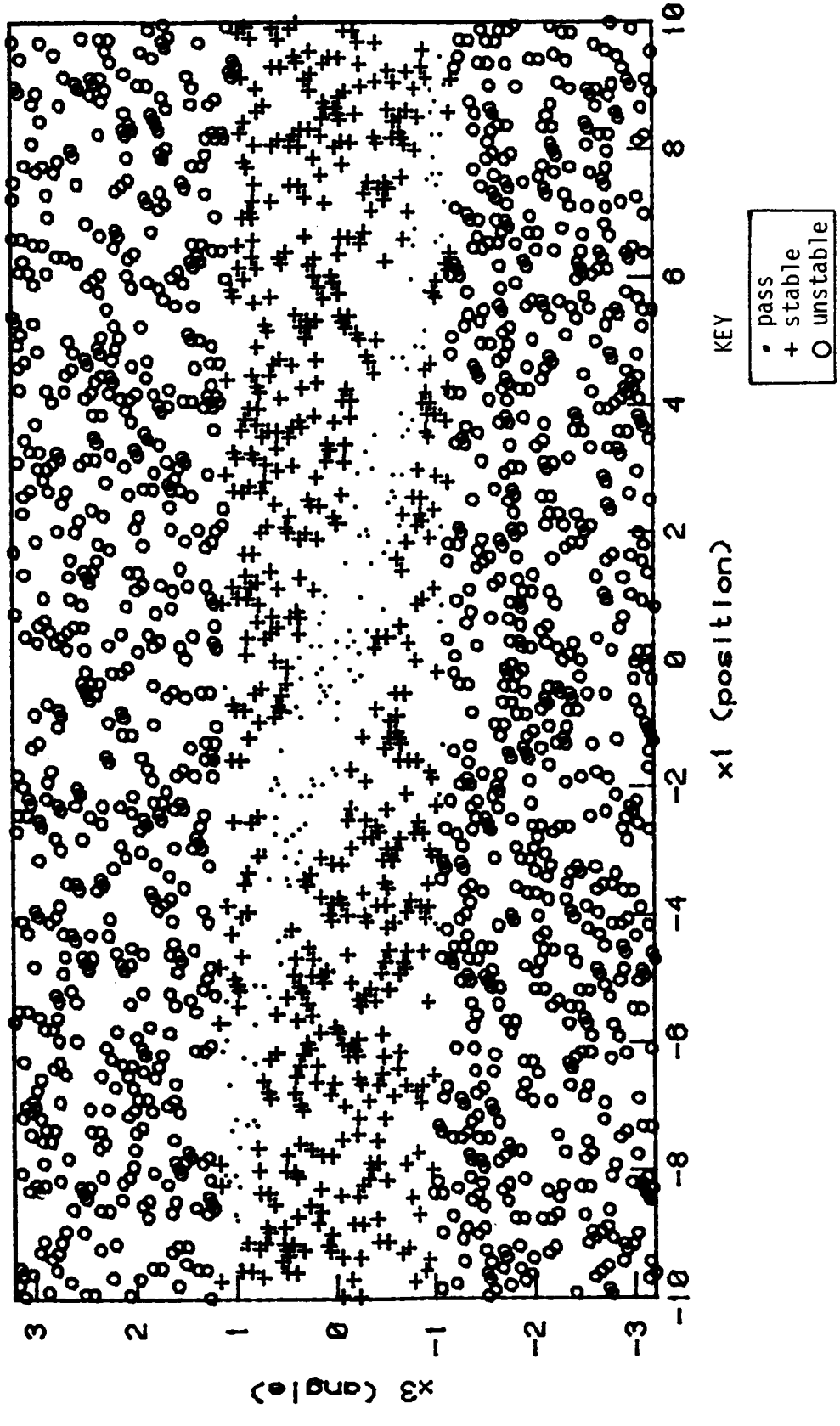

Figure 19: 2000 Initial Conditions for Pole Placement Control

when an appropriate mixture of fast and slow poles were used. There is no direct method to determine this mixture.

It is generally true in linear systems that faster poles give the system a larger domain since they imply that the system recovers quickly from perturbations. As shown above, this is not necessarily true of nonlinear systems. The example with poles at $s = -1, -1, -5, -5$, recovers from a larger group of perturbations in $t \leq 5$, yet its linear design has some slower poles than the case with all poles at -5. This is because the linear approximation only holds for behavior near the equilibrium point. The domain investigation uses initial conditions far from the origin; here the nonlinear properties of the system dominate its behavior. Thus, the decision to use faster or slower poles cannot always be intuitively based on the linearized behavior.

3.5 Monte Carlo Search For Linear State Feedback Gains

The connection, or map, between the placement of poles in a linearized design and the resulting behavior in the nonlinear system is nonintuitive. The limitation in the use of linear state feedback control on nonlinear systems is in the absence of this map from design parameters to system performance.

A more direct design approach is used here. The goal remains to find the linear feedback controller gains that enable the system to recover from the largest set of perturbations. However, instead of looking for linearized system poles or optimal gains for a specific initial condition, a direct search of controller gains is made using the domain of performance as the selection filter. This global design method

searches for systems that can recover from the largest class of state perturbations.

The controller has the feedback form of equation 3.8. A range for each element of the k vector is selected and the elements are set with a random search using a uniform distribution over the respective ranges. This gain vector is used in a domain simulation of the nonlinear system with initial conditions selected randomly from the region of state space. At the end of each domain simulation, the minimum radius of the domain of performance is stored and another gain vector is picked. The largest minimum radius found from this nested Monte Carlo procedure corresponds to the system that can recover from the largest set of randomly oriented state perturbations.

The gains are randomly selected from the set:

$$\{0 \leq k_1 \leq 50,\ 0 \leq k_2 \leq 50, \qquad (3.22)$$
$$0 \leq k_3 \leq 200,\ 0 \leq k_4 \leq 100\}$$

where each subscripted k is an element of the gain vector. Five hundred gain vectors were selected and each gain was simulated using 1000 initial conditions from the range in equation 3.7.

The best gain was found to be:

$$k = [7.2,\ 13.2,\ 103.8,\ 39.4] \qquad (3.23)$$

Figure 20 shows the domain of performance for this gain using 2000 initial conditions. The minimum radius is:

$$\hat{r}_{perf} = \hat{r}_{stab} = 1.20 \pm 0.03 \qquad (3.24)$$

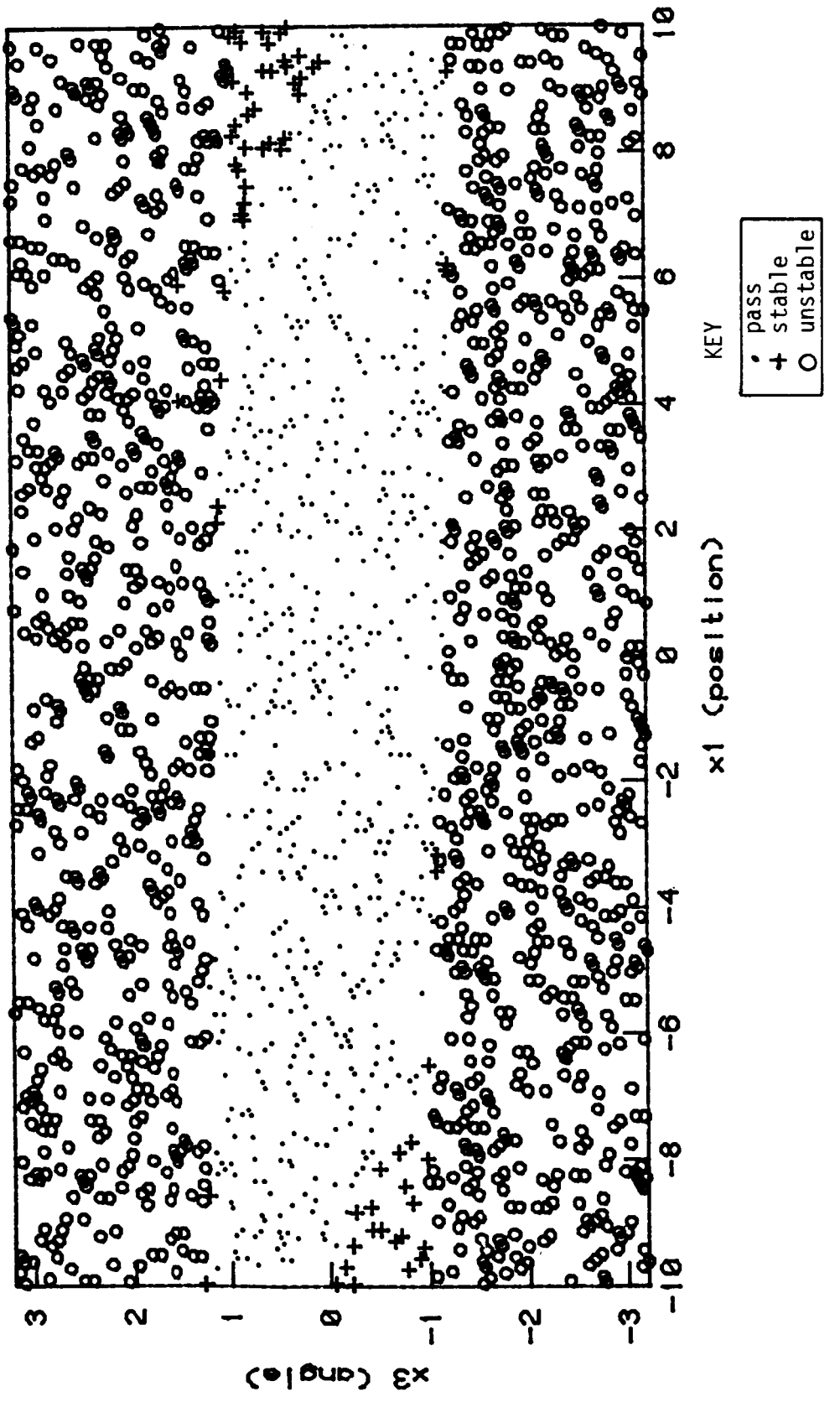

Figure 20: 2000 Initial Conditions for Linear Feedback Control

The minimum radius of the pass and stability regions are identical. They differ only where the cart is far from the origin and the pendulum is leaning in the same direction as the cart displacement. In these cases, the time to get the pendulum balanced and move the cart back to the origin is slightly longer than the performance limit.

Using the gain in equation 3.23, the poles of the closed loop system (equation 3.18) are at s = -22.66, -1.02, $-1.26 \pm 1.22j$, where j is the unit imaginary number. Hence, the best mixture of poles is for one to be very fast and the other three to be rather slow.

While this design has a larger minimum radius than that found by trial and error placement of poles or local optimizations, it may not be the controller with the largest possible domain. The range of gains was sampled only 500 times. Further sampling could turn up some that would perform better.

3.6 A Nonlinear Controller

Of the controllers presented in this chapter, the one that recovered from the largest class of state perturbations was the linear state feedback using a search over a range of gains. The design did not depend on parameter selection and the domain of attraction was used to determine global behavior. A critical limitation, however, exists in the system's recovery from perturbations in the direction of pendulum angle (x_3). To try to increase the angular range, a nonlinear controller with nonlinear gain for the angle component of the state feedback will be used.

The nonlinear controller for the inverted pendulum uses the

following feedback form:

$$F = [k_1 x_1 + k_2 x_2 + f(x_3) x_3 + k_4 x_4] \tag{3.25}$$

$$f(x_3) = \begin{cases} a_1 x_3: & -b \leq x_3 \leq b \\ a_2 x_3 + c: & x_3 \geq b \\ a_2 x_3 - c: & x_3 \leq -b \end{cases}$$

The nonlinear gain function f is shown in Figure 21.

To reduce the dimension of the gain search, the gains for x_1 and x_2 are fixed at the values found for the best linear gain in equation 3.23. The angular gains are from the range:

$$\{0 \leq a_1 \leq 300,\ 0 \leq a_2 \leq 400,\ 0 \leq k_4 \leq 80\} \tag{3.26}$$

The break point in the nonlinear gain f is set to b = 0.9. The intercept c is calculated for each selection of a_1 and a_2 so that the function is continuous.

Five hundred gains were randomly selected from a uniform distribution over the range in equation 3.26. Each was simulated with 1000 initial conditions distributed over the range in equation 3.7. The system with the largest domain had gains:

$$k_1 = 7.2 \tag{3.27}$$

$$k_2 = 13.2$$

$$a_1 = 118.7$$

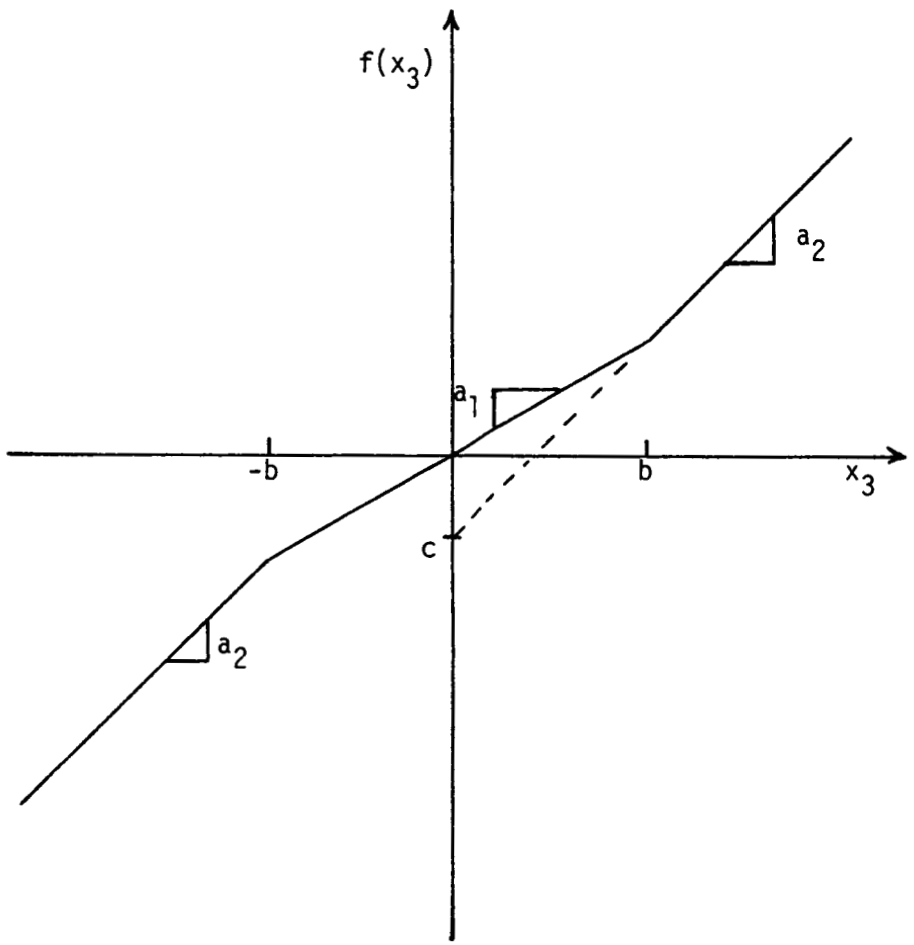

Figure 21: Nonlinear Control Gain Function

$$a_2 = 253.$$

$$k_4 = 43.5$$

The domain of attraction using 2000 initial conditions is shown in Figure 22 and the minimum radius is:

$$\hat{r}_{perf} = \hat{r}_{stab} = 1.32 \pm 0.03 \tag{3.28}$$

For this controller, the domain of performance and the domain of attraction are identical over the sampled range of initial conditions.

While this controller is an improvement over the linear one, it is probably not optimal. First, the gains on cart position and velocity could be included in the Monte Carlo search. Secondly, all the gains could be made nonlinear with adjustable break points. Lastly, a state space discrete controller, such as those proposed by Young [18], could be used instead. This control design example was chosen to show that nonlinear controllers can be designed with the same techniques as linear ones.

3.7 Summary

In designing controllers for nonlinear systems, the nonlinearity cannot be ignored. Controllers that are designed with a linear approximation may or may not be adequate to control the nonlinear system. The linearized design only guarantees behavior near the equilibrium. While this is sufficient to determine local stability, it is often inadequate to evaluate the system's global behavior. Further, controllers that optimize a local behavior often do so at the expense of global perfor-

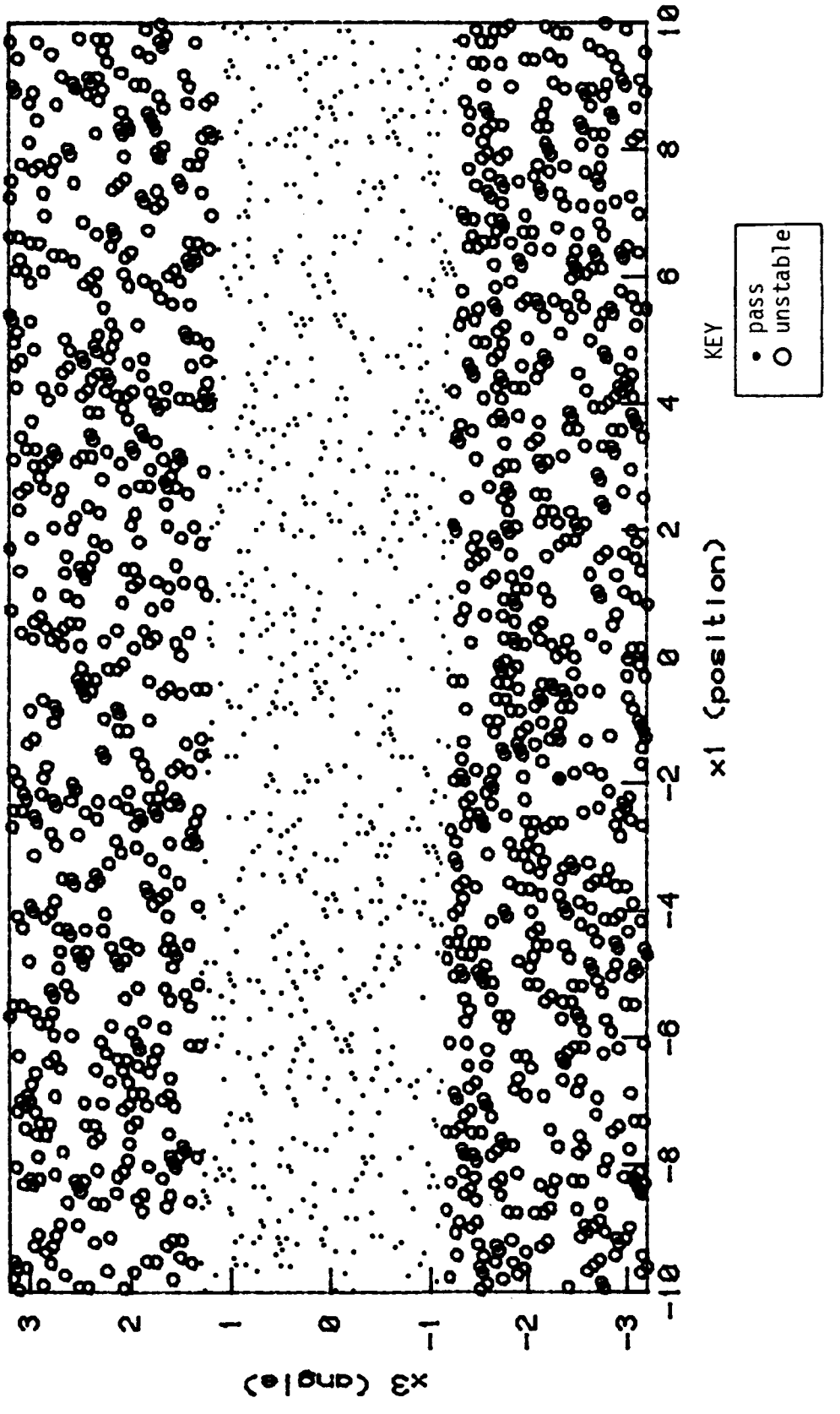

Figure 22: 2000 Initial Conditions for Nonlinear Control

mance. By using the domain of attraction as a selection filter in controller design, the global behavior of the nonlinear system is directly known. The nested Monte Carlo method permits design of linear and nonlinear controllers that have large domains of attraction and performance. The elimination of design parameters, such as weighting factors or initial conditions, further simplifies the design problem.

A distinction has been made between domain of performance and domain of attraction. For systems that are initially unstable, domain of attraction may be sufficient as a performance measure. However, stable systems, particularly those that are globally attracting, can only be analyzed with the domain of performance. The only difference is in the goals; the domain of attraction is used to delineate stability and the domain of performance indicates the region that meets the performance criteria.

A tabulation of minimum radii for the various controllers presented in this chapter is found in Table 3.

Table 3: Inverted Pendulum Controller Summary

Controller	$\hat{r}_{perf}$	$\hat{r}_{stab}$
Minimum Error	0.35 ± 0.05	0.81 ± 0.03
Minimum Time	0.89 ± 0.03	0.89 ± 0.03
Pole Placement	0.45 ± 0.03	1.20 ± 0.03
Linear Search	1.20 ± 0.03	1.20 ± 0.03
Nonlinear Search	1.32 ± 0.03	1.32 ± 0.03

4 THE CELSS MODELS

4.1 Overview

A Closed Ecological Life Support System (CELSS) is usually conceived as having mass closure but an external supply of energy. It is possible to model such a system using conservation of mass equations that describe the storage tank behavior. Flows between tanks can be treated as controllable variables. Averner [1] used this approach balancing the elemental masses (hydrogen, oxygen, nitrogen, etc.) in the system. Stahr, et al. [15] developed a model where bulk masses (water, carbon dioxide, edible food, etc.) are followed through the system. The latter approach will be used here because it lends itself to examinations of the interplay between storage tank size, system mass, and control design.

Initial design studies for closed life-support systems concentrate on the equilibrium requirements for supporting the crew [11]. These studies give some indication of mass and volume requirements by specifying the flows that will be necessary through various processors, and thus give some indication of the minimum unit size. However, the life support system must be capable of maintaining vital functions during temporary failures of some of its components. Extra storage must be provided, processors must have the capability of operating above (or below) their equilibrium flows, and total amounts of flowing masses in the system must be specified. This part of the design can only be done by considering the system's dynamic behavior as none of these parameters enter into the static equilibrium calculation.

To examine the dynamic interaction of internal system mass and storage tank sizes, the model of a CELSS shown in Figure 23 is used. This abstract model is a simplification of the true complexity of the system. It does, however, contain some essential components of a CELSS: constant mass, finite storage tank sizes, and limited processor capacities.

To understand the model better, its behavior at steady state is examined. The crew consumes food at a rate of one unit/day (steady state) from food storage. With the crop growing to maturity in 60 days, the 6 plant chambers produce a harvest every 10 days. This harvest must have an edible mass of 10 units for the system to remain at steady state.

Under normal conditions, one third of the harvest is edible. The inedible part is placed in waste storage. As food is consumed, the crew's waste also goes into this tank. The waste is reoxidized in the waste processor and the resulting nutrients, water, etc., are placed in the plant chambers. To insure adequate growth for the steady state, the processor flow must be 3 units/day.

Both food and waste storages have capacities. If a capacity is exceeded, the tank's output flow must be increased. The waste processor also has a capacity. If its capacity is exceeded, some of the flow is bypassed. Clearly overflow conditions can occur given finite storage tanks and the possibility of a component failure.

The flows in this model are mixtures of solids, gases and liquids. Thus, the "nutrient" flow refers to nutrients, water, carbon dioxide,

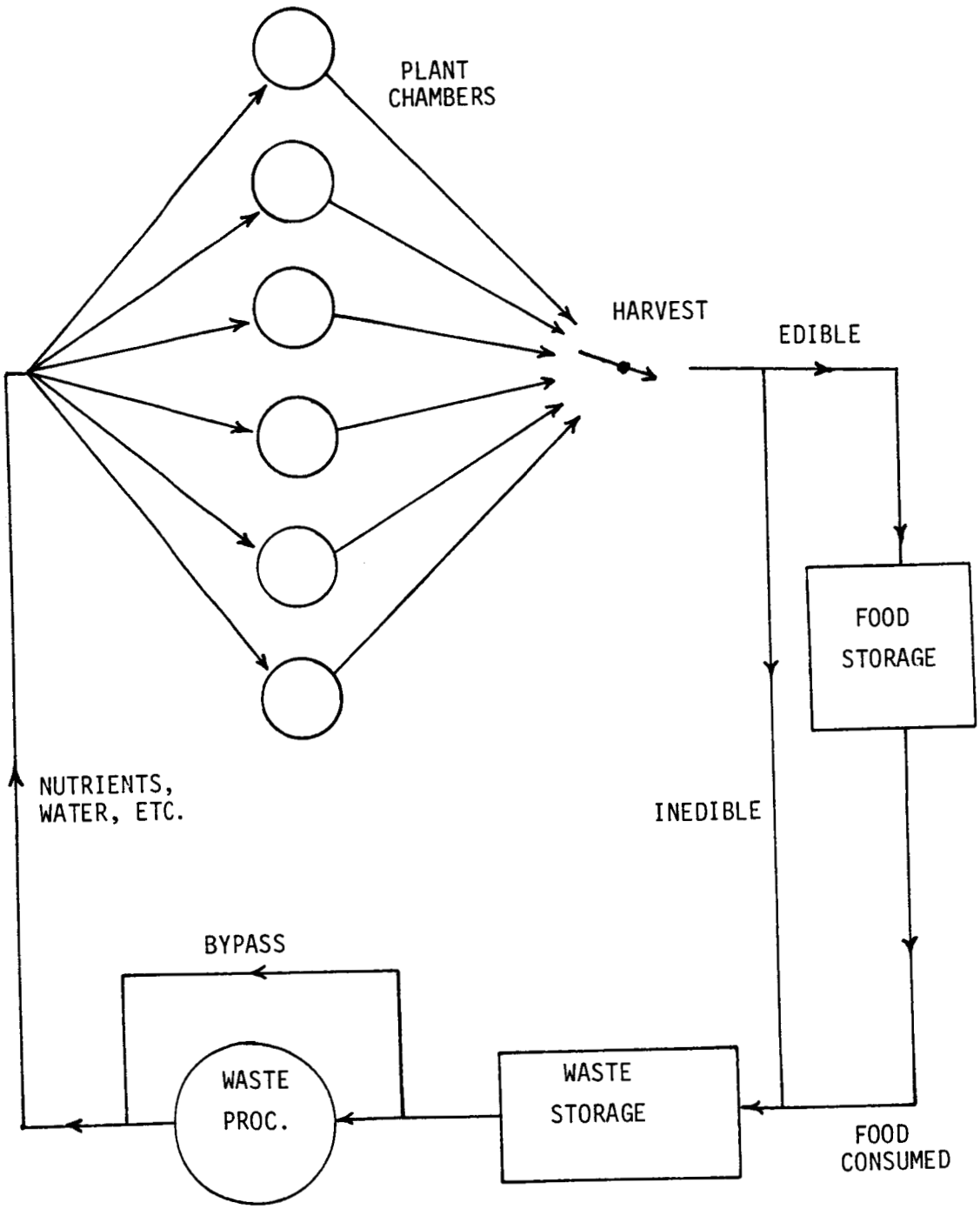

Figure 23: A CELSS Model

and other material needed for plant growth. The "harvest" contains excess water, oxygen, edible and inedible plant matter, and other byproducts of plant growth. The proper mixing of the elements is assumed. In this model the plant growth depends only on the rate of the nutrient flow.

The plants in each chamber are at different stages of growth to allow harvests at 10-day intervals. As a simplification, an independent supply of seeds is assumed. The steady state plant growth is shown in Figure 24 (top). This curve follows the general behavior of plant growth [13]. The plant mass reaches 10% of the harvest mass in the first 20 days from a nutrient flow of 0.1 units/day. The plants grow faster in the second 20 days reaching 50% of its total mass. So far no edible mass has grown. In the last 20 days, 2/3 of the nutrient flow goes into edible growth. Hence, the result is a harvest that is 1/3 edible.

If the nutrient flow into the plant chamber is not at the steady state two things happen [8]. First, the total plant mass does not increase as indicated in Figure 24 (top). This effect is due to conservation of mass. Second, if this occurs during the last 20 days of the growth cycle (when the edible part grows), the percent of the nutrient flow that becomes edible is affected (Figure 24, center). The nutrient flow into the 6 chambers is always divided to do the least damage to the growing plants.

If the waste processor's capacity is exceeded, the bypass flow goes into the plant chambers (see Figure 23). This overflow accumulates as "inert matter" in the plant chambers and does not contribute to the plants' growth. If there is inert matter in the plant chamber during the

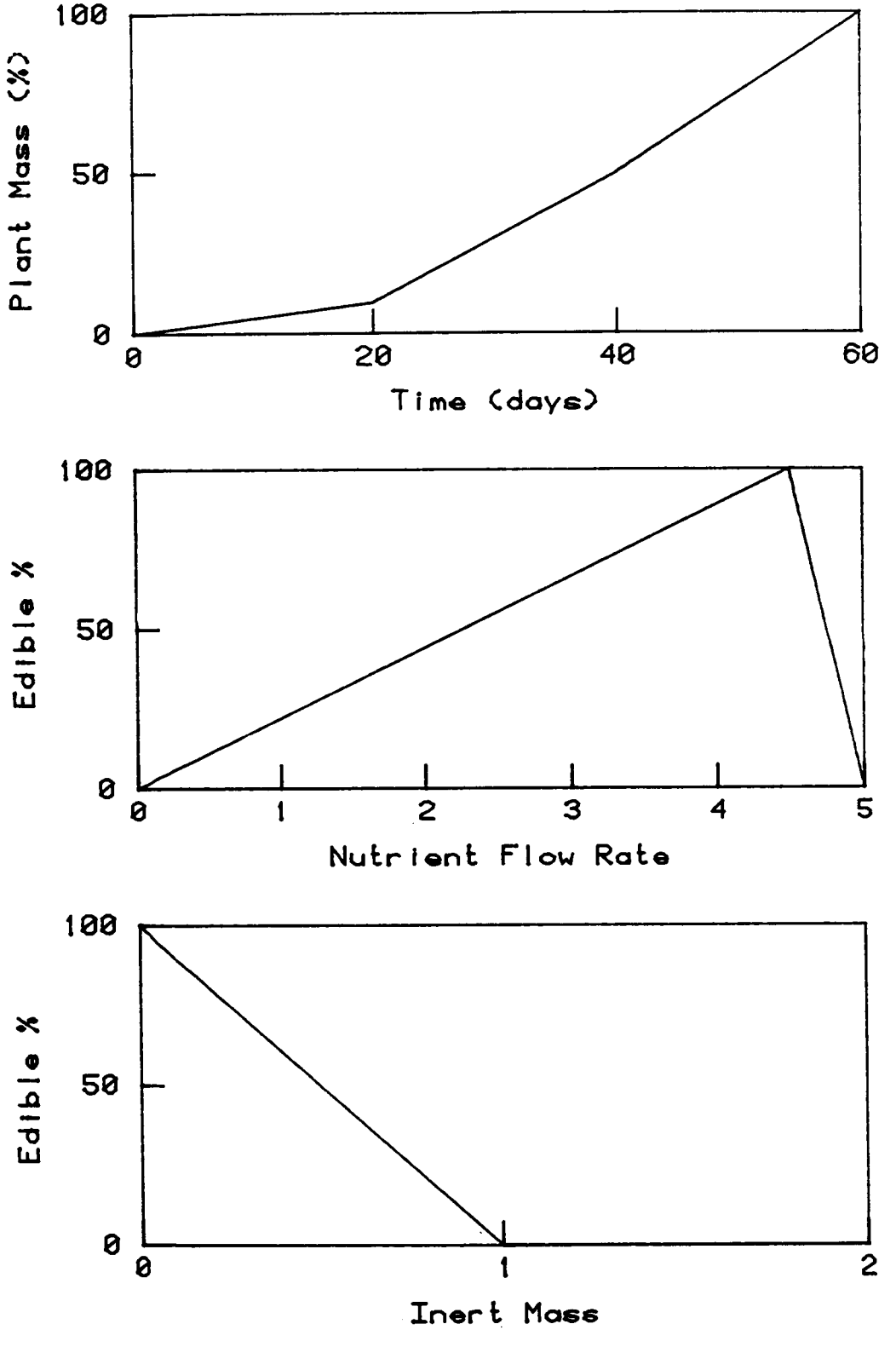

Figure 24: Plant Growth Functions

last 20 days (when the edible part of the plant is growing) its growth is inhibited (see Figure 24, bottom). The inert matter is removed from the plant chamber during harvest, and is sent to the waste storage.

Control is exerted on the system by adjusting the nutrient flow to the plant chambers. Flow regulation decisions may be based on a variety of information about the system. For example, the growth of plants could be set to compensate for a poor harvest, or the flow of nutrients could be adjusted to return the waste storage tank to its steady value. Evaluating the effectiveness of these feedback schemes is critical in the controller design. This, along with an investigation of the effects of storage tank size will be covered in the following sections.

4.2 The State Equations

Three versions of the CELSS model were considered: one with three plant growth chambers, one with six, and the other with twelve. While the steady behavior of these three are similar, their differences in harvest rates and storage tank needs are considerable and have far reaching consequences.

The three-chamber model looks similar to the one in Figure 23 except for the number of growth chambers. The plant growth curves are the same as those in Figure 24. It has harvests every 20 days whereas the six-chamber version is harvested at 10-day intervals. The plant growth time is 60 days for both. Similarly, the twelve-chamber model has the same form but is harvested every 5 days.

The CELSS models consist of state equations that represent mass conservation for storage tanks and the plant growth chambers. The state

equations are of the form:

$$\dot{x}(t) = f(x(t),u(t),g(t)) \tag{4.1}$$

where x is the vector of masses, u is the control, and g is the vector used to represent switching functions associated with harvesting and tank capacities.

For example, the food storage state is:

$$\dot{x}_{food} = q_{in} - q_{out} + g_1(x_{food}, t) \tag{4.2}$$

The flow into the tank (q_{in}) is the edible part of the harvest. It is a delta function because the harvesting is periodic. The output flow (q_{out}) is the required rate of food going to the crew (a continuous function). The function $g_1(x_{food})$ is a switching function that is used to represent an empty or overflowing food tank. The waste storage tank has a similar state equation except that its switching function g also contains information on the waste processor capacity.

Each plant chamber has three state equations associated with it. The first is the mass of the edible part of the plant. It is set to zero for any chamber associated with the first 40 days of the plant's growth. During the last 20 days of plant growth the state equation is:

$$\dot{x}_{edible} = q_{in} \cdot f_1 \cdot f_2 + g_2(x_{edible}, t) \tag{4.3}$$

The input flow (q_{in}) is the nutrient flow from the waste processor. Functions f_1 and f_2 are the edible growth functions represented in Figure 24 (center and bottom, respectively). f_2 is the inert mass state variable associated with each chamber. The switching function g_2

represents periodic harvesting.

The second state variable for each chamber is the inedible part of the plant. For plants over 40 days old, it grows by using the nutrient flow (q_{in}) that is not being used for edible growth:

$$\dot{x}_{inedible} = q_{in} \cdot [1 - f_1 \cdot f_2] + g_3(x_{inedible}, t) \tag{4.4}$$

The functions f_1 and f_2 are the same as for the edible state variable. The switching function g_3 represents periodic harvesting. For chambers holding plants that are less than 40 days old, the inedible fraction uses all of the nutrient flow:

$$\dot{x}_{inedible} = q_{in} \tag{4.5}$$

The third state variable associated with each chamber represents the inert mass. This is the accumulation of unprocessed waste in the plant chambers due to the bypass flow. Its state equation is:

$$\dot{x}_{inert} = q_{in} + g_4(x_{inert}, t) \tag{4.6}$$

where q_{in} is the bypass flow sent to the chamber. Since the inert mass affects edible growth as an accumulated quantity (see Figure 24, bottom), it is most advantageous to divide the bypass flow evenly between all plant chambers. The function g_4 represents periodic harvesting.

The total number of state variables depends on the number of plant chambers. When three are used, there are 9 mass storage variables (1 edible, 3 inedible, 3 inert, 1 food storage, 1 waste storage). For the six-chamber model there are 16 (2 edible, 6 inedible, 6 inert, 1 food storage, 1 waste storage). The twelve-chamber model has 30 (4 edible,

12 inedible, 12 inert, 1 food storage, 1 waste storage). Since the system has constant mass, only n-1 of the n mass storage variables can be independently selected. These are the state variables. The explicit time dependence of the harvest in the continuous-time system appears as an added state variable, creating an "augmented state space" [17]. This augmented state vector has dimension n.

The harvesting time interval depends on the number of plant chambers. With three the interval is 20 days; with six it is 10 days; and with twelve it is 5 days. The harvest looks like a periodic delta function.

By sampling the continuous-time system state at the harvesting frequency, a return map (Poincare surface of section) can be made [10]. This map is a discrete-time system where the time dependencies of the forcing functions are now implicitly included in the formulation. The system (equation 4.1) now appears as:

$$x(k+1) = x(k) + T \cdot [f_d(x(k),u(k),g(k))] \qquad (4.7)$$

where k is the time index representing steps of T units.

The continuous-time system function f is now replaced with an equivalent discrete-time function f_d. The key difference in the two is in how delta functions are treated. In the former case they are evaluated at the appropriate time. However, with the larger time steps of the discrete-time simulation, the delta functions need to be approximated. This is accomplished by evaluating them first in the sequence of calculations for each time step. In this way the discrete-time simulation generates the same behavior as the continuous one in most

situations.

One limitation with the discrete-time calculation is that it cannot properly simulate continuous phenomena as observed in the behavior of the system during a component failure or tank overflows due to continuous (not delta function) inputs. In the examples that follow, there are no occurrences of such overflows. But when a component failure occurs, the continuous-time simulation must be used to follow the system trajectory. The discrete-time simulation can then be used to examine the subsequent evolution of the system once the component is repaired. Thus, the system's ability to recover from random component failures can be investigated through simulations of random initial conditions using the discrete-time calculation.

4.3 Equilibrium Behavior

The three CELSS models described in the previous sections were designed with a steady state that provides harvests equal to the crew demand of one unit/day. The relationship between the continuous-time and discrete-time simulations of these models can be seen by examining the system behavior at this equilibrium. The three- and six-chamber models are demonstrated in this section. Similar behavior is observed in the twelve-chamber model.

Figure 25 shows the three-chamber model operating at steady state. The continuous simulation's behavior is represented by the plotted line and the circles are the output of the discrete simulation. Figure 26 shows the equivalent steady state for the six-chamber system.

Each harvest causes a vertical jump in the storage curves while

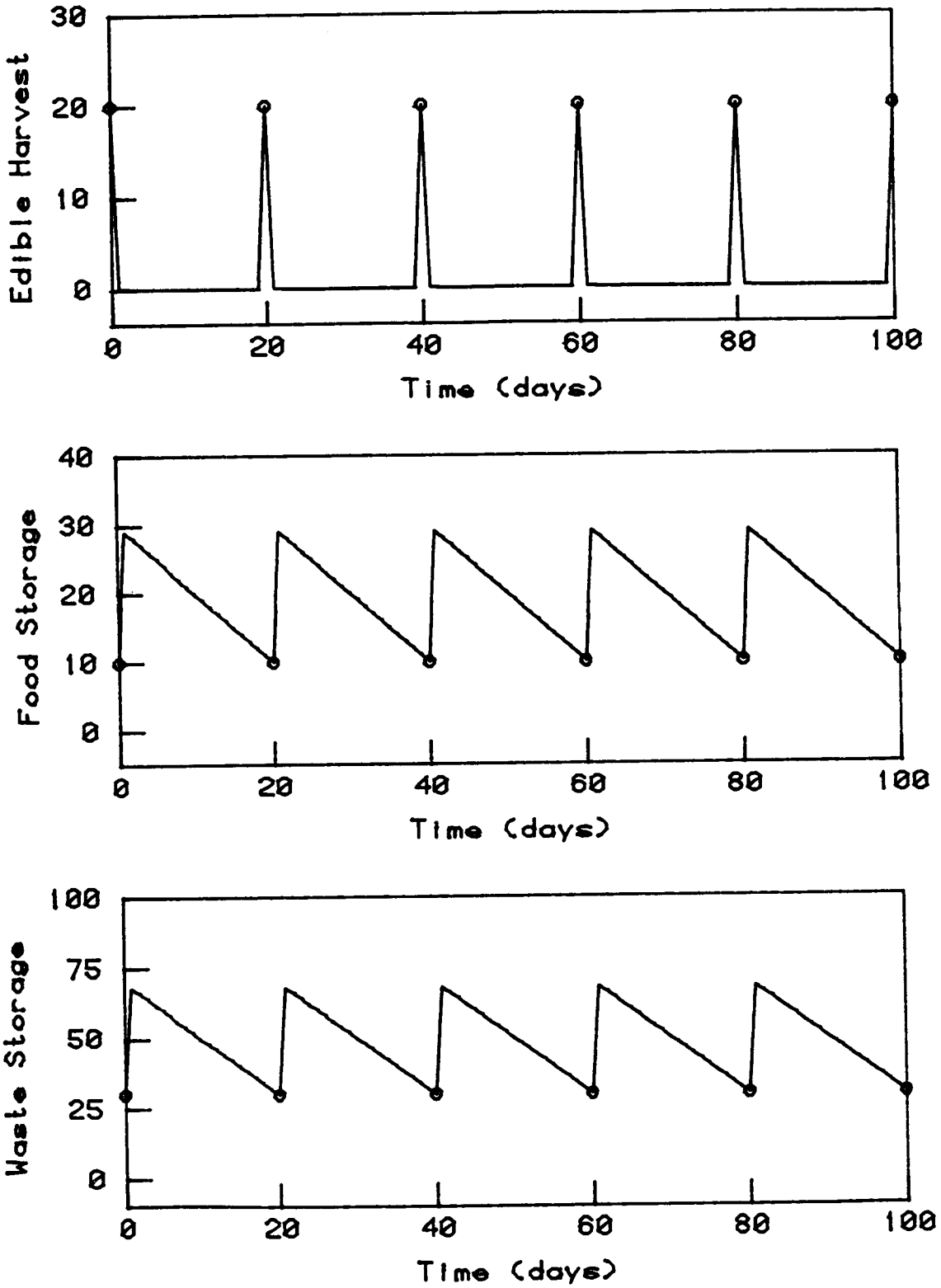

Figure 25: Continuous- and Discrete-Time Equilibrium; Three-Chamber Model

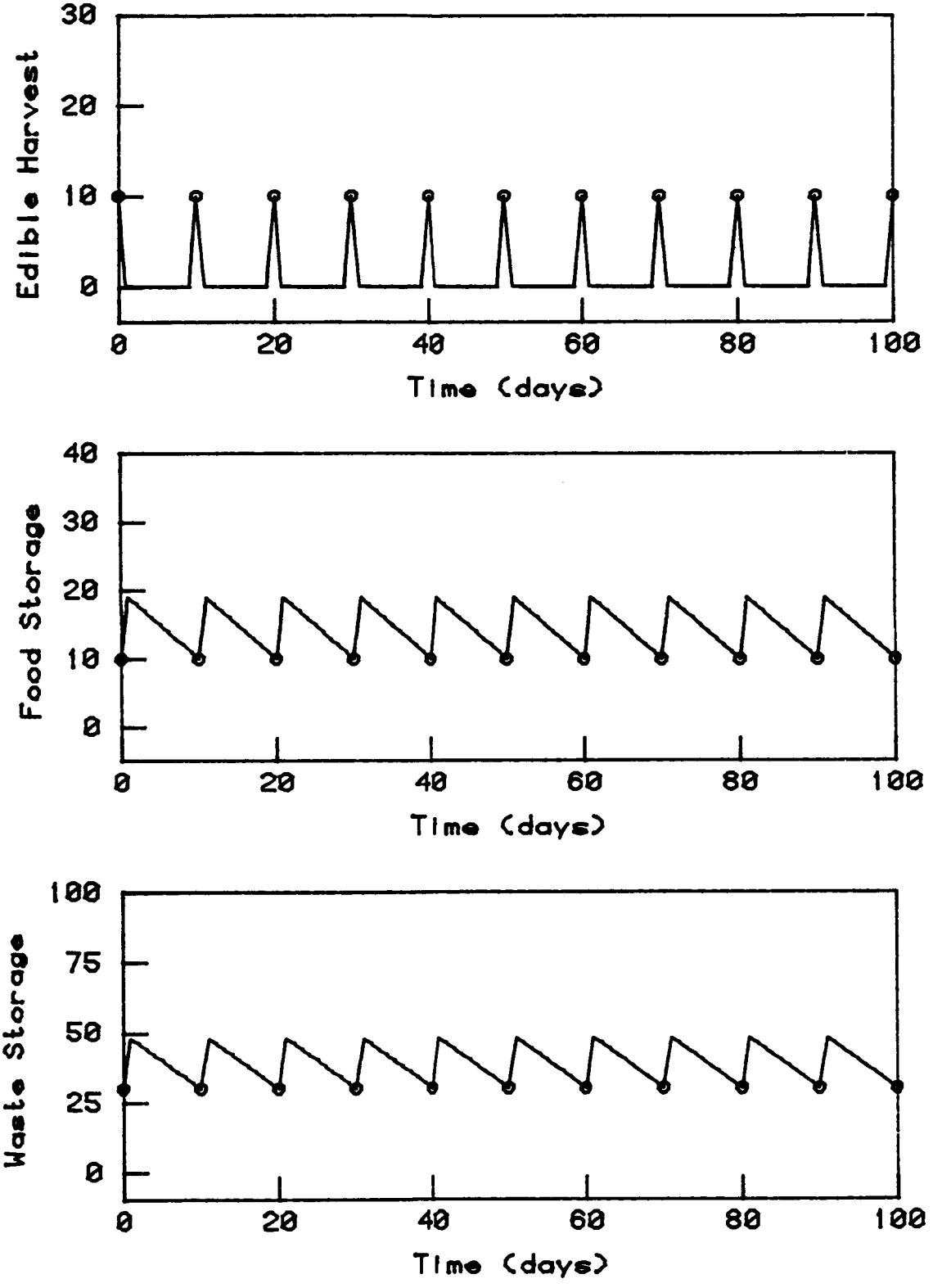

Figure 26: Continuous- and Discrete-Time Equilibrium;
Six-Chamber Model

continuous output flows cause smooth downward slopes. This sawtooth pattern indicates that the continuous simulation's equilibrium state is not a point but a cycle. The discrete simulation has a time step equal to the harvest interval so its output does not show this cyclical behavior. Its steady state is an equilibrium point. The stability of this steady state will be examined in the next chapter.

In these examples, the food and waste tanks are never empty. This buffer level is large enough to maintain the output flows for 10 days. This buffer level can be set wherever desired. However, the survivability of the system to survive failures depends a great deal on the size and location of these buffers.

The system mass and size of the storage tanks needed depend on the number of plant chambers the model has. Both the three- and six-chamber models have food and waste buffers of 10 and 30, respectively. However, the mass tied up in the plant chambers is not the same. The three-chamber model has 96 mass units in its plant chambers at steady state while the six-chamber model has 81 units. Further, the three-chamber model's larger harvest mass (20 days of food and inedible waste) requires larger food and waste tanks than the six-chamber model does. With these static considerations, the lighter and smaller six-chamber system would appear to be a better choice. However, in the next chapter the dynamic behavior of the two models is compared and the superiority of the six-chamber system is not as obvious.

4.4 A Processor Failure and the Need For Control

Some of the system dynamics can be seen when a waste processor

failure is considered. In this example, the supply of water and nutrients to the plants is stopped from the fifth to the fifteenth day. During this 10-day failure the output of the waste storage is set to zero to avoid a bypass of the processor. From a static design viewpoint the steady state contains enough food and waste in their respective buffers to ride out the 10-day processor failure. Control is exerted on the system through adjustments of the output flow of the waste storage. All storage tanks are large enough to prevent overflows.

One strategy is to maintain the waste storage output flow at its steady state value. Using the continuous-time simulation, the effects of this no-control strategy on a 10-day failure are shown in Figure 27 for the three-chamber model and in Figure 28 for the six-chamber model. The system returns to an equilibrium in 60 days. This is not the original steady state, however. The food buffer of 10 units is gone and the waste buffer has increased from 30 units to 40. This transfer of mass leaves the system in a configuration that would be disastrous if another processor failure occurred.

In addition to moving to a new steady state, the three-chamber model needs a waste storage capacity of at least 93 units to absorb the transient without causing an overflow. For the six-chamber model a waste capacity of 74.25 is needed. This dynamic behavior could not be predicted from the static design.

To return the system to its original steady state with 10 day buffers, some sort of control action is needed. Figure 29 shows a feedback control that adjusts the nutrient flow to the plant chamber. If the harvest is too small, the controller increases the nutrient flow which

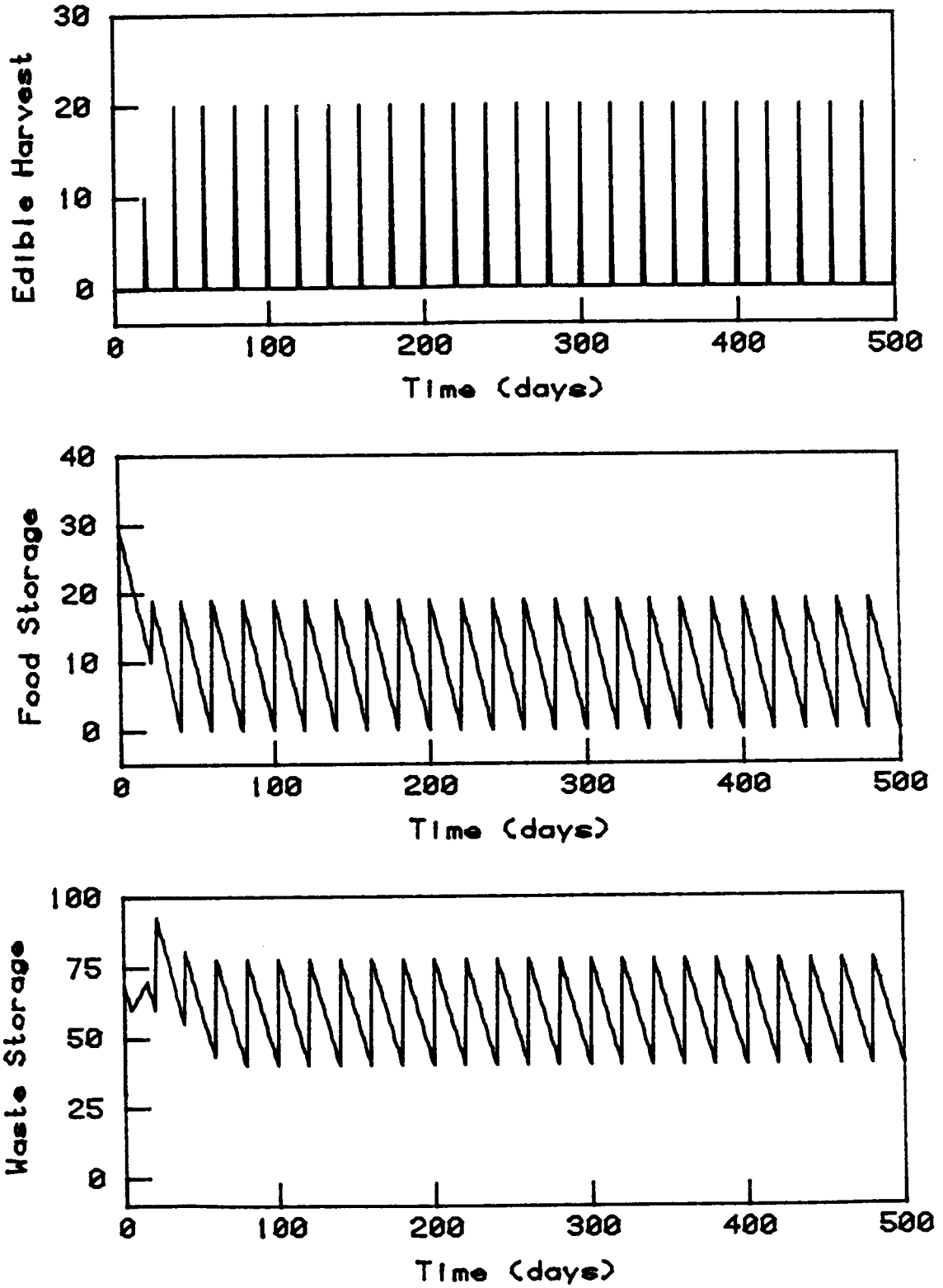

Figure 27: Processor Failure with No-Control;
Three-Chamber Model (Continuous-Time)

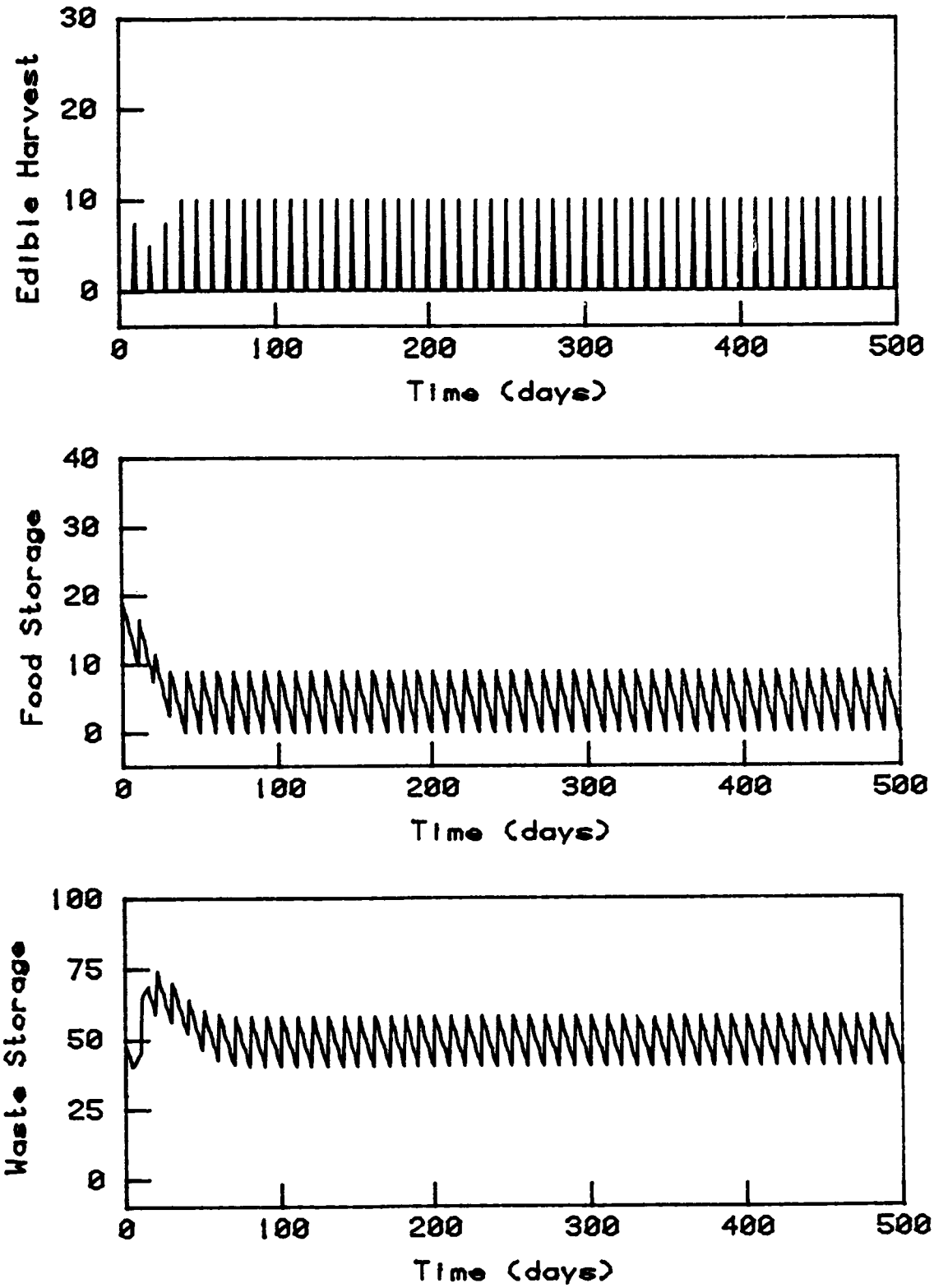

Figure 28: Processor Failure with No-Control;
Six-Chamber Model (Continuous-Time)

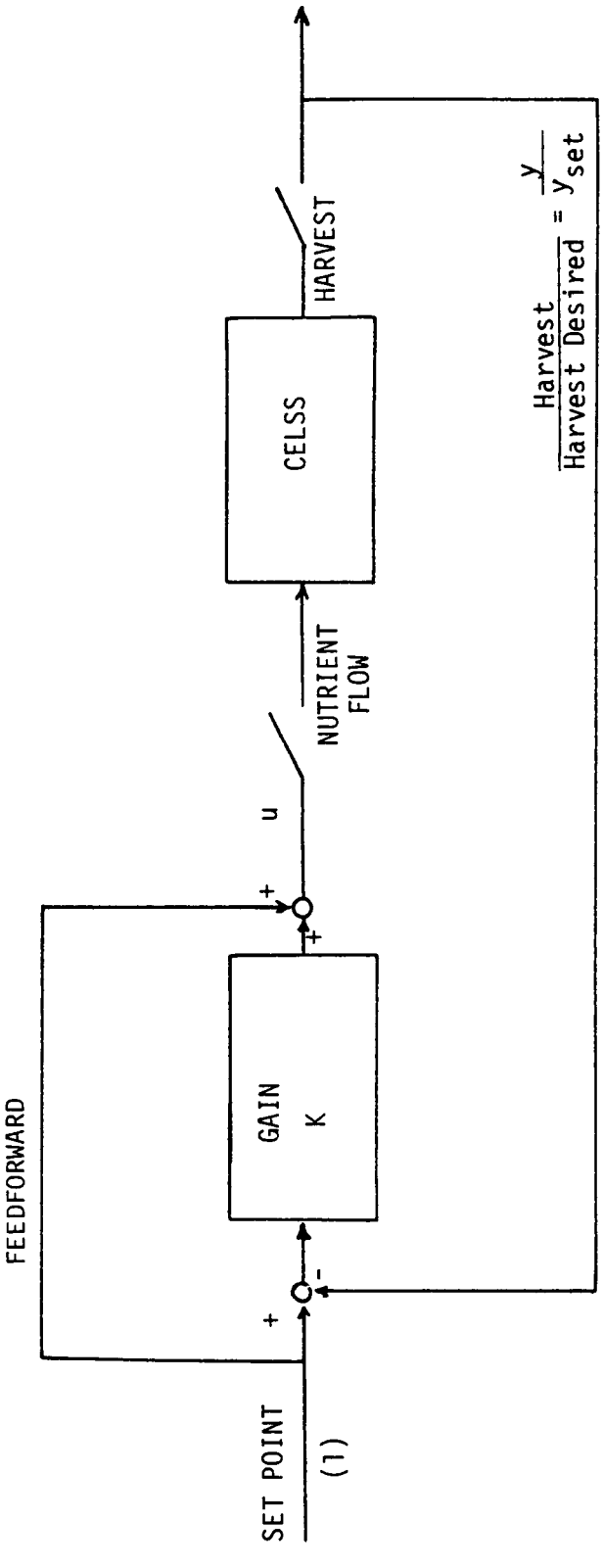

Figure 29: CELSS with Proportional Control

in turn increases plant growth. The gain adjusts the magnitude of the change in nutrient flow relative to the harvest error. The feedforward of the set point avoids offset errors in the control.

The feedback controller is expressed mathematically as:

$$u = u_{steady} [1 + k(1 - y/y_{set})] \tag{4.8}$$

where u is the nutrient flow to the plants and y is the edible harvest. The proportional gain is k, u_{steady} is the steady state nutrient flow, and y_{set} is the desired edible harvest mass. At each harvest the controller calculates the nutrient flow which is then maintained until the next harvest. Thus, this is a discrete-time controller. If the control function results in a nutrient flow large enough to harm the plants, the controller applies the flow that is at the maximum point of the growth curve (see Figure 24, center).

This controller is applied to the processor fail example. With a gain k = 1 the system behavior can be seen in Figures 30 and 31, for the three- and six-chamber models, respectively. The food and waste buffers are recovered after the failure, however, the recovery time is between 100 and 120 days. Such a long delay after a failure is due to the system dynamics. Even though the longest time constant in the model is the plants' 60-day growth time, the system shows evidence of the disturbance for much longer periods. As was the case with the no-control example (Figures 27 and 28), larger storage tanks are needed to avoid overflows than is indicated by a static design.

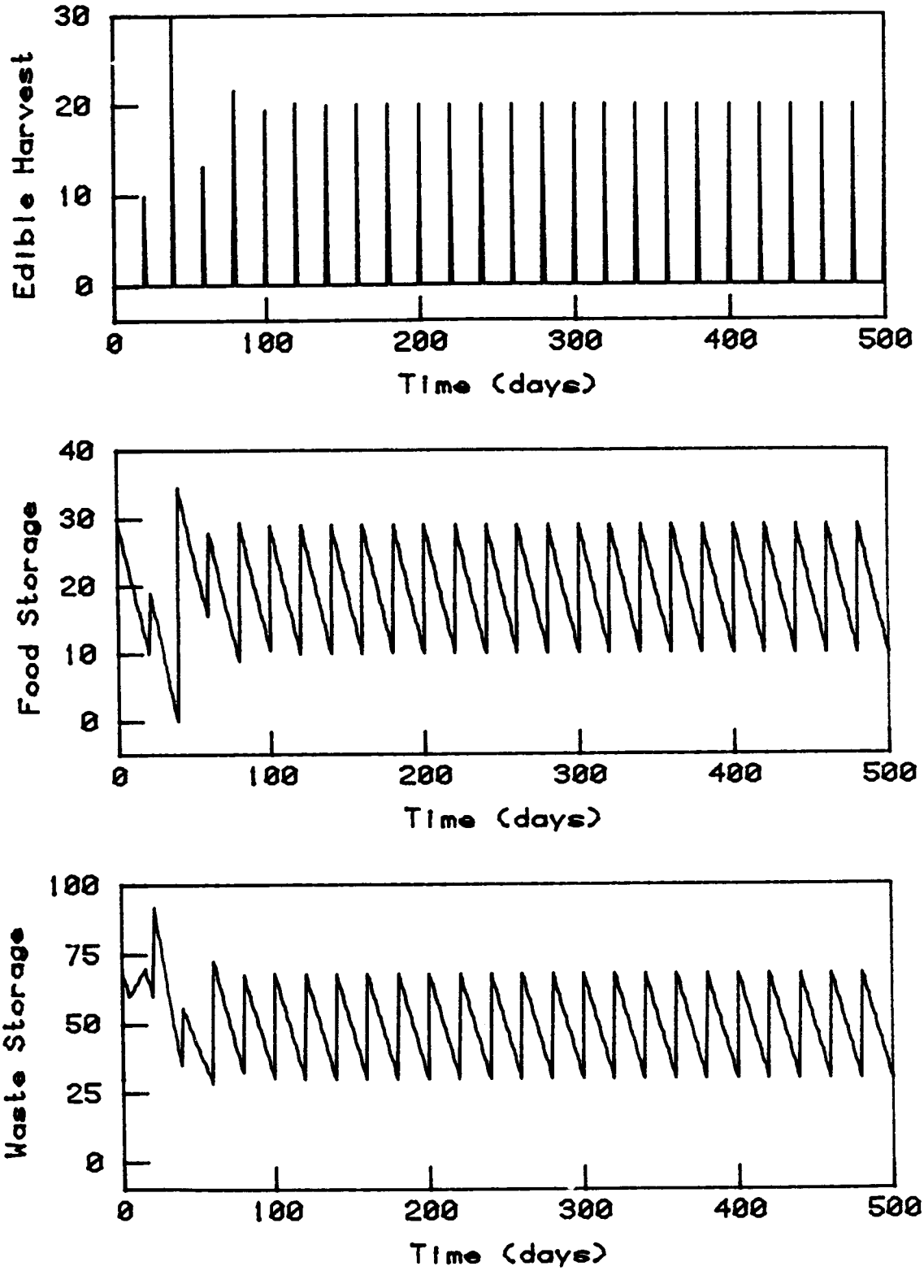

Figure 30: Processor Failure with Proportional Control; Three-Chamber Model (Continuous-Time)

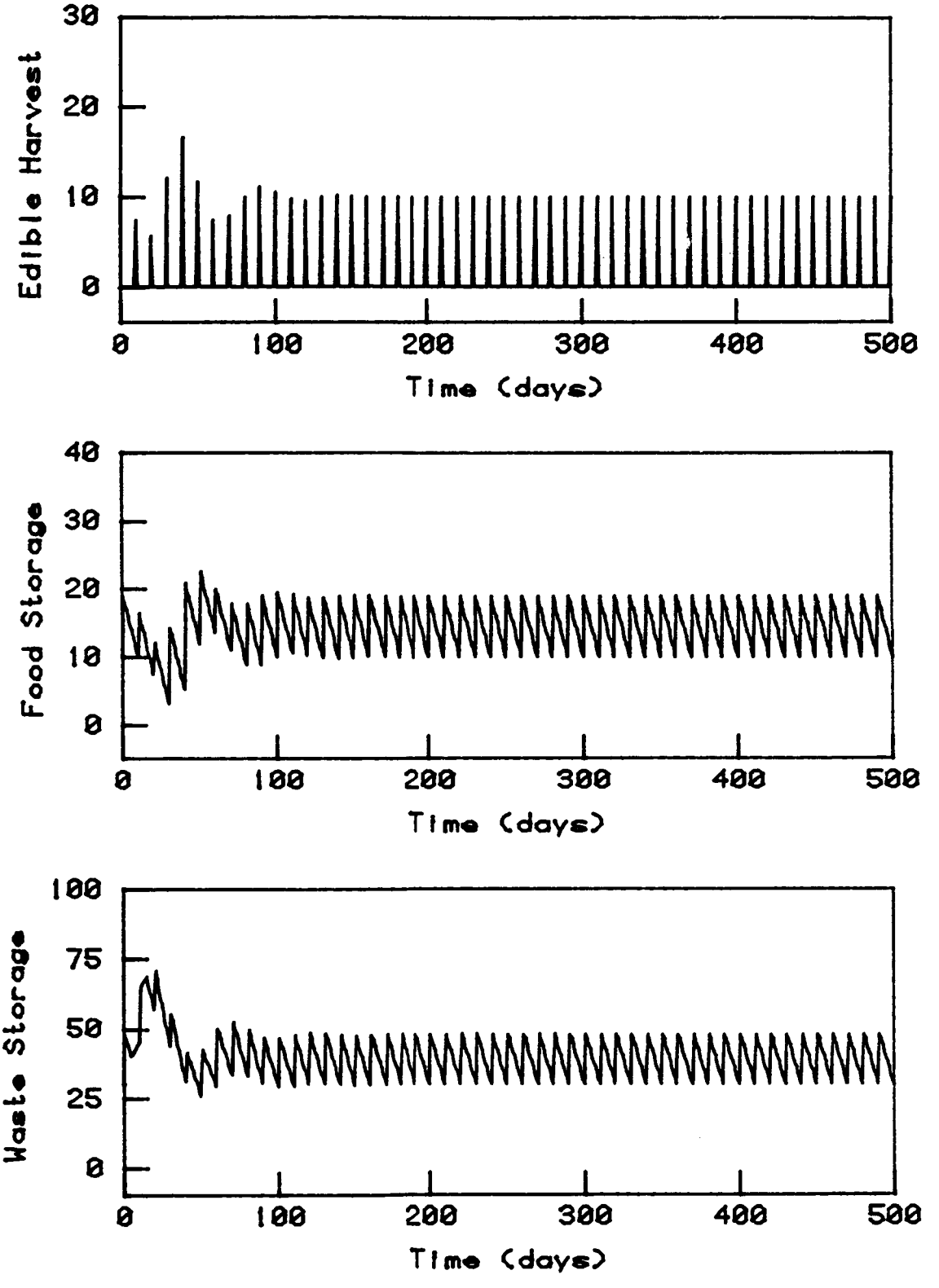

Figure 31: Processor Failure with Proportional Control; Six-Chamber Model (Continuous-Time)

5 DOMAIN OF ATTRACTION IN CELSS ANALYSIS

The methods of system analysis using the domain of attraction presented in Chapters 2 and 3 are particularly suited to investigating many aspects of the CELSS models. Their high dimensionality and nonlinear state equations make them difficult to analyze by any other technique. The goal is to investigate the dynamic consequences of a change in the waste storage capacity and the total system mass, as well as how information is used by the controller.

A random component failure is simulated as a random initial condition. The size and shape of the region of initial conditions that are attracted to the specified operating point indicate the system's ability to recover from random failures.

Three-, six-, and twelve-chamber models are considered. The waste processor capacity is 4.5 units/day. Waste flows exceeding this amount are bypassed.

5.1 Uniformity of Sample Points

Since the system has constant mass, the state space is bounded. Therefore, not only can the entire state space be sampled in the selection of initial conditions, it is also possible to find all attractors in the system. The constant mass constraint, however, makes it impossible to get a uniform distribution of initial conditions.

Consider a system with n mass storage variables: x_1 through x_n. Since the system has constant mass, only n-1 of these are needed to describe the state. Therefore, it is possible to randomly select the

first n-1 mass variables, but this fixes the value of x_n. Given the system's mass, it is possible to set bounds on the n state variables:

$$0 \leq x_i \leq M_i, \quad i = 1,2, \ldots n \tag{5.1}$$

where M_i is the maximum value for x_i. The M_i may be simply set to the total mass or more refined calculations can be done to set each variables' maximum.

The set of initial conditions used in the domain of attraction procedure are found as follows. The variables x_1 through x_{n-1} are set as random variates uniformly distributed over their respective ranges. The final state variable is found by subtracting the sum of the n-1 variables from the total mass. If x_n is within its limits, the n state variables are accepted as members of the set. If the last variable is out of its range, the entire collection of n variables is discarded. This process is repeated until the required number of initial conditions are found.

The mass constraint forces the admissible initial conditions into nonuniform distributions. Figure 32 shows histograms of the marginal distribution of the edible and waste storage initial conditions for the three-chamber model. The six-chamber model is shown in Figure 33. The other state variables have similar distributions. Few large values are present because once a large value is selected there is a high probability that the total-mass constraint will be exceeded.

Such nonuniform distributions must considered in determining the domain of attraction's volume and minimum radius. Clearly, the fraction of initial conditions in the domain is not proportional to the domain's

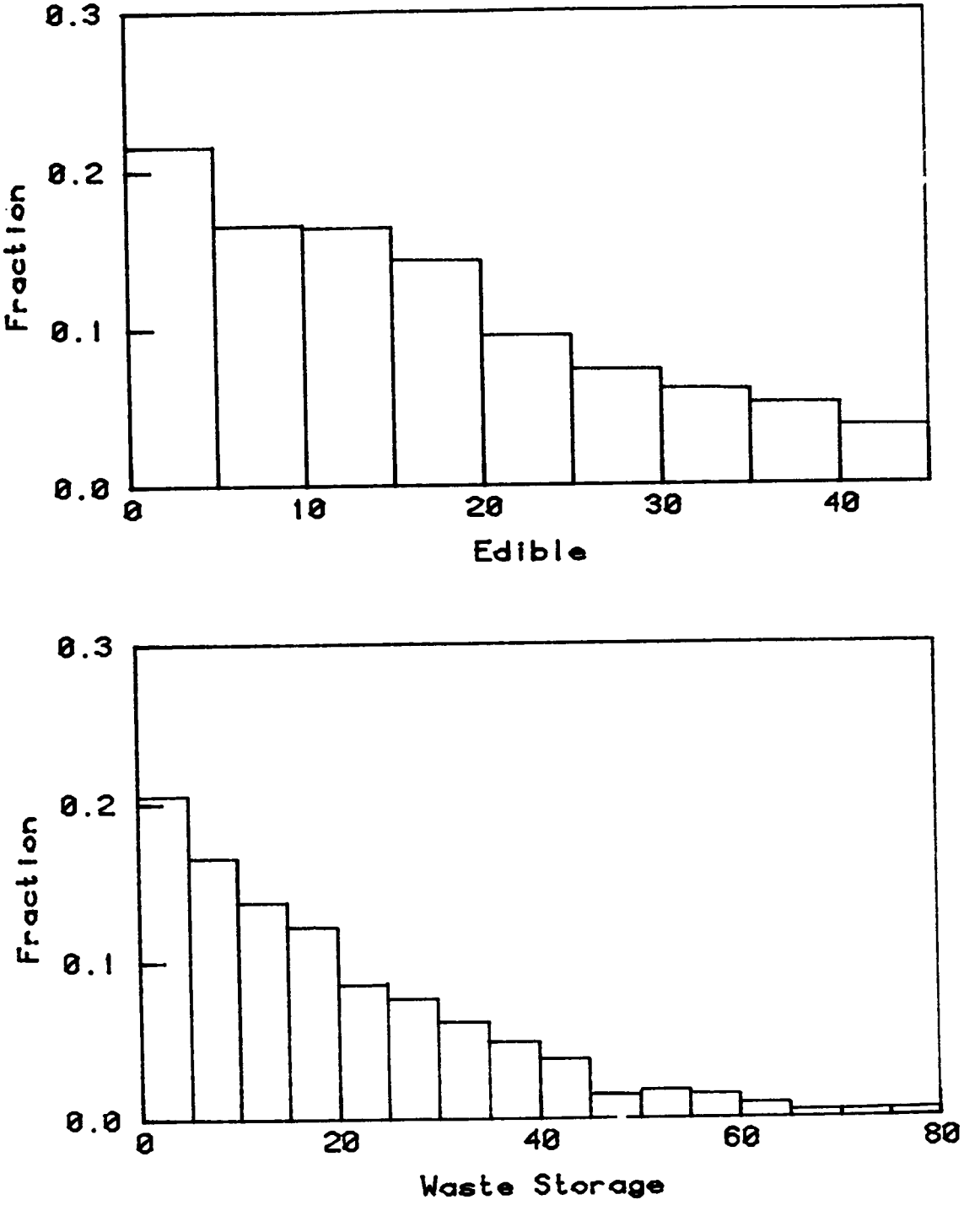

Figure 32: Sample Distribution Histogram; Three-Chamber Model

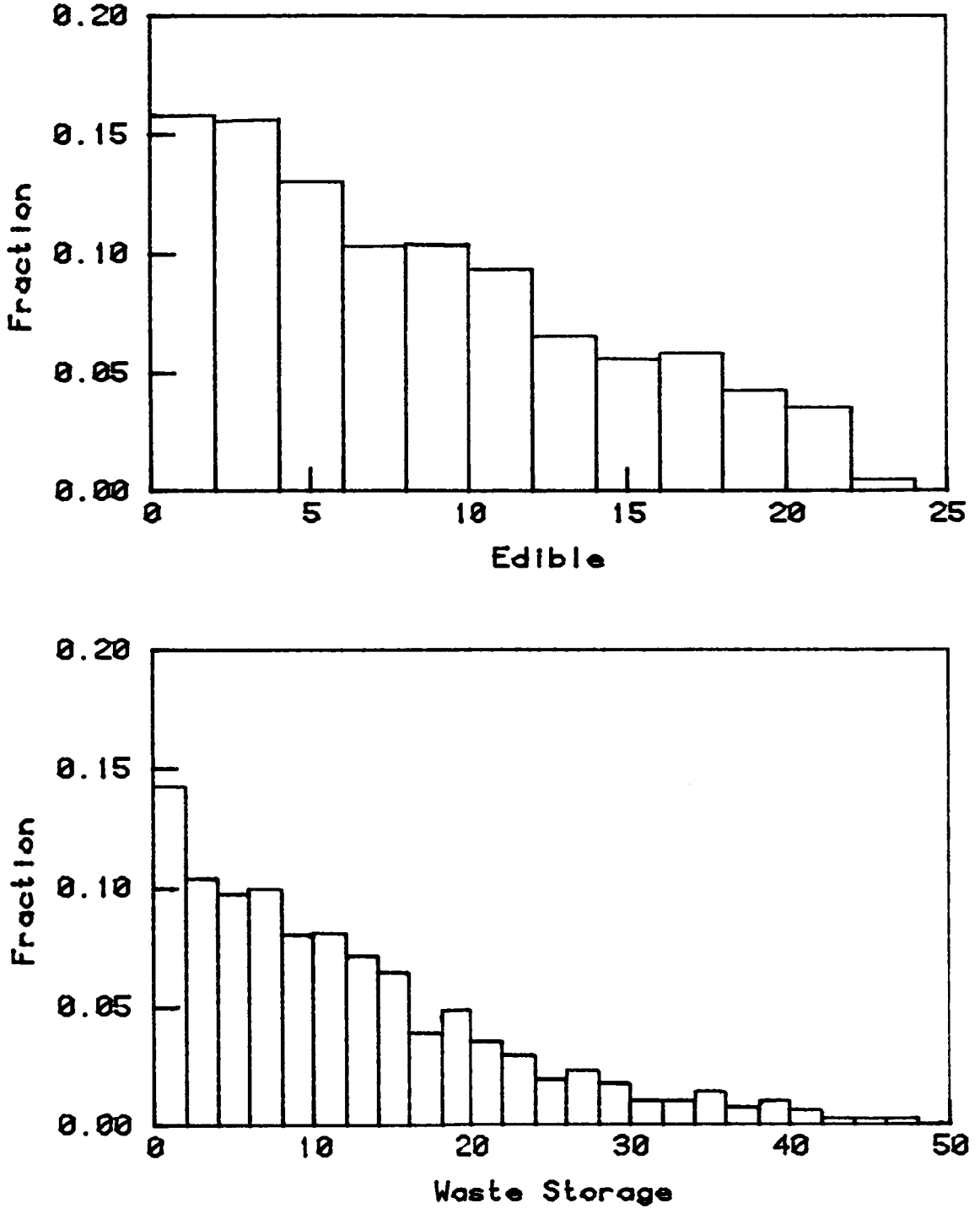

Figure 33: Sample Distribution Histogram; Six-Chamber Model

volume. However, if the state space is divided into moderately sized, identical cubes (actually they are 9-, 16-, or 30-dimensional hypercubes in these models), the initial conditions can be assumed to be uniformly distributed in each. The number of points in each cube gives the local density. Therefore, the volume of the domain of attraction is:

$$V = \sum_{i=1}^{K} \frac{(N_p)_i}{d_i} \tag{5.2}$$

where $(N_p)_i$ is the number of pass points and d_i is the local density of points in cube i. The number of cubes in the state space is K.

Estimating the domain's boundary requires knowledge about the local point spacing. Its expected value is determined by taking the n^{th} root of local volume per point for an n-dimensional state space. The minimum radius is the distance to the nearest fail point minus the local point spacing.

The state space, while bounded, is very large for these two models. The three-chamber model has a 9-dimensional state space with a volume of 8.9×10^{14}. A 10,000 point sample of initial conditions would have an average spacing of 16.4. The six-chamber model has a 16-dimensional volume of 3.0×10^{20}; its average point spacing for 10,000 points is 10.7. The 30-dimension twelve-chamber model has a volume of 8.0×10^{26} with an average spacing of 5.8 for a 10,000 point sample. As shown in the distributions of Figures 32 and 33, the local density and point spacing can be expected to vary considerably throughout the state space.

5.2 System Behavior and Storage Capacity

The CELSS model behavior is strongly dependent on the selection of

storage tank capacities. Here, variations of the waste tank capacity are considered. Simulations are made to delineate the domain of attraction using a random selection of 10,000 initial conditions. These initial conditions are viewed as the point the system arrived at after a random component failure. It is assumed that the component has been fixed so the subsequent model evolution can be followed with the discrete-time simulation. Proportional control with gain k = 1 is used in the examples that follow (see Figure 29). System mass is set so there is enough for 10-day waste and food buffers.

When the three-chamber model is used with waste storage capacity larger than 82.4, all 10,000 initial conditions are attracted to the equilibrium point that generates food at the rate the crew consumes it (see Figure 25). This steady state is therefore globally attracting and stable. It should be noted that this attractor is an equilibrium point only in the discrete-time simulation used here. In a continuous-time simulation it would be a stable limit cycle. Such a steady state is called the pass steady state or the pass equilibrium point because a CELSS operating at this point meets its crew's food and environmental needs.

When the waste storage tank is smaller than 70, all 10,000 initial conditions are attracted to equilibrium points that have edible harvests of zero. Each value for the waste capacity has a corresponding, unique equilibrium that is globally attracting. All of these points are called fail points.

In the intermediate range of storage sizes, from 70 to 82.4, both a pass and a fail equilibrium point coexist. The fraction of the state

space attracted by each is shown in Figure 34. These volume fractions have errors of ± 0.005. As the tank size increases, the region attracted by the fail equilibrium shrinks while that of the pass increases. For waste capacities below 70 the pass point is unstable and, for storages larger than 82.4, the fail point is unstable. Thus, there is a bifurcation and reverse bifurcation in the stable points as the waste capacity is increased. There are no other attractors in the three-chamber system.

One possible design goal is to maximize the domain of attraction about the pass equilibrium. If this domain covers the entire state space then the system is able to recover from all perturbations. However, it is desirable to have a system with small storage tanks and mass. Figure 34 indicates that all initial conditions are attracted when the waste capacity is 82.4. A typical, continuous-time trajectory for this system is shown in Figure 35. here it can be seen there are no edible harvests for 100 days. Further, it takes the system 240 days to return to the steady state. This trajectory is stable, but it is not survivable.

A performance criteria can be established such that all pass initial conditions must settle to the pass equilibrium point in $t \leq 300$ days. Figure 36 compares the volume of this performance domain with the domain of attraction. To meet the performance limit over the entire state space, a waste storage capacity of 83 is needed. The minimum radius as a function of waste storage size for the two domains is identical (see Figure 37). Thus, the extra volume in the stable region appears to be far from the equilibrium. Other performance criteria could be used such as a limited time without food, etc.

An alternative approach to reducing storage capacities is to reduce

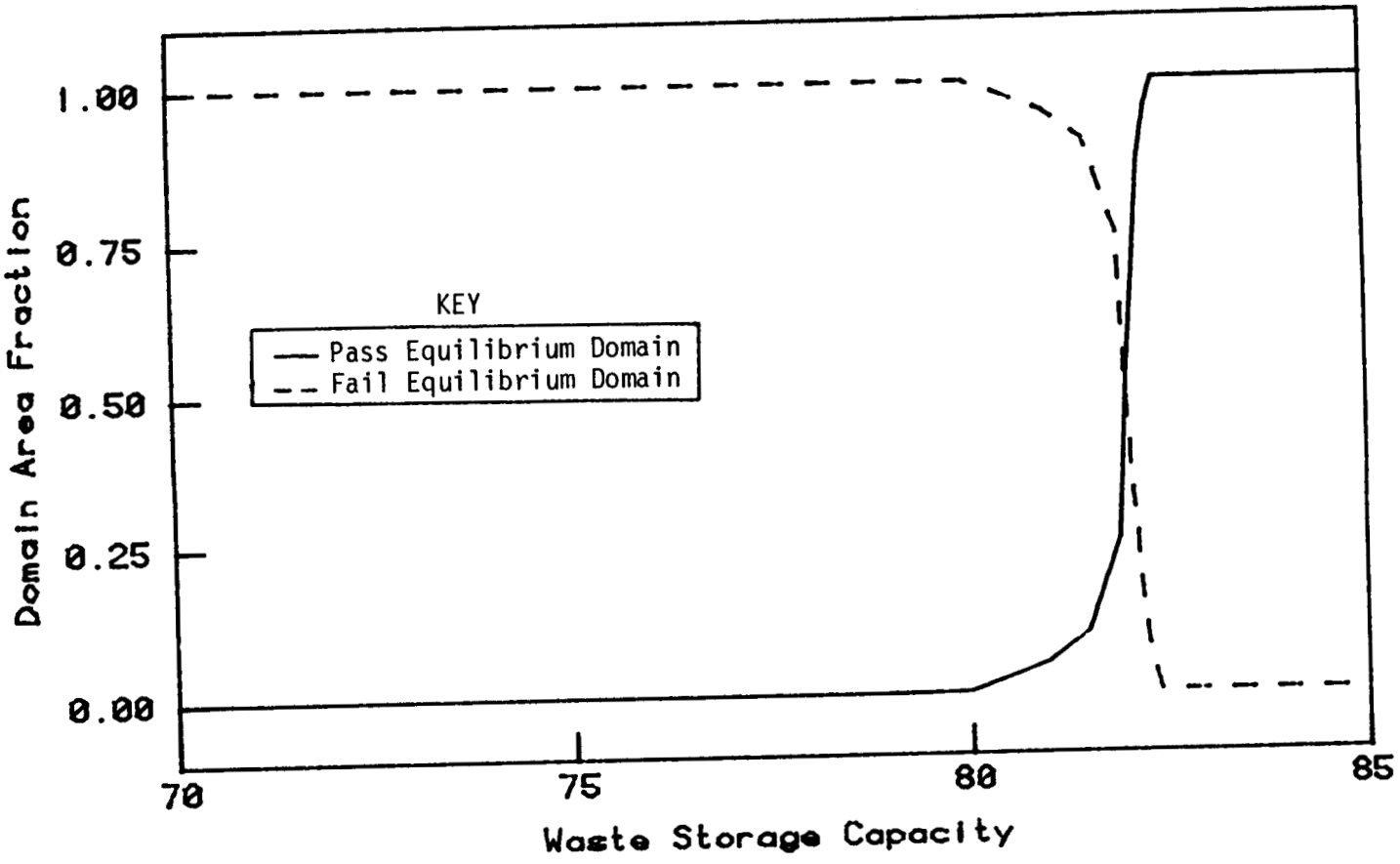

Figure 34: Domains of Attraction; Three-Chamber Model

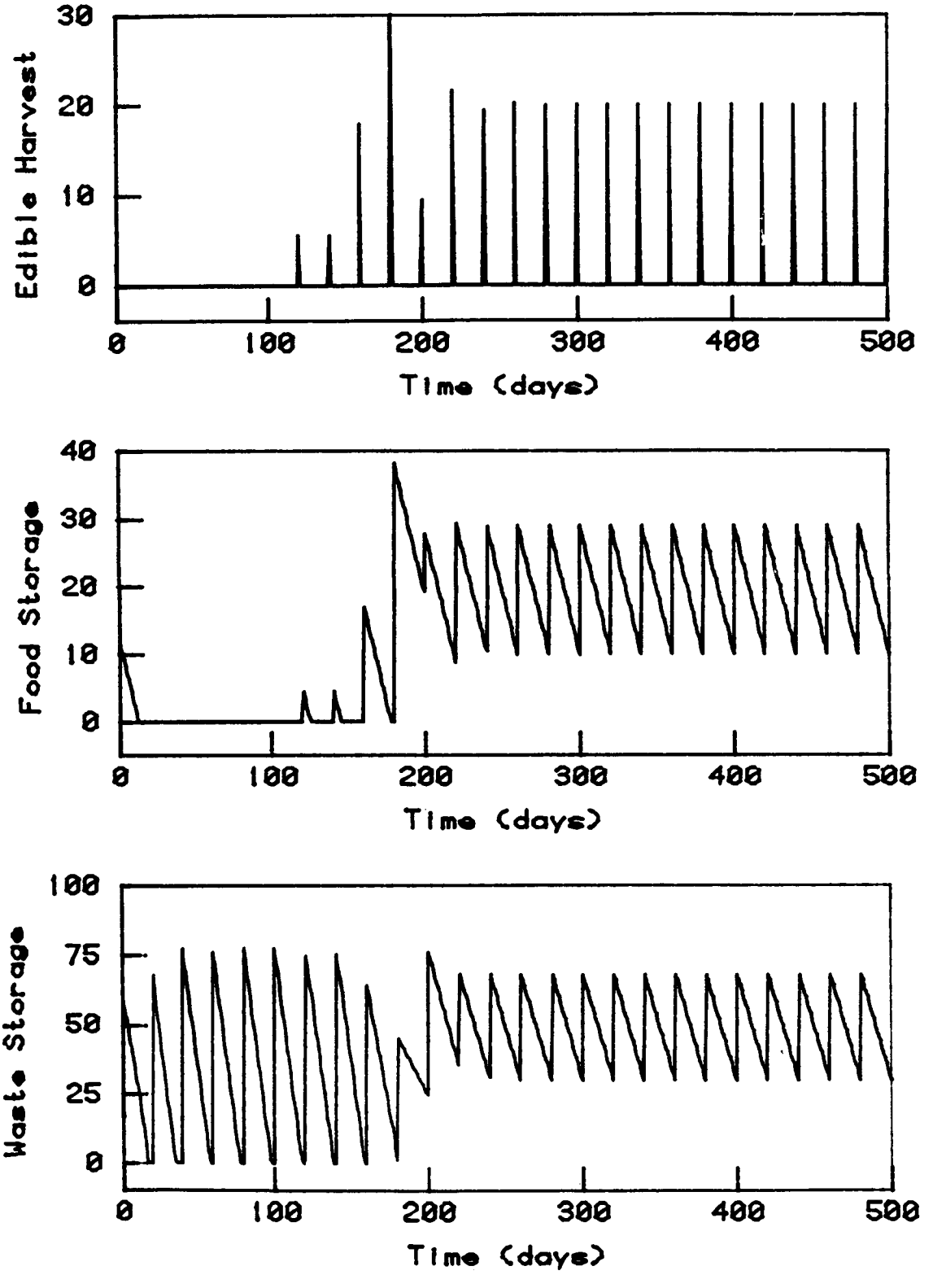

Figure 35: Long Transient Settling Time;
Three-Chamber Model (Continuous-Time)

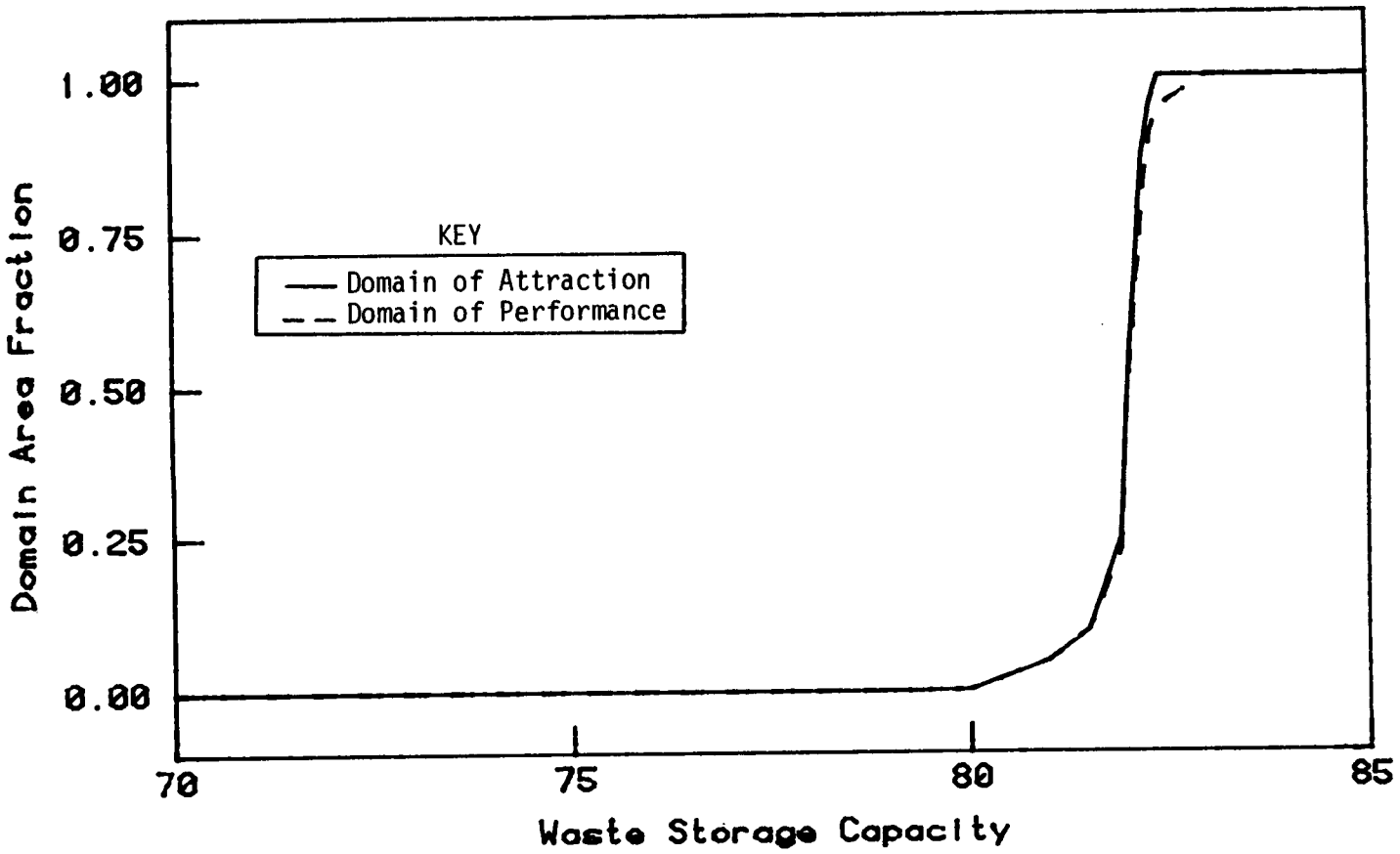

Figure 36: Pass Domain of Attraction and Performance; Three-Chamber Model

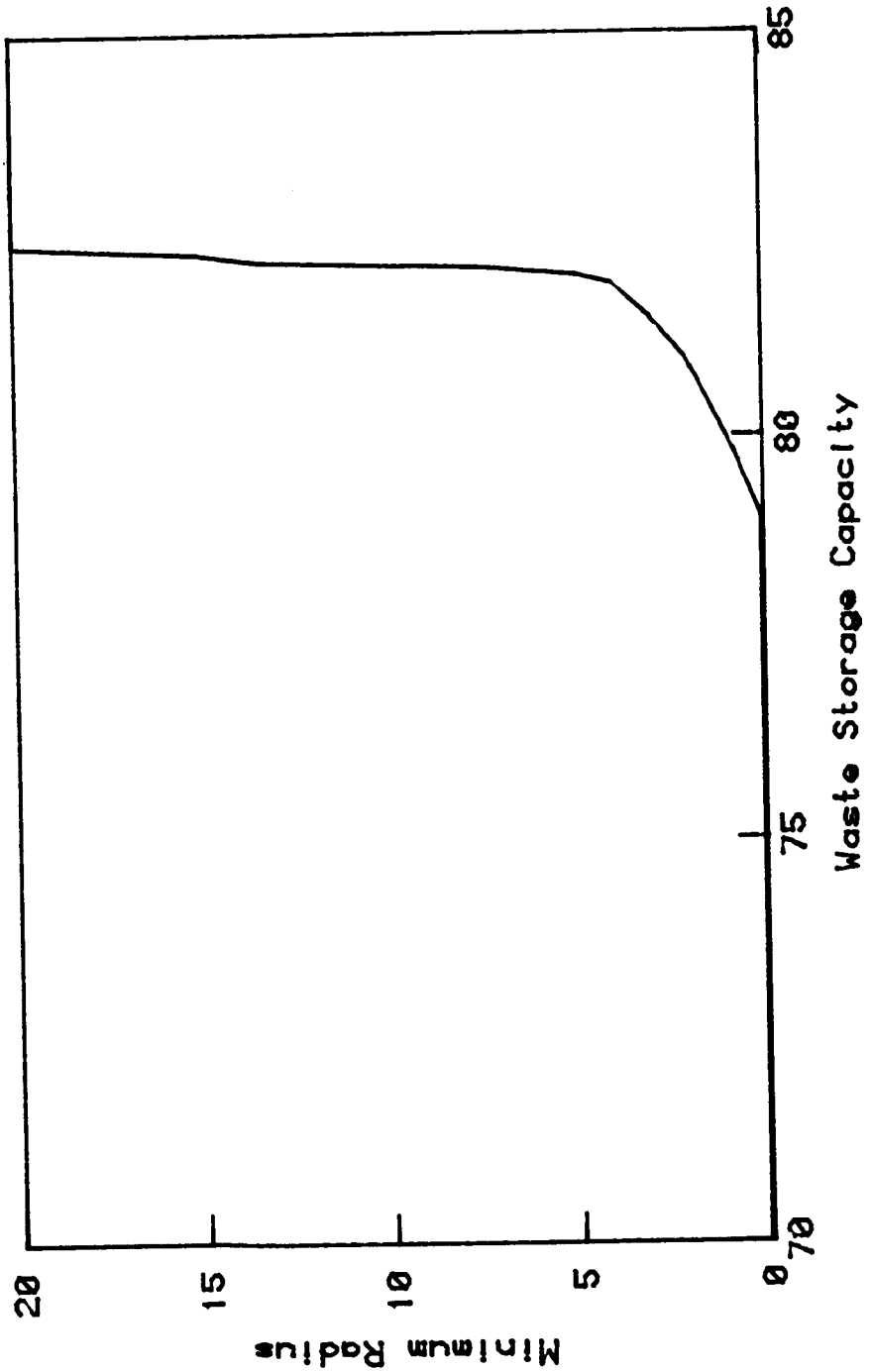

Figure 37: Pass Domain of Attraction; Three-Chamber Model

total system mass. For instance, if a 5-day buffer is used in the food and waste tanks, the total three-chamber system mass is reduced to 116. The domain sizes for the pass and fail equilibria are shown in Figure 38. As with the 10-day buffer example (Figure 34), there is a bifurcation pattern between the pass and fail attractors. However, the pass equilibrium is globally attracting for waste capacities above 73. Therefore, in addition to reducing system mass by 20, the waste storage can be made 9.6 units smaller without changing the system's stability. Smaller buffers, however, cause there to be longer transients when food is not available.

The six-chamber model has all of the same dependencies on storage capacities and system mass as the three-chamber model. However, it has a more complicated bifurcation pattern as well as attractors that are not equilibrium points.

Figure 39 shows the percent of the state space attracted to the pass and fail equilibrium points. The pass steady state attracts the entire space for waste capacities larger than 54. The fail equilibrium is globally attracting for storages smaller than 43.2. While the waste capacity needed for the pass domain to cover the entire space is smaller than that needed in the three-chamber model, many of the initial conditions still take a long time to settle. This is shown in Figure 40 where the performance domain has a settling time limit of 300 days.

In the intermediate range of waste storage capacity, the equilibrium points go through a series of bifurcations that create higher-dimensional attractors. The motion on these attractors is bounded and may be quite complex. For example, Figure 41 shows a trajectory that,

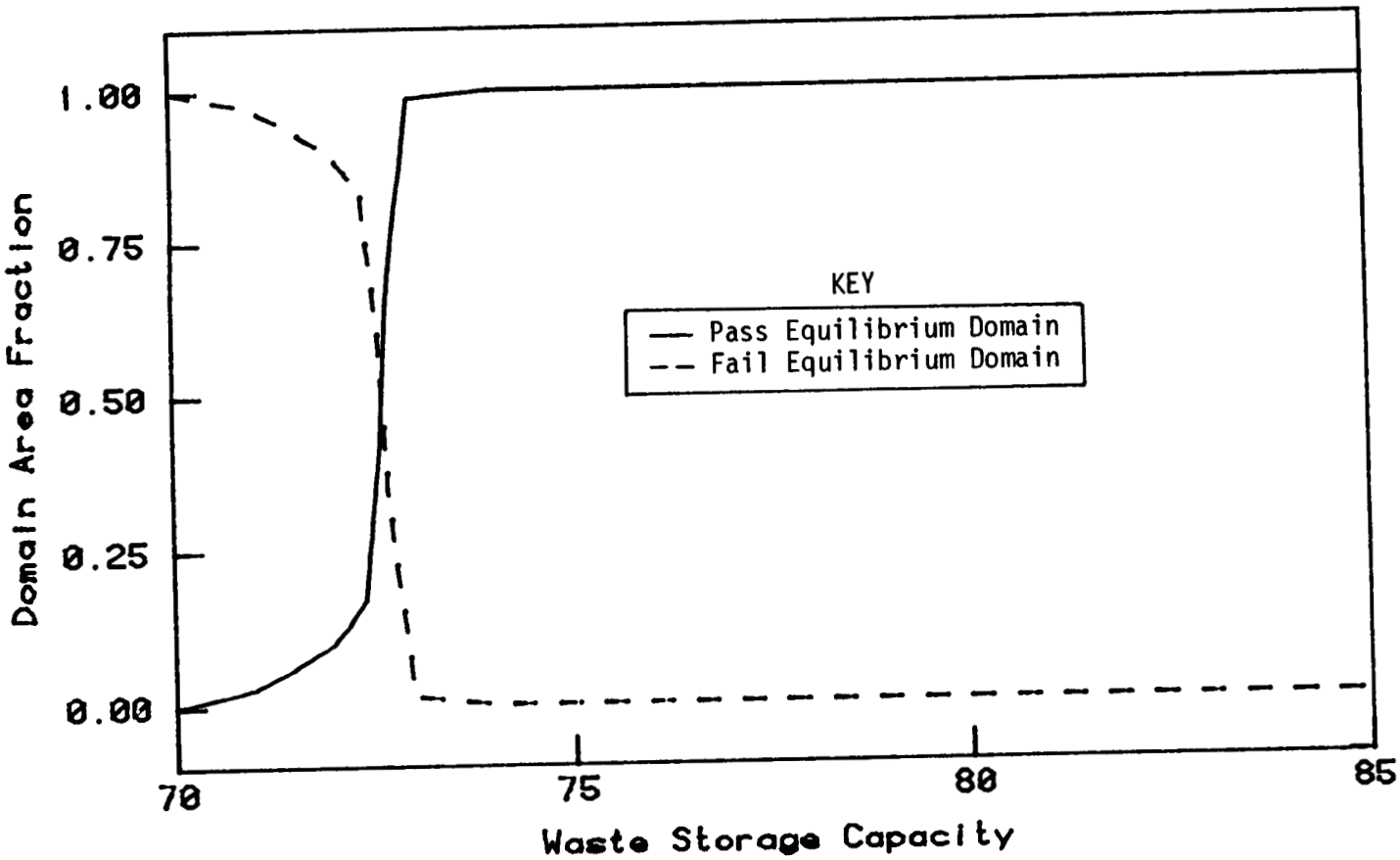

Figure 38: Domains of Attraction with Total Mass=116; Three-Chamber Model

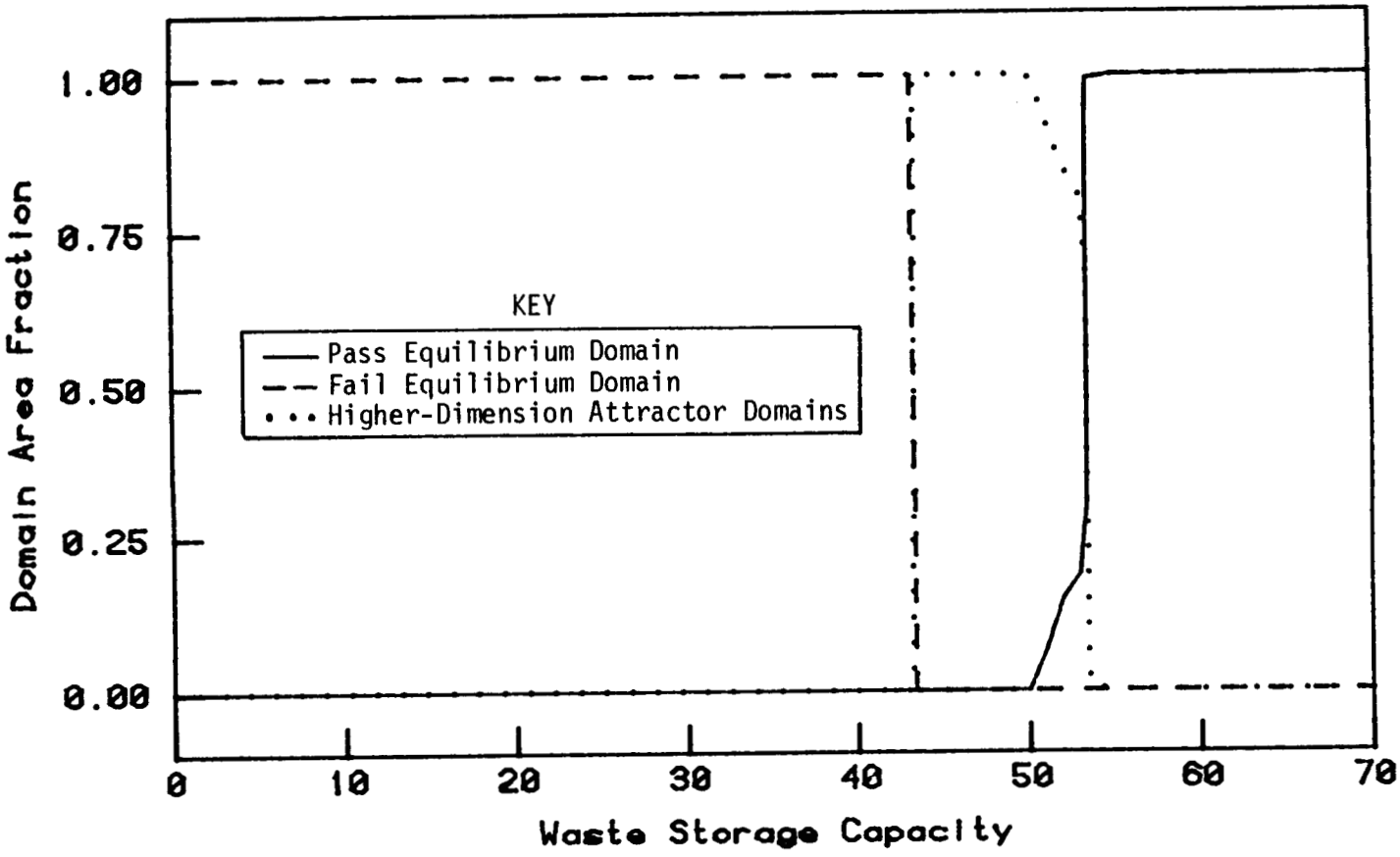

Figure 39: Domains of Attraction; Six-Chamber Model

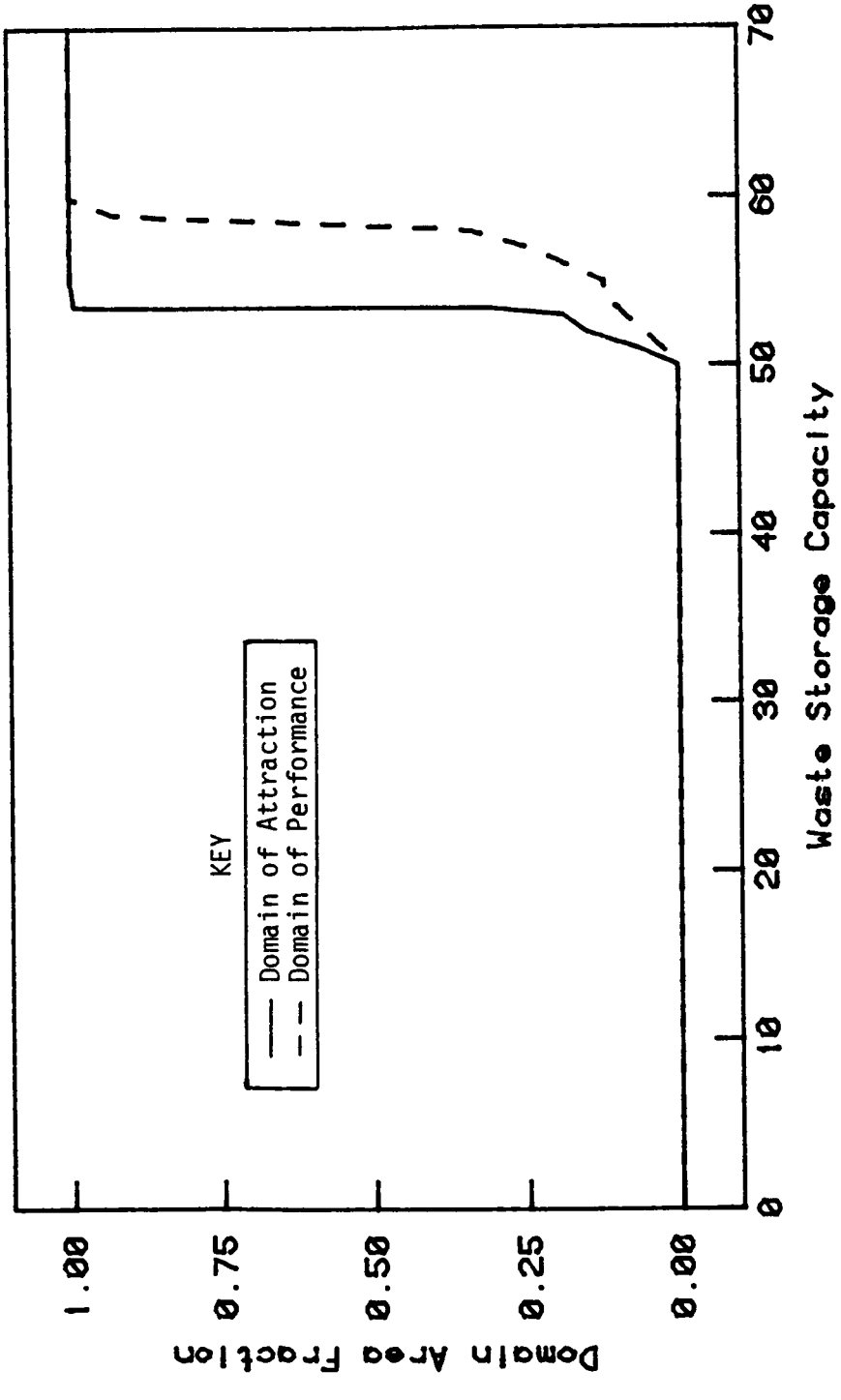

Figure 40: Pass Domain of Attraction and Performance; Six-Chamber Model

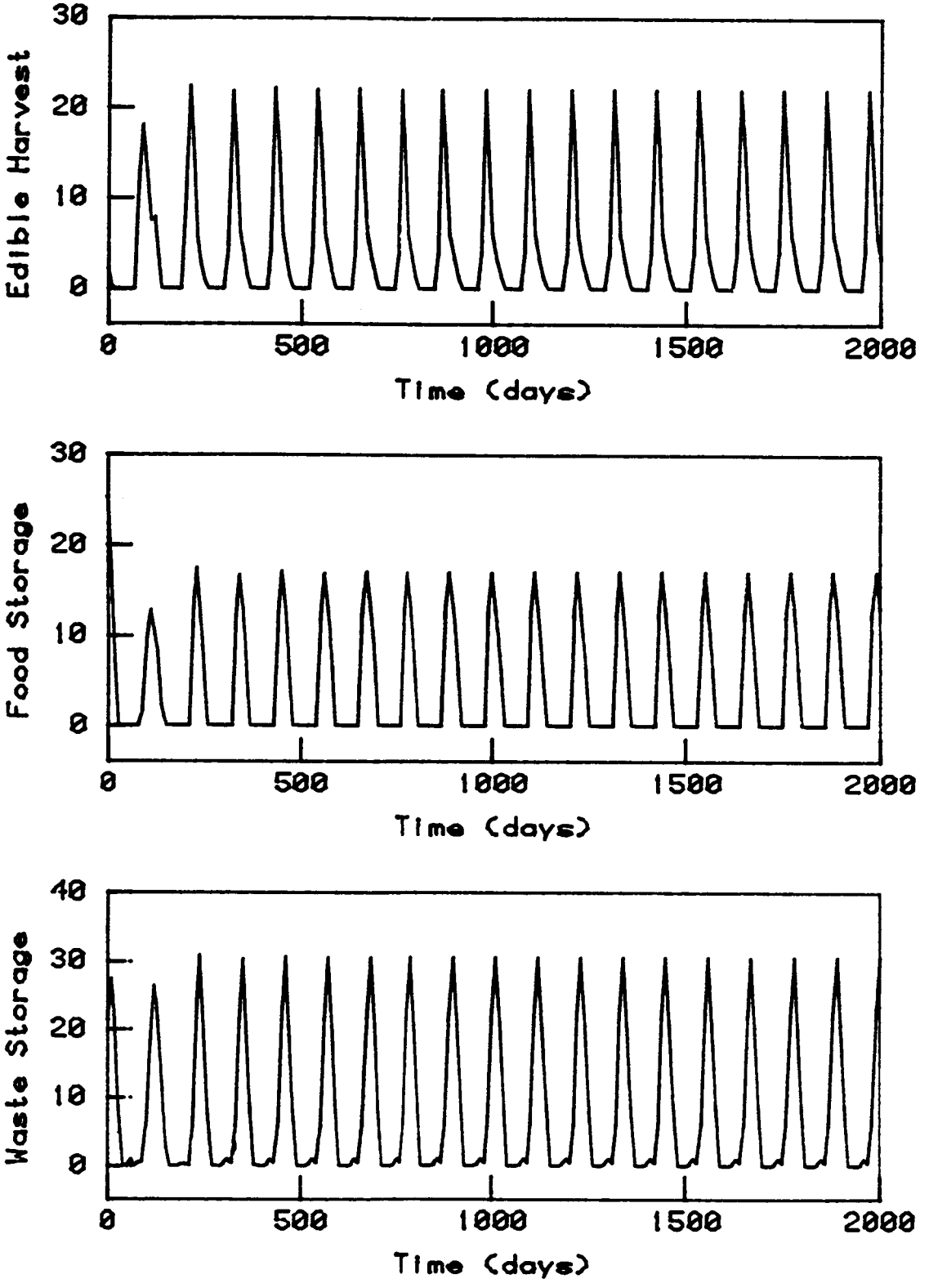

Figure 41: Limit Cycle Trajectory;
Six-Chamber Model (Discrete-Time)

after an initial transient, becomes periodic. This figure shows the output of a discrete-time simulation where the output samples have been connected to form the trajectory. Thus, the edible harvest plot shows harvest levels oscillating in a repeating pattern. This limit cycle behavior is globally attracting for a waste capacity of 46.

When the waste storage capacity is 53.4, two-thirds of the initial conditions are attracted to the discrete-time trajectory shown in Figure 42. This motion is called chaotic. It is characterized by trajectories that never repeat, a continuous spectrum, and a Lyapunov exponent greater than zero [10]. The first Lyapunov exponent was found to be 0.3. The chaotic motion takes place on what is called a "strange attractor" [14].

While it is desirable to use the smallest waste capacity possible, it is not acceptable to go into this region of higher-dimension attractors. The limit cycle and chaotic motion shown in Figures 41 and 42 are not survivable because there are long periods with no edible harvest and no food in the storage. No stable attractors capable of providing a continuous food supply were found in the six-chamber model, other than the pass equilibrium point.

In a twelve-chamber model, limit cycle behaviors can be found that meet the crew's needs. This system has a pass equilibrium point that provides harvests of 5 units every 5 days. The total mass with 10-day food and waste buffers is 113.5. There are 30 state variables in this model. Figure 43 shows the fraction of the state space attracted to the equilibrium points and higher-dimension attractors. A waste capacity of 48 guarantees global stability but, as was true in the other models, the

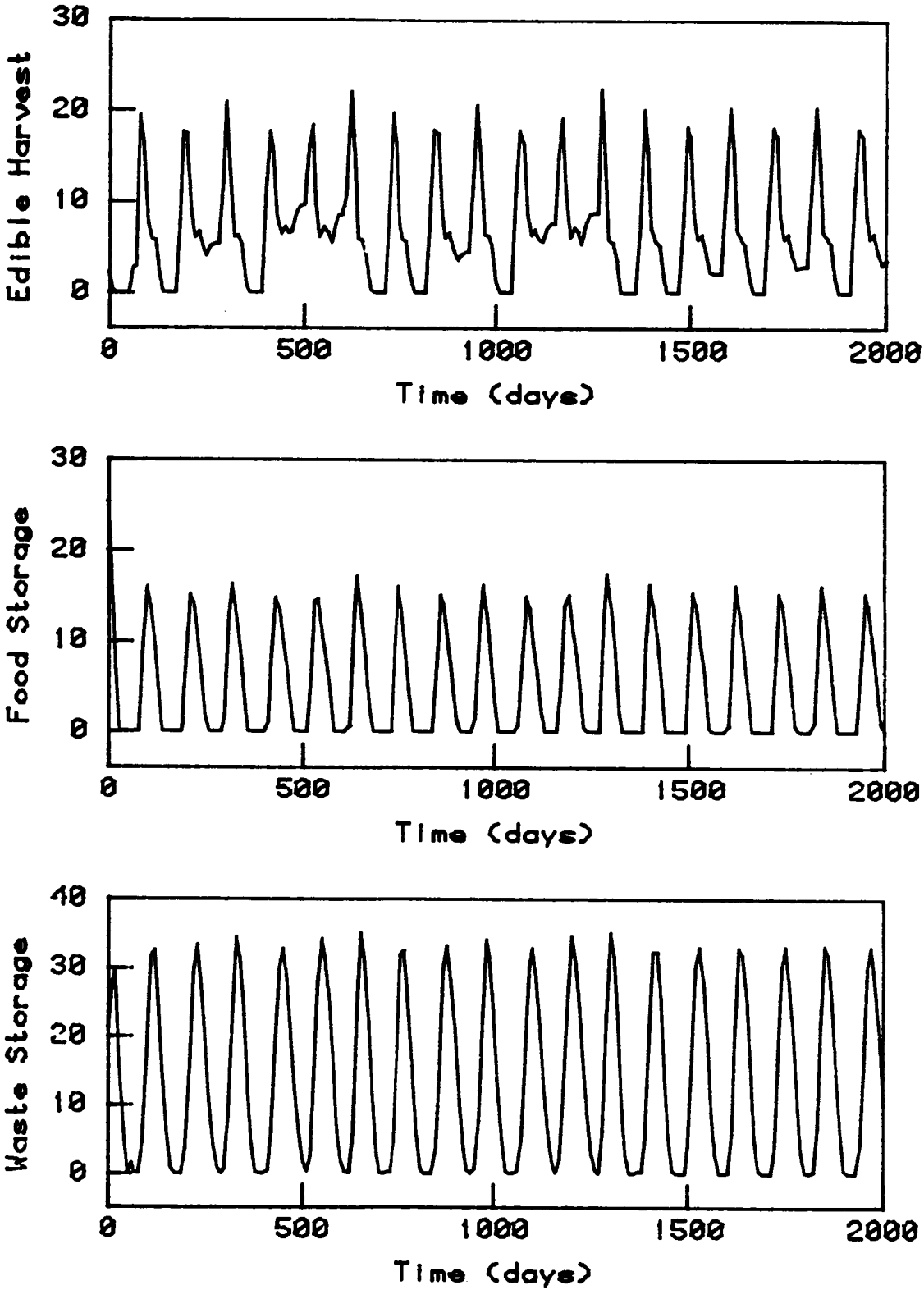

Figure 42: Chaotic Trajectory;
Six-Chamber Model (Discrete-Time)

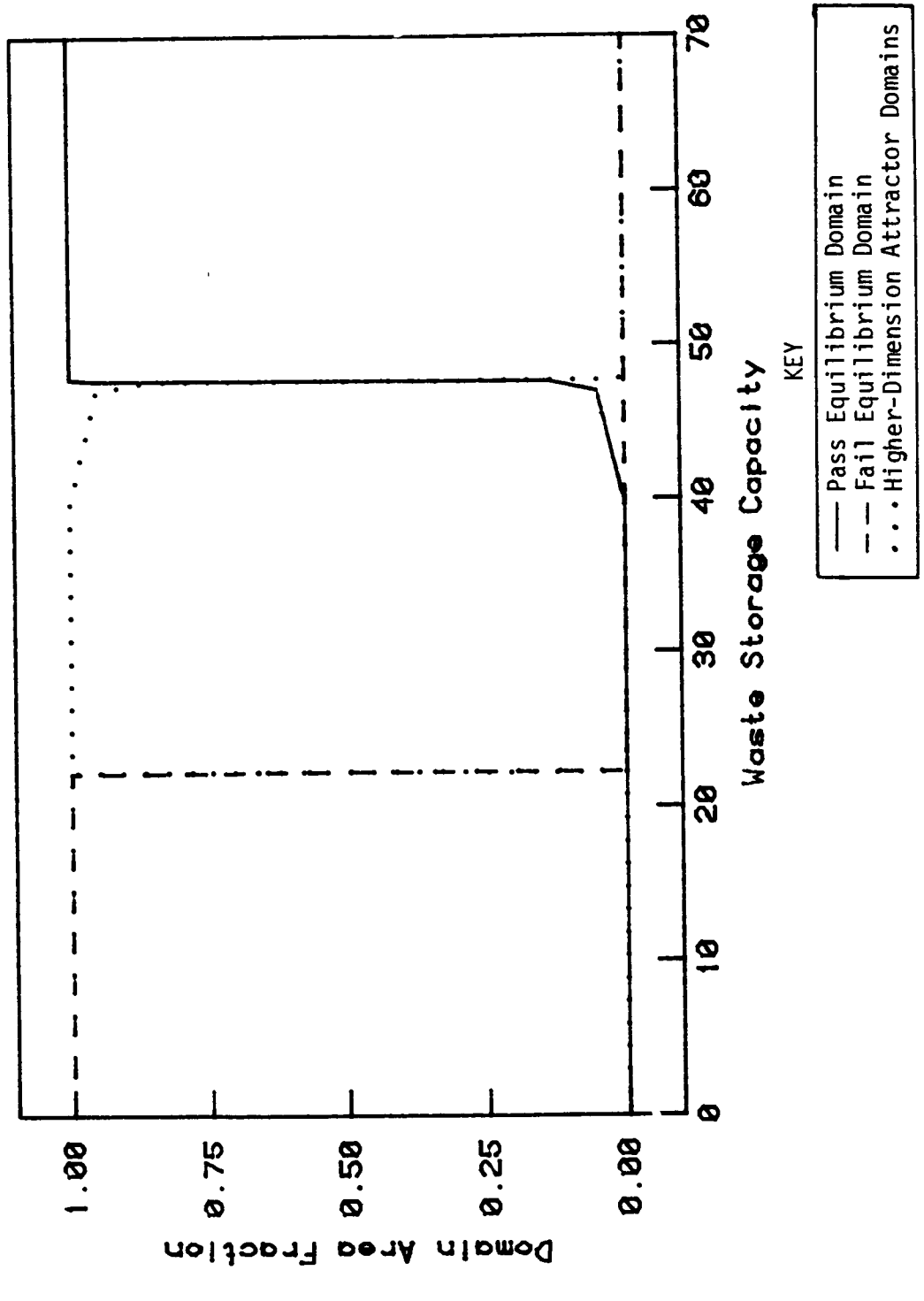

Figure 43: Domains of Attraction; Twelve-Chamber Model

settling time may be long for some of the initial conditions.

A waste capacity of 37.3 gives a globally attracting cycle (see Figure 44). There is always a 1 unit per day flow of food to the crew making this cycle survivable. Further, it attracts the entire state space with a waste capacity smaller than that which would support a pass equilibrium point. Ordinarily, cycles are engineered out of systems because they wear out components. However, biological systems are not hurt by constant oscillation; in fact this behavior may be more natural. Another benefit is that repairs and maintenance can be performed without disturbing the system every 110 days as the low point in the flow goes through the component.

This cycle is aperiodic. It has "envelope" and "carrier" frequencies that do not have a common divisor. The attractor creating this type of trajectory can be pictured as motion on a torus [10]. However, for the purposes of insuring that the crew's needs are met, the aperiodic component of this motion is not significant.

The twelve-chamber model also has chaotic motion. Figure 45 shows the motion (discrete-time simulation) on a strange attractor that is globally attracting at a waste capacity of 37.6. While there are long periods where the crew's food needs are met, such occurrences are difficult to predict. It should be noted, however, that there may be strange attractors that can insure the needed food flow. These would be as acceptable, from a survival point of view, as the cycle shown in Figure 44. To demonstrate the complexity inherent in a chaotic trajectory, Figure 46 shows the edible harvests for 13.7 years.

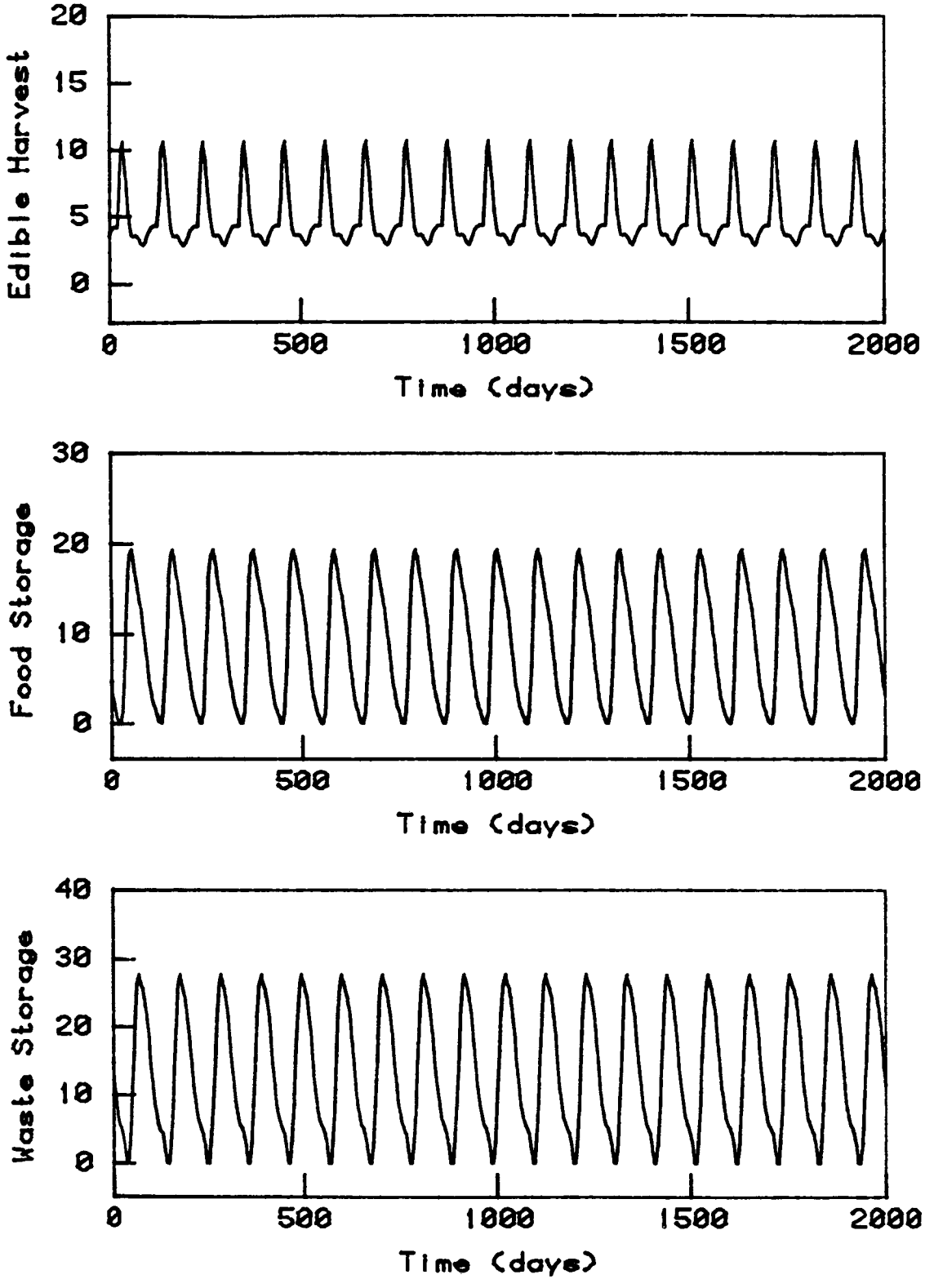

Figure 44: Oscillating Trajectory;
Twelve-Chamber Model (Discrete-Time)

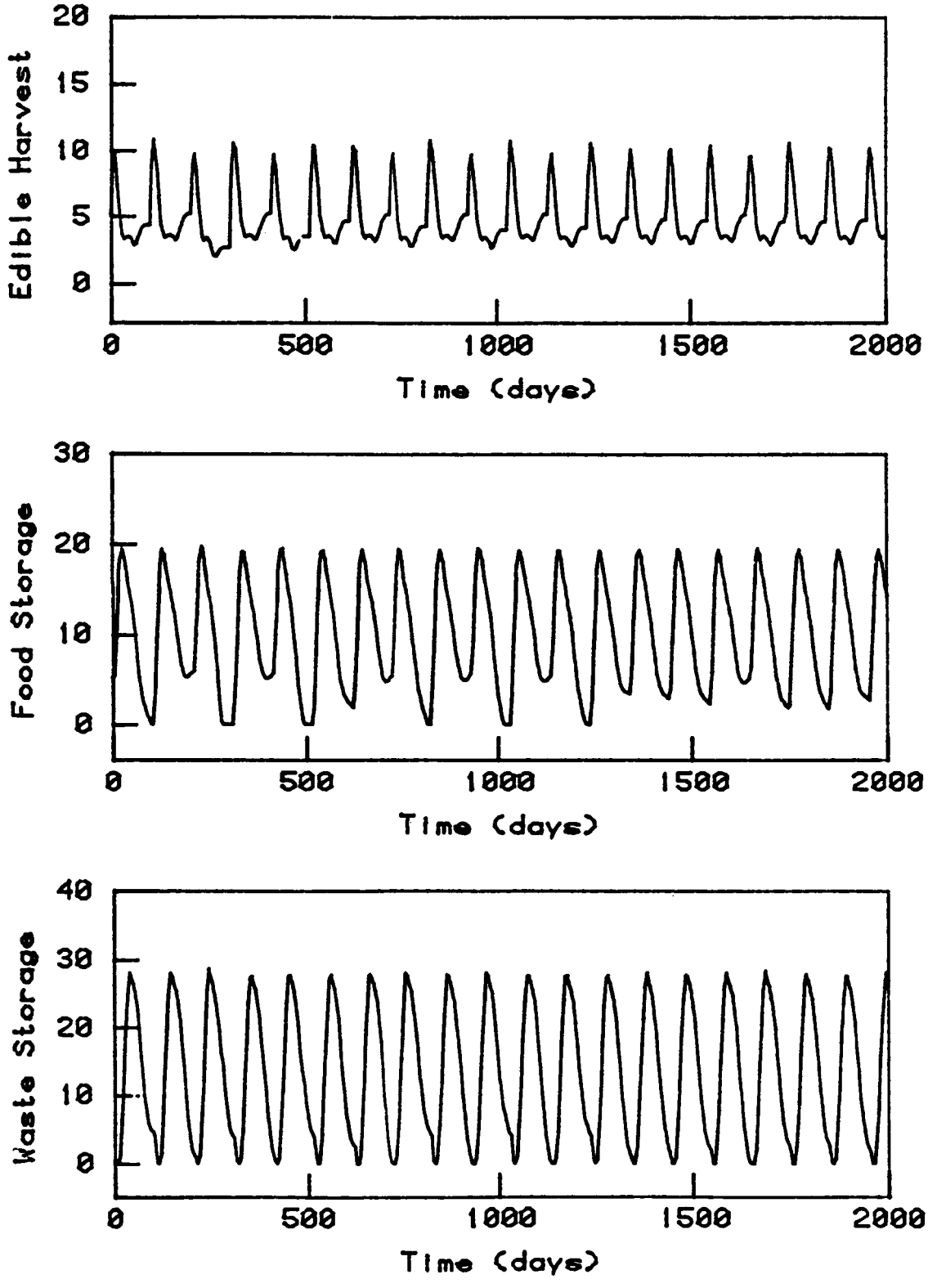

Figure 45: Chaotic Trajectory;
Twelve-Chamber Model (Discrete-Time)

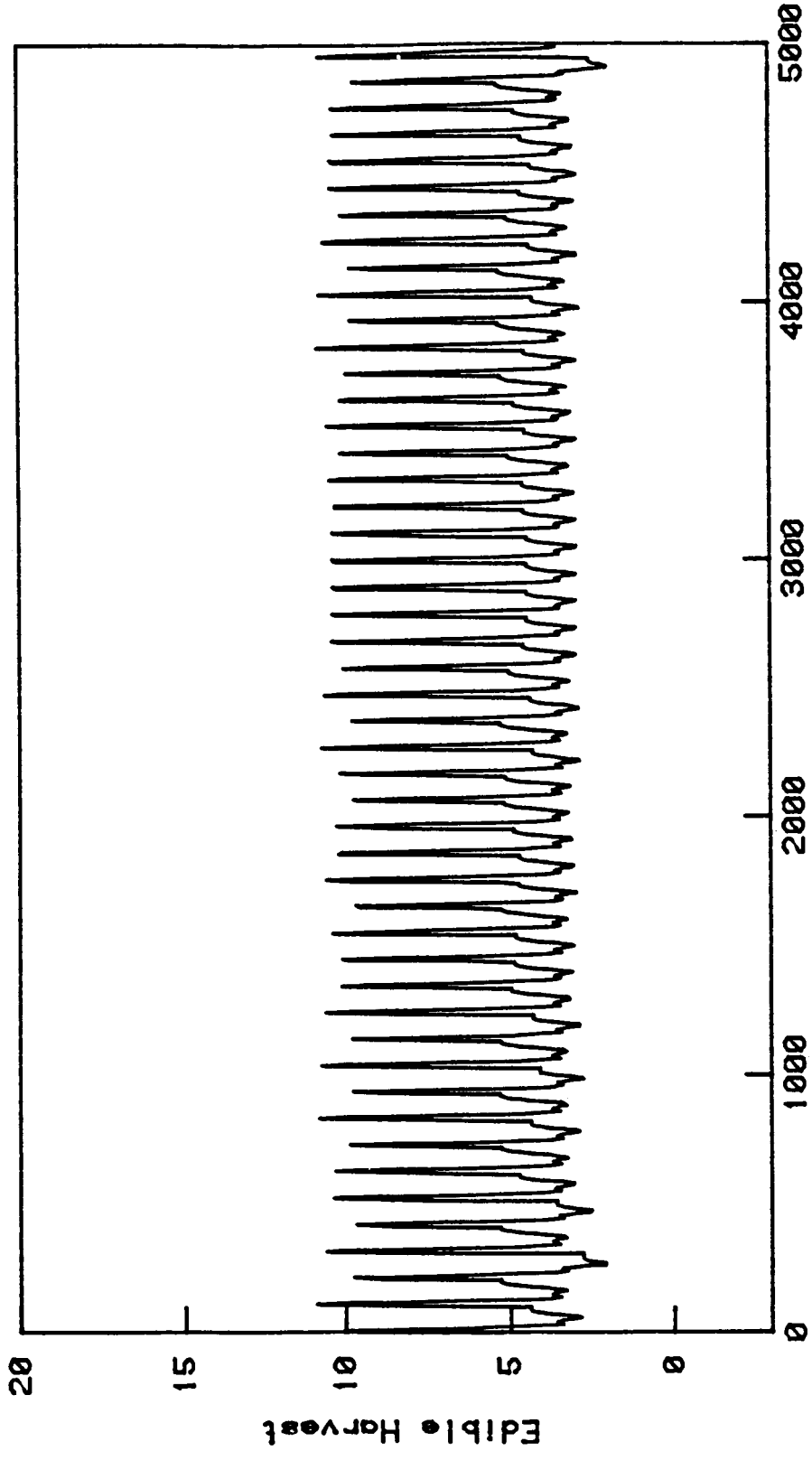

Figure 46: Chaotic Harvest; Twelve-Chamber Model (Discrete-Time)

In summary, changes in waste storage capacity and the number of plant chambers significantly alters the system's behavior. All three models show a pattern of bifurcation and reverse bifurcation as the waste capacity is increased. The three-chamber model has only two equilibrium points while the six- and twelve-chamber models have two equilibrium points and a collection of higher-dimension attractors. As the waste capacity is reduced, the settling time of the pass initial conditions increases. In addition to permitting the use of smaller storage tanks, the six- and twelve-chamber models have oscillating, stable, globally attracting trajectories. These occur at waste capacities smaller than those that permit surviving equilibrium point behavior.

5.3 Information Flow in a CELSS

Since the CELSS system is a closed cycle, it is not apparent what piece of information will be most useful to a controller. To investigate the effectiveness of different information use, the three-chamber model was chosen with a waste capacity of 82. The design goal is to maximize the volume and the minimum radius of the domain of attraction of the pass equilibrium point. The domain is delineated with 10,000 initial conditions.

In the first example, the waste flow to the processor is set at the steady state value of 3 units/day. This no-control situation is the equivalent of an open-loop investigation in traditional process control. The domain of attraction for this case is 0.056 ± 0.005 of the state space volume. The minimum radius is 1.5 ± 1.1.

A proportional control is added to the system. Its general form is:

$$u = u_{steady}\,[1 + k(1 - y/y_{set})] \tag{5.3}$$

where u is the waste flow to the processor, u_{steady} is the steady state processor flow, and k is the proportional gain. The observed variable is y and the desired value for y is y_{set}. The quality of the control depends on the selection of the state variable y that is used in the controller feedback.

Figure 47 shows some possible paths for feedback information flow in a CELSS. Three feedback configurations are shown, for which domain of attraction simulations are repeated with 100 proportional gains randomly selected from the range:

$$0 \leq k \leq 5 \tag{5.4}$$

The gain that provides the largest minimum radius is the controller for that feedback system that can recover from the largest set of random state perturbations.

When the waste flow is set by comparing the level in the waste storage with the steady state, the largest domain of attraction volume is 0.099 ± 0.005 of the state space and its minimum radius is 2.1 ± 1.1. Its gain is $k = 0.51$. It should be noted that volume fractions from 0.050 to 0.099 can be obtained by using gains in the range from 0 to 1.5. A gain of zero is the no-control situation. Using the waste storage level as the control input has a marginal effect on the system's ability to recover from random failures.

The presence of inert matter in the plant chamber reduces edible

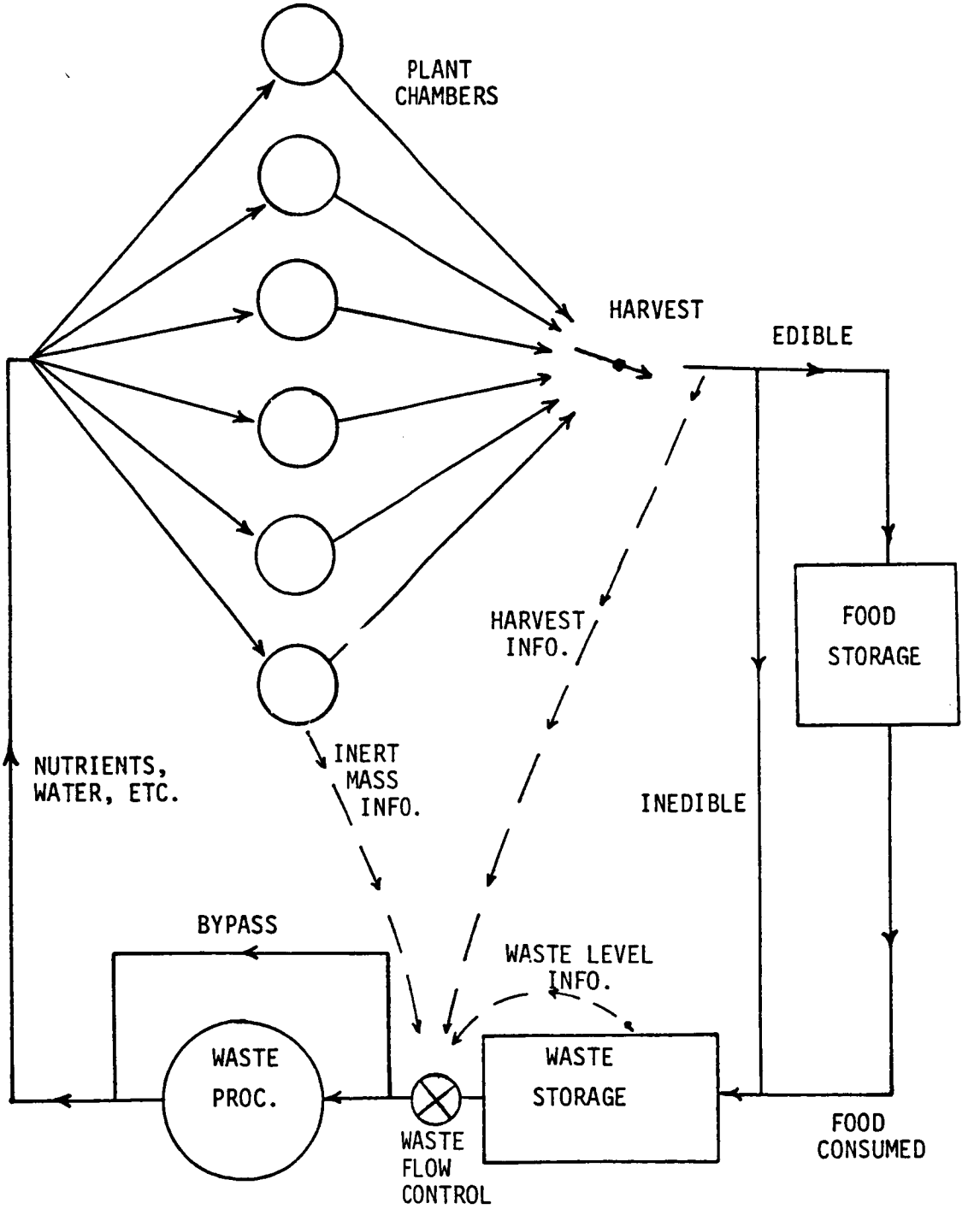

Figure 47: Information Flow in a CELSS

growth (see Figure 24). A controller can compensate by increasing the nutrient flow to the plants, which increases the edible fraction. Searching the range of gains with this feedback design gives a maximum domain of attraction volume of 0.180 ± 0.005 of the state space. The minimum radius is 5.2 ± 1.1. This control has a larger domain than the waste-feedback or no-control configurations. Although the gain for this domain is $k = 1.4$, there is a wide range of gains that give comparable results. Volumes from 0.100 to 0.180 are achieved with any gain larger than $k = 0.5$. As the gain gets larger, the controller reaches its maximum flow for very small inert masses. Such saturation indicates that most results above a certain gain will be identical.

The harvest can also be used as input to the controller. Although this configuration is like the one used in the waste capacity investigation of the previous section, here the capacity is fixed and the control gain is searched to find the system that recovers from the largest set of random failures. The largest domain of attraction was found for the gain $k = 1.2$. The domain's volume is 0.585 ± 0.005 of the state space and its minimum radius is 18.3 ± 1.1. The domain is rather sensitive to gain. For gains from 1.0 to 1.25 the domain volume fraction is between 0.500 and 0.585. However, there is a sharp drop in domain volume for gains outside this range.

Global system behavior was slightly improved over the no-control situation by using the waste storage level or inert mass as the feedback information. However, a large increase in the domain of attraction was obtained when harvest information was used. This can be understood by redrawing the CELSS in a more conventional process control configura-

tion. Figure 48 shows the system drawn with forward and backward paths. Control is exerted on the system by adjusting the waste processor flow. Using the waste storage level as the control input gives very little improvement in the size of the domain of attraction. Since this domain represents stability, it is expected that feedforward control would have no influence on its size. Hence, making use of the waste storage information mimics the traditional behavior of a feedforward path. The inert mass in the plant chambers provides feedback on the inner mass loop which gives more system stability. Feedback on the outside mass loop, using harvests as the control input, does even more to improve the stability domain.

This analogy with process control helps to explain the effectiveness of various feedback configurations. It is, however, only a single input, single output controller investigation. More complex controllers, such as those that use state feedback, would probably be able to achieve larger domains of attraction and performance than these output feedback controls.

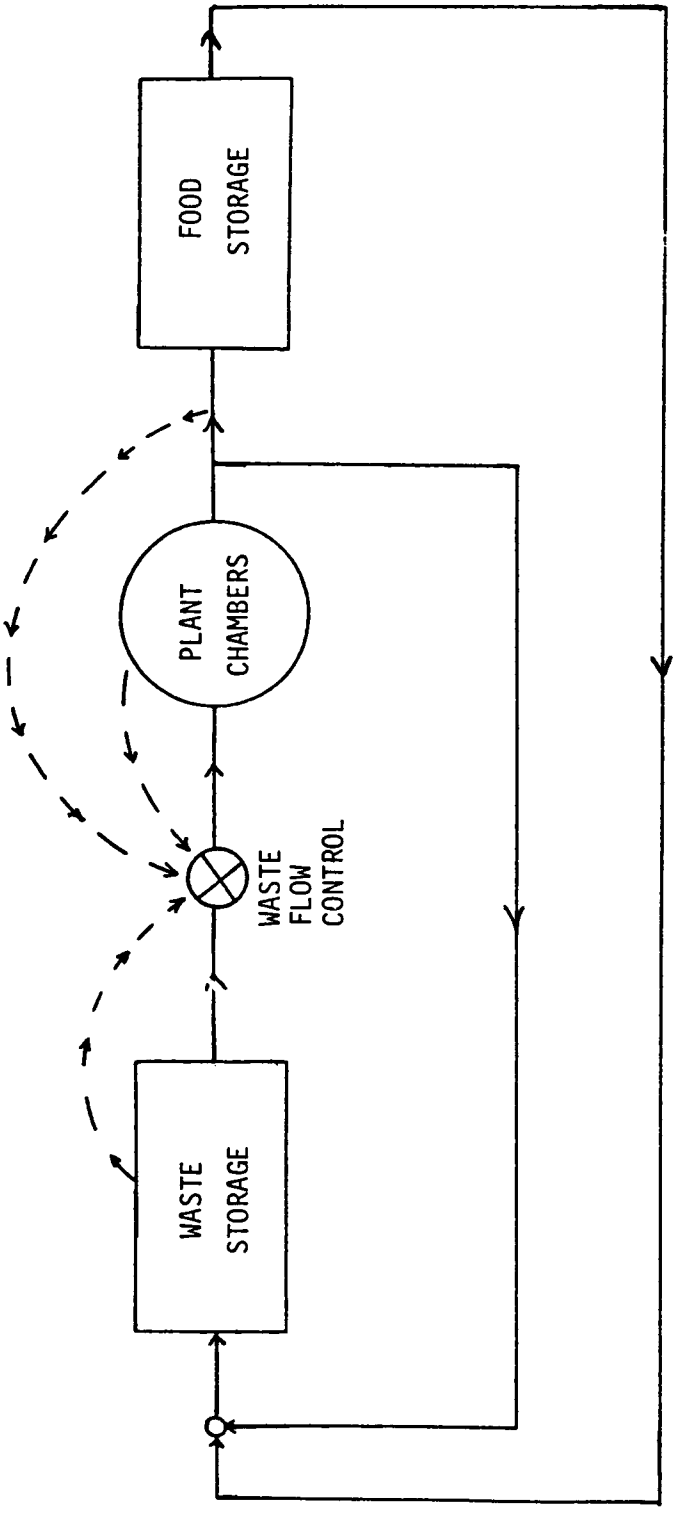

Figure 48: The CELSS as a Process Control System

6. SUMMARY

In this dissertation, a technique for analyzing and designing controllers for nonlinear systems based on measures of the domain of attraction has been presented. These methods are particularly suited to investigating the dynamic consequences of changes in the waste storage capacity, the system mass, and how information is used for control in CELSS models. The models' high-dimensionality and nonlinear state equations make them difficult to analyze by any other technique.

The domain is the region of initial conditions that asymptotically approach an attractor. The attractor may be an equilibrium point, a limit cycle, or other higher-dimension attractors. A refinement of this region is the domain of performance which is the region of initial conditions that meet a performance criteria.

In nonlinear systems, local stability does not insure stability over a larger region. The domain of attraction marks out this stability region. In this way, it is a measure of nonlinear system's ability to recover from random state perturbations. In linear systems, local stability guarantees global stability so this concept is not enlightening. However, the use of a domain of performance as a global measure is useful in both linear and nonlinear systems.

When considering random perturbations, the minimum radius of the domain is a measure of the magnitude of perturbations for which recovery is guaranteed. An advantage of this measure is that it is a vector length and, therefore, is applicable to systems with any dimension. The representation of global system performance in a single scalar permits

easy comparisons of system and controller designs.

The domain of attraction or performance is delineated by randomly selecting initial conditions from the region of state space being investigated. If these are from uniform distributions, the number of points in the domain is proportional to its volume. The minimum radius of the domain's boundary is found by subtracting the typical point spacing distance from the nearest initial condition not in the domain. In constrained systems, the sample distribution cannot be uniform. The minimum radius is now found by subtracting the local point spacing distance from the nearest point not in the domain. By numerically inverting the nonuniformity of the sample points, the domain volume can be obtained. Error determinations for the volume and minimum radius are found by repeating the domain simulations with independent samples.

The use of the domains of attraction and performance were demonstrated in controller design for an inverted pendulum. This global design technique was contrasted with more traditional, local design methods. Since the problem is nonlinear, the traditional designs only insured some sort of local behavior. There is no map between local design decisions and the nonlinear system's global behavior. Thus, it is not apparent what parameter changes need to be made to improve the global performance.

When the domain of attraction or performance is used in the controller design, the global behavior of the system is used as the design criteria. Consider the case where a controller form is selected and the gains need to be set. A controller can be designed by randomly selecting gains, simulating the resulting domains, and using the minimum radius as

the selection parameter. For the inverted pendulum, this technique was used to find a linear state-feedback controller that was able to recover from a larger class of state perturbations than those found by local techniques. A nonlinear controller was also designed which had larger domains of attraction and performance than the linear one.

An advantage to this global design technique is that the design process is automated once the system model is formulated, the region of state space to be investigated is established, and the form of the controller is set. The domain simulations are made from randomly selected initial conditions over the state space. Each domain simulation results in a minimum radius representing the system's ability to recover from random state perturbations. The complexity of the controller has no effect on this process, other than to increase the number of parameters that need to be set for each domain simulation. The system dimension is not a problem because the selection is made using a scaler.

The domain of attraction was used in the CELSS examples not only to find good control gains, but also to investigate system behavior as a function of system parameters. It was found that the three-chamber model has only two equilibrium points in the discrete-time simulation. One point provides edible harvests that meet the crew's food requirements. The other has edible harvests that are always zero. The former, surviving equilibrium is called the pass equilibrium point and the latter one is called the fail equilibrium. For small waste storage capacities the fail point is the only attractor. As the waste storage increases this equilibrium bifurcates into pass and fail stable points. Then there is a reverse bifurcation leaving only the pass equilibrium point.

The six- and twelve-chamber models showed a similar bifurcation, then reverse bifurcation pattern. However, in the intermediate range of tank capacity, there were also stable, higher-dimension attractors present. These have bounded trajectories that are limit cycles, aperiodic oscillations, and chaotic motion. While there were no survivable oscillating trajectories found for the six-chamber model, the twelve-chamber system had survivable behaviors that are cyclical.

An investigation of the effectiveness of using different information as controller input showed that the CELSS can be viewed in a process control configuration. Here, controls that look like traditional feedforward control have no effect on the system stability. Feedback control, however, improves system stability. In this representation the multi-loop form of the CELSS becomes apparent.

To achieve the minimum mass and storage capacity in a CELSS, systems with more frequent harvests are preferred. Less mass is tied up in the plant chambers and the harvests are small, requiring less storage capacity. However, these systems have a large number of state variables. Real-time controllers may be burdened by this high-dimensionality.

Smaller waste capacities may be used to force the system into a cyclical mode. While this is not usually acceptable in mechanical systems, it appears to have benefit in a CELSS. The waste capacity is reduced while not requiring an increase in the food storage capacity. Also, by waiting for the low point in the system flow, repairs and maintenance could be performed without disturbing the system.

The abstract CELSS models presented in this dissertation only give

a hint of the complexity of dynamic behavior that will be observed in a real system. Modeling the atmosphere as a separate loop would probably create new system behaviors due to the interaction of the gaseous and solid/liquid loop. State feedback controllers may be successfully designed to globally stablize the system about a variety of operating behaviors.

7. REFERENCES

1. Averner, M. An Approach to the Mathematical Modelling of a Controlled Ecological Life Support System. Washington D.C.: NASA (NASA CR-166331), 1981.

2. Babcock, P.S., D.M. Auslander, and R.C. Spear. "Dynamic Considerations for Control of Closed Life Support Systems". Proceedings of the 25th Annual Meeting of the Committee on Space Research (COSPAR), Graz, Austria, July, 1984. (To be published).

3. Franklin, G.F., and J.D. Powell. Digital Control of Dynamic Systems. Reading, MA: Addison-Wesley, 1980.

4. Guckenheimer, J., and P. Holmes. Nonlinear Oscillations, Dynamical Systems, and Bifurcations of Vector Fields. New York: Springer-Verlag, 1983.

5. Gustan, E. and T. Vinopal. Controlled Ecological Life Support System: Transportation Analysis. Moffett Field, CA: NASA Ames Research Center (NASA CR-166420), 1982.

6. Hammersley, J.M., and D.C. Handscomb. Monte Carlo Methods. New York: Wiley & Sons, 1964.

7. Hunt, L.R., R. Su., and G. Meyer. "Global Transformation of Nonlinear Systems". IEEE Transaction on Automatic Control. vol. 27,

1982.

8. Incropera, F. "Leaf Photosynthesis: The Influence of Environmental Variables". Journal of Environmental Quality. Vol.4, No.4., 1975.

9. Jordan, D.W. and P. Smith. Nonlinear Ordinary Differential Equations. Oxford: Clarendon Press, 1979.

10. Lichtenberg, A.J. and M.A. Lieberman. Regular and Stochastic Motion. New York: Springer-Verlag, 1983.

11. Modell, M. and J. Spurlock. "Closed-Ecology Life Support Systems (CELSS) For Long-Duration, Manned Missions". American Society of Mechanical Engineering. Paper 79-ENAs-27, 1979.

12. Rubenstein, R.Y. Simulation and the Monte Carlo Method. New York: Wiley & Sons, 1981.

13. Salisbury, F. and C. Ross. Plant Physiology. Belmont, CA: Wadsworth, Inc., 1979.

14. Sparrow, C. The Lorenz Equations: Bifurcations, Chaos, and Strange Attractors. New York: Springer-Verlag, 1983.

15. Stahr, J., D.M. Auslander, R.C. Spear, and G. Young. An Approach to the Preliminary Evaluation of Closed Ecological Life Support System (CELSS) Scenarios and Control Strategies. Moffett Field, CA: NASA

Ames Research Center (NASA CR-166368), 1982.

16. Su., R., G. Meyer, and L.R. Hunt. "Robustness in Nonlinear Control". in Differential Geometric Control Theory. Boston: Birkhauser, 1983.

17. Takahashi, Y., M.J. Rabins, and D.M. Auslander. Control and Dynamic Systems. Reading, MA: Addison-Wesley, 1972.

18. Young, G.E. A Design Methodology for Nonlinear Systems Containing Parameter Uncertainty: Application to Nonlinear Controller Design. Berkeley: University of California, Dissertation, 1982.

APPENDIX A:
CELSS Documents Published as NASA Reports

1. Johnson, Emmett J.: Genetic Engineering Possibilities for CELSS: A Bibliography and Summary of Techniques. NASA CR-166306, March 1982.

2. Hornberger, G.M. and Rastetter, E.B.: Sensitivity Analysis as an Aid in Modelling and Control of (Poorly-Defined) Ecological Systems. NASA CR-166308, March 1982.

3. Tibbitts, T.W. and Alford, D.K.: Controlled Ecological life Support System: Use of Higher Plants. NASA CP-2231, May 1982.

4. Mason, R.M. and Carden, J.L.: Controlled Ecological Life Support System: Research and Development Guidelines. NASA CP-2232, May 1982.

5. Moore, B. and MacElroy, R.D.: Controlled Ecological Life Support System: Biological Problems. NASA CP-2233, May 1982.

6. Aroeste, H.: Application of Guided Inquiry System Technique (GIST) to Controlled Ecological Life Support Systems (CELSS). NASA CR-166312, January 1982.

7. Mason, R.M.: CELSS Scenario Analysis: Breakeven Calculation. NASA CR-166319, April 1980.

8. Hoff, J.E., Howe, J.M. and Mitchell, C.A.: Nutritional and Cultural Aspects of Plant Species Selection for a Controlled Ecological Life Support System. NASA CR-166324, March 1982.

9. Averner, M.: An Approach to the Mathematical Modelling of a Controlled Ecological Life Support System. NASA CR-166331, August 1981.

10. Maguire, B.: Literature Review of Human Carried Microbes' Interaction with Plants. NASA CR-166330, August 1980.

11. Howe, J.M. and Hoff, J.E.: Plant Diversity to Support Humans in a CELSS Ground-Based Demonstrator. NASA CR-166357, June 1982.

12. Young, G.: A Design Methodology for Nonlinear Systems Containing Parameter Uncertainty: Application to Nonlinear Controller Design. NASA CR-166358, May 1982.

13. Karel, M.: Evaluation of Engineering Foods for Controlled Ecological Life Support Systems (CELSS). NASA CR-166359, June 1982.

14. Stahr, J.D., Auslander, D.M., Spear, R.C. and Young, G.E.: An Approach to the Preliminary Evaluation of Closed-Ecological Life Support System (CELSS) Scenarios and Control Strategies. NASA CR-166368, July 1982.

15. Radmer, R., Ollinger, O., Venables, A. and Fernandez, E.: Algal Culture Studies Related to a Closed Ecological Life Support System (CELSS). NASA CR-166375, July 1982.

16. Auslander, D.M., Spear, R.C. and Young, G.E.: Application of Control Theory to Dynamic Systems Simulation. NASA CR-166383, August 1982.

17. Fong, F. and Funkhouser, E.A.: Air Pollutant Production by Algal Cell Cultures. NASA CR-166384, August 1982.

18. Ballou, E. V.: Mineral Separation and Recycle in a Controlled Ecological Life Support System (CELSS). NASA CR-166388, March 1982.

19. Moore, B., III, Wharton, R. A., Jr., and MacElroy, R.D.: Controlled Ecological Life Support System: First Principal Investigators Meeting. NASA CP-2247, December 1982.

20. Carden, J. L. and Browner, R.: Preparation and Analysis of Standardized Waste Samples for Controlled Ecological Life Support Systems (CELSS). NASA CR-166392, August 1982.

21. Huffaker, R. C., Rains, D. W. and Qualset, C. O.: Utilization of Urea, Ammonia, Nitrite, and Nitrate by Crop Plants in a Controlled Ecological Life Support System (CELSS), NASA-CR 166417, October 1982.

22. Gustan, E. and Vinopal, T.: Controlled Ecological Life Support System: Transportation Analysis. NASA CR-166420, November 1982.

23. Raper, C. David, Jr.: Plant Growth in Controlled Environments in Response to Characteristics of Nutrient Solutions. NASA CR-166431, November 1982.

24. Wydeven, T.: Composition and Analysis of a Model Waste for a CELSS. NASA Technical Memorandum 84368, September 1983.

25. Averner, M., Karel, M., and Radmer, R.: Problems Associated with the use of Algae in Bioregenerative Life Support Systems. NASA CR-166615, November 1984.

26. Radmer, R., Behrens, P., Fernandez, E., Ollinger, O., Howell, C., Venables, A., Huggins, D. and Gladue, R.: Algal Culture Studies Related to a Closed Ecological Life Support System (CELSS). NASA CR-177322, October 1984.

27. Wheeler, R. and Tibbitts, T.: Controlled Ecological Life Support System: Higher Plant Flight Experiments. NASA CR-177323, November 1984.

28. Auslander, D., Spear, R., Babcock, P. and Nadel, M.: Control and Modeling of a CELSS (Controlled Ecological Life Support System). NASA CR-177324, November 1984.

29. Karel, M. and Kamarei, A.R.: Feasibility of Producing a Range of Food Products from a Limited Range of Undifferentiated Major Food Components. NASA CR-177329, April 1984.

30. MacElroy, R.D., Smernoff, D.T., and Klein, H.: Life Support Systems in Space Travel. (Topical Session of XXVth COSPAR meeting, Graz, Austria) NASA CP-2378, May 1985.

31. MacElroy, R.D., Martello, N.V., Smernoff, D.T.: Controlled Ecological Life Support Systems: CELSS '85 Workshop, NASA TM-88215, January 1986.

32. Tibbitts, T.W.:Controlled Environment Life Support System: Calcium-Related Leaf Injuries on Plants. NASA CR-177399, March 1986.

33. Tibbitts, T.W., Wheeler, R.M.: Controlled Environment Life Support System: Growth Studies with Potatoes, NASA CR-177400, March 1986.

1. Report No.	2. Government Accession No.	3. Recipient's Catalog No.
NASA CR-177401		

4. Title and Subtitle	5. Report Date
Nonlinear System Controller Design Based on Domain of Attraction: An Application fo CELSS Analysis and Control	March 1986
	6. Performing Organization Code: SLX
7. Author(s): P.S. Babcock, IV	8. Performing Organization Report No.: 34
9. Performing Organization Name and Address: Department of Mechanical Engineering, University of California - Berkeley, Berkeley, CA 94720	10. Work Unit No.: T 4081
	11. Contract or Grant No.: NCC 2-67
12. Sponsoring Agency Name and Address: National Aeronautics and Space Administration, Washington, D.C. 24056	13. Type of Report and Period Covered: Contractor Report
	14. Sponsoring Agency Code: 199-61-12

15. Supplementary Notes

Point of Contact: Robert D. MacElroy, NASA Ames Research Center, MS 239-4, Moffett Field, CA 94035, 415-694-5573 or FTS 8-464-5573

16. Abstract

A technique for analyzing and designing controllers for nonlinear systems based on measures of the domain of attraction is presented. These methods are particularly suited to investigating Closed Ecological Life Support Systems (CELSS) models. In particular, the dynamic consequences of changes in the waste storage capacity and system mass, and how information is used for control in CELSS models are examined. The models' high dimensionality and nonlinear state equations make them difficult to analyze by any other technique. The domain of attraction is the region of initial conditions that tend toward an attractor and it is delineated by randomly selecting initial conditions from the region of state space being investigated. Error determinations are found by repeating the domain simulations with independent samples. A refinement of this region is the domain of performance which is the region of initial conditions that meet a performance criteria. In nonlinear systems, local stability does not insure stability over a larger region. The domain of attraction marks out this stability region; hence, it can be considered a measure of a nonlinear system's ability to recover from state perturbations. When considering random perturbations, the minimum radius of the domain is a measure of the magnitude of perturbations for which recovery is guaranteed. An advantage of this measure is that it is a vector length and, therefore, is applicable to systems with any dimension. The use the domains of attraction and performance are demonstrated in controller design for an inverted pendulum. This global design technique is contrasted with more traditional, local design methods. Design of both linear and nonlinear controllers are shown. Three CELSS models, with 9 to 30 state variable, are presented. Measures of the domain of attraction are used to show the global behavior of these models under a variety of design and controller scenarios. It is shown that all of the models have stable equilibria that bifurcate, then reverse bifurcate as the waste storage capacity increases. High-dimension models also show limit cycle and chaotic trajectories.

17. Key Words (Suggested by Author(s))	18. Distribution Statement
CELSS, nonlinear systems, domain of attraction, simulation models	Unclassified - Unlimited STAR Category 54

19. Security Classif. (of this report)	20. Security Classif. (of this page)	21. No. of Pages	22. Price*
Unclassified	Unclassified	120	

*For sale by the National Technical Information Service, Springfield, Virginia 22161